Projecte Fi de Carrera

Enginyeria de Telecomunicació

Analysis and Optimization of the Satellite-to-Plane Link of an Aeronautical Global System

Ricard Alegre Godoy

Director: María Ángeles Vázquez Castro

Departament de Telecomunicació i Enginyeria de Sistemes

Escola Tècnica Superior d'Enginyeria (ETSE)
Universitat Autònoma de Barcelona (UAB)

Setembre 2010

El sotasignant, *María Ángeles Vázquez Castro*, Professor de l'Escola Tècnica Superior d'Enginyeria (ETSE) de la Universitat Autònoma de Barcelona (UAB),

CERTIFICA:

Que el projecte presentat en aquesta memòria de Projecte Fi de Carrera ha estat realitzat sota la seva direcció per l'alumne *Ricard Alegre Godoy*.

I, perquè consti a tots els efectes, signa el present certificat.

Bellaterra, *2/09/2010*.

Signatura: *María Ángeles Vázquez Castro*

Contents

List of Acronyms

ACM	Adaptive Coding and Modulation
AES	Aeronautical Earth Station
AFR	Array Fed Reflector
AL	Application Layer
ANSP	Air National Service Provider
ATM	Air Traffic Management
ATN	Aeronautical Telecommunications Network
AWGN	Additive White Gaussian Noise
BBFRAME	Base Band Frame
BBH	Base Band Header
BEC	Binary Erasure Channel
BER	Bit Error Rate
BO	Bandwidth Occupation
BSC	Binary Symmetric Channel
C	Continuity
CFLTR	Channel Filter
CFR	Correct Frame Rate
CoS	Class of Service
CRC	Cyclic Redundancy Check
DBA	Dynamic Bandwidth Allocation
DBFN	Digital Beam Forming Network
DOCON	Down-Converter
DVB-S2	Digital Video Broadcasting over Satellite 2on Generation
DVB-RCS	Digital Video Broadcasting Return Channel over Satellite
ECAC	European Civil Aviation Conference
EG	Euclidean Geometry
eIRA	extended Irregular Repeat and Accumulate
EIRP	Equivalent Isotropic Radiated Power
ET	Expiration Time
FDM	Frequency Division Multiplexing
FEC	Forward Error Correction
FWD	Forward
GeIRA	Generalized Irregular Repeat and Accumulate

GEO	Geosynchronous Earth Orbit
GES	Ground Earth Station
GFMAC	Galois Field Multiply and Accumulate
GSE	General Stream Encapsulation
G/T	Gain over Temperature
GW	Gateway
HEO	Highly Elliptical Orbit
HMPA	Hybrid Matrix Power Amplifier
HPA	Hybrid Power Amplifier
IFEC	Interburst Forward Error Correction
IFLTR	Intermediate Filter
IDMUX	Input Demultiplexer
IMUX	Input Multiplexer
IRA	Irregular Repeat and Accumulate
k	Boltzmann constant
KKT	Karush Kuhn Tucker
LDPC	Linear Density Parity Check
LL	Link Layer
LL-FEC	Link Layer Forward Error Correction
LNA	Low Noise Amplifier
LOS	Line of Sight
LT	Luby Transform
LTWTA	Linear Traveling Wave Tube Amplifier
MAC	Medium Access Control
MDS	Maximum Distance Separable
MF-TDM	Multi Frequency Time Division Multiplexing
MF-TDMA	Multi Frequency and Time Division Multiple Access
MODCOD	Modulation and Codification
MPE	Multi Protocol Encapsulation
NCC	Network Control Center
NLOS	Non Line of Sight
NOFR	Non Orthogonal Frequency Reuse
NPR	Noise Power Ratio
OBO	Output Back-Off
OBP	On Board Processor
OFLTR	Output Filter
PER	Packet Error Rate
PG	Progressive Geometry
PHY-FEC	Physical Layer Forward Error Correction
QoS	Quality of Service
RAT	Resource Allocation Table
RRM	Radio Resource Management
RS	Reed Solomon
RTN	Return
SBFN	Single Beam Feed Network
SINR	Signal to Interference plus Noise Ratio

SLA	Service Level Agreement
SNR	Signal to Noise Ratio
TC	Transported Capacity
TD_{95}	Time Delay 95 percentile
UPCON	Up-Converter
UT	User Terminal
WAN	Wide Area Network

List of Figures

List of Tables

Introduction

Background of the project

This project is part of a European project solicited by EUROCONTROL in the Single European Sky ATM Research (SESAR) programme called ANTARES. The project's prime contractor is Thales Alenia Space Italy and it is driven by several institutions such as Aedel Aerospace, Airtel ATN (IRL), Capgemini Norge (N), Commsonic (GB), Evolving Systems Consulting (CZ), Frequentis (A), Honeywell International (CZ), Indra Espacio (E), Iguassu Software Systems (CZ), IZT (D), Next (I), OHB-System (D), SINTEF ICT (N), Skysoft (P), DLR(D), Space Engineering (I), Syderal (CH), Thales Alenia Space Espana (E), Thales Alenia Space France (F), Thales Avionics (GB), Thales UK (GB), University of Salzburg Scientific Computing (A). The objectives of the project are to develop the communications protocols and satellite system for aviation communication. This satellite system is intended as a backup system for the currently operative beacon based system, but in the end because of advantages in terms of reliability, capacity etc. of this kind of system will, after some years, become the main system.

Motivation and Objectives

The purpose of this work is the analysis at system-level and a joint optimization at physical/link layer level of a satellite-to-plane link, forward link, of an aeronautical global system.

The general design framework is driven by the highly increasing air-traffic, which is expected to follow an exponential increase in the near future. Hence, currently distributed ground beacons-based approach may not scale enough and a turn to a rather centralized general approach will be assumed throughout the work.

In particular, the modular design covered in the present work has consisted of: system-level architecture at link layer, functional definition, algorithms and protocols at link layer for radio resource management and forward error correction need and solutions at link layer considering physical layer design.

It is also presented a study of the co-channel interference in satellite mulitbeam system since ANTARES is a particular multibeam system. The objective has been to provide neat thorough payload-dependant models to aid the overall final system design. This study is complementary to parallel work within our group on system-modelling and optimization of general multibeam systems with traffic constraints.

The objectives are to meet all the requirements, mandatory for aviation communication as it is established by the European Civil Aviation Conference (ECAC), whether they are relative to the link budget accomplishment, error rate ratios or qualities of service requirements needed at the analyzed layers in the work, physical layer and link layer. For this reason the methodology used is beginning with an exhaustive analysis of the system, the parts to optimize and its requirements to be able to take the right decisions to improve the overall performance of the system. Then we will simulate the proposed designs to observe if the requirements are met.

As it has been mentioned before the ANTARES project is driven by several institutions, regarding to this it must be mentioned that during the development of the work not all the information needed was available as it was being developed by other contractors. This can be seen either as a disadvantage or an advantage since when all the information is available the obtention and analysis of results, and the optimizations tasks are easier. However as this has not been possible we have been pushed to do also and engineering task, suppose suitable values or configurations , analyze the obtained results and iterate with new values if necessary.

Structure

This work is structured as follows, after this brew introduction, is presented in Chapter 1 the reason for designing the ANTARES system, its operation at system level and its mandatory requirements imposed by the ECAC. Later on, in Chapter 2 are explained the design options for the Radio Resource Management in ANTARES, defining the architectures at system and medium access control level. It is also detailed in the named chapter the physical access to the medium in order to meet the specified requirements. In Chapter 3 is discussed and analyzed the need for using LL-FEC codes in the system and which are the most suitable codes.

Chapter 4 explains, from a top view, the different payloads used in satellites, different payloads will lead to different link budget computations that will affect on our interference analysis on Chapter 5. This analysis is carried out in a generalized multibeam scenario and in a baseline option for ANTARES.

Finally Chapter 6 presents the simulation results for the Chapter 2, 3 and 5 and it takes conclusion into the results. Chapter 7 concludes the project by

resuming and analyzing the work done, as well as indicating future research lines. An appendix, A, is added to give detailed information of some of the computation carried out in the work. Appendix B provides brief guidelines for the LL-FEC implementation in ANTARES.

Chapter 1

ANTARES Global System

1.1 Introduction to aviation communications

Currently data aviation communications are based on transmitting information to ground beacons using VHF. These ground beacons retransmit the information through the Aeronautical Telecommunications Network (ATN) to its correct destination.

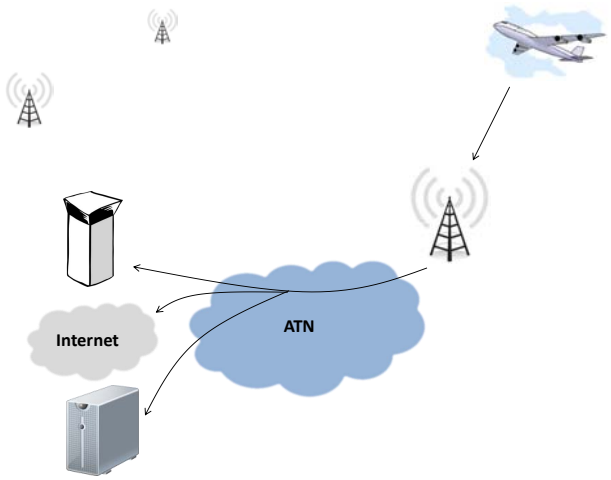

Figure 1.1: Aviation communications scheme

Ground beacons are distributed along airplane flight routes in order to maintain data communications continuous. However it is expected an exponential increase of the air traffic in the next years as well as the aperture of new aerial

routes. These changes will lead to the increase of ground radio beacons and data traffic. Hence the need to implement a backup satellite system for aviation communication in order to manage traffic in a more centralized way, increase the capacity of the system, being able to manage the incoming higher volumes of air traffic data and also unify all European countries under the same standard.

1.2 ANTARES System and Requirements

1.2.1 Architecture

The ANTARES system is basically a three Geosynchronous Earth Orbit (GEO) satellite multibeam system, designed for providing control communications between base stations and aircrafts, and vice versa through a satellite. The architecture of the system is shown in Figure 1.2.

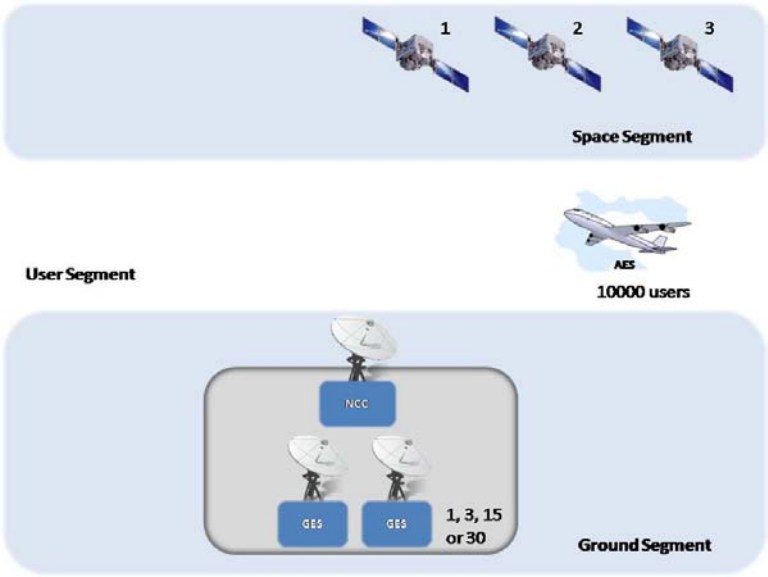

Figure 1.2: ANTARES system architecture

The elements constituting the system are described here after:

- GEO satellites: The three GEO satellites should be enough to provide coverage to flight areas, the use of additional Highly Elliptical Orbit (HEO) is envisaged in order to provide coverage to the poles and remote areas. Each of the GEO satellites is backuped by an additional satellite separated $\alpha = 50^o$ to increase the robustness of the system, providing an

additional link in case of degradation of the main one or substituting the main satellite in case of failure.

- Aeronautical Earth Stations (AES): The user segment system is compound of 10 thousand AESs, normally airplanes equipped with omnidirectional antennas on the top of the fuselage.
- Network Control Center (NCC): Is in charge of controlling all the satellite networking functions, one NCC per satellite is previewed.
- Ground Earth Stations (GES): Provide the interface with the ATN, the traffic network for airplanes communications. As a first approach one GES would be enough to manage all the system, however some Air National Service Providers (ANSP) have demanded specific GES for them, hence the values considered are 1, 3 or 5.

The system performs as follows, in the forward link when a GES wants to send information the NCC transmit a forward and a return signaling carrier to the GES and AES to indicate the forward and return traffic carriers. The NCC must receive back the signaling information in order to correct errors such as satellite Doppler. Then GES uses the assigned forward traffic carrier to transmit information to the AES, and the AES at the same time use the return traffic carrier to send information to the GES. While GES and AES are exchanging information a synchronization procedure is carried out between GES, AES and NCC to keep the continuity of the traffic carriers.

1.2.2 Types of Links

The system will work over two frequency bands, the Ku band and the L band as it is shown in Table 1.1.

	Fixed Link		Mobile Link	
Uplink	Ku band	11.7-12.7 GHz	L band	1646.5-1656.5 MHz
Downlink	Ku band	14-14.5 GHz	L band	1545-1555 MHz

Table 1.1: Types of Links

The fixed link comprehends from the GES to the satellite (unique beam structure) while the mobile link comprehends from the satellite to the AES (multi-beam structure).

1.2.3 Protocol Stack

The protocol stack of the system is shown in Figure 1.3.

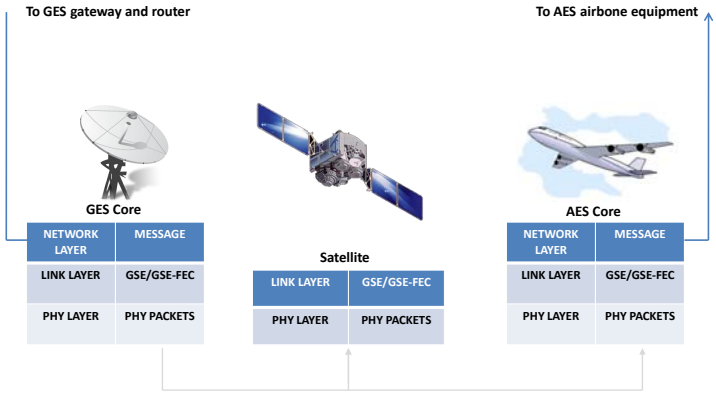

Figure 1.3: ANTARES end-to-end protocol stack

Messages from upper layers, ATN messages, are encapsulated into link layer frames using General Stream Encapsulation (GSE). In case it is decided to use Link Layer Forward Error Correction (LL-FEC), at this point the redundancy would be added as a GSE frame. After that GSE stream are encapsulated into physical layer packets ready to be sent. The encapsulation process followed is shown in Figure 1.4.

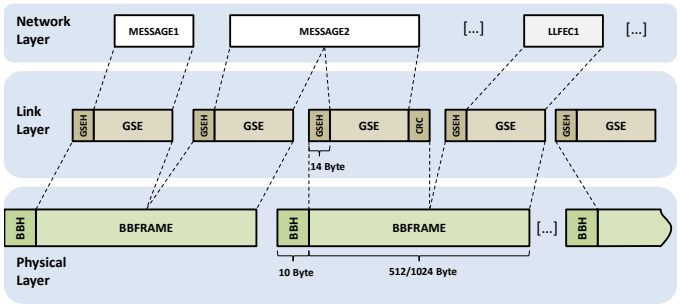

Figure 1.4: ANTARES general encapsulation process

1.2.4 Global System Parameters

In Table 1.2, 1.3, 1.4 and 1.5 are resumed the forward link parameters of the ANTARES system. At this point of development of the project more than one value is considered for some parameters.

Parameter	Value
Carrier Bandwidth (BW)	200kHz
B_{guard}	0.1
L1 Block Size (BS)	4096/8192 bits
Overhead L2	0.04
Overhead L1/L2 (OV L1/L2)	0.1
Modulations	QPSK, 8PSK 16APSK
Codifications (r)	1/3, 1/2, 2/3
Roll-off (α)	0.25
$\overline{R_{b,AES}}$	608.47 bps
σ_{AES}	138.57
$\overline{R_{b,AES}} + 3{\cdot}\sigma_{AES}$	1024.2 bps
$\overline{R_{b,AES}} - 3{\cdot}\sigma_{AES}$	192.76 bps

Table 1.2: Global system parameters

Parameter	Value
Number of satellites	3
Orbit	GEO
Payloads	Conventional, Flexible, Beam Hopping

Table 1.3: Satellite segment parameters

Value	Parameter
Number of users (N_{AES})	10000
Number of antennas	1

Table 1.4: User segment parameters

Parameter	Value
Number of GES (N_{GES})	1, 3, 5
Number of NCC	1

Table 1.5: Ground segment parameters

1.2.5 ANTARES System Requirements

Three types of requirements can be distinguished for the system:

- Resources demanded by each GES to send information to the AESs.
- Quality of Service (QoS) requirements for delivering the messages.

- User Terminal (UT) requirements for decoding the information.

GESs of the ANTARES system will be demanding a certain quantity of resources in order to send information to its assigned AESs. Depending on the final number of implemented GESs in the system, 1, 3, or 5 as it is specified in Table 1.5, the amount of resources requested per GES will vary. These values can be obtained from the traffic distribution of one single AES, $\overline{R_{b,AES}}$ and σ_{AES} specified in Table 1.2 and knowing the number of users the system must support, 10000, as depicted in Table 1.4. The histogram for the traffic distribution of one AES is as shown in Figure 1.5.

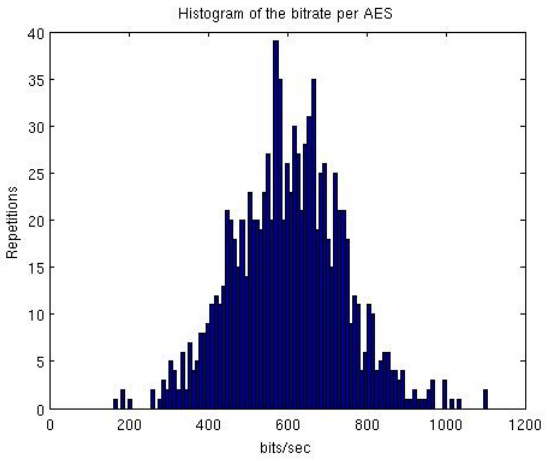

Figure 1.5: Histogram of the bitrate per AES

In order to estimate the aggregated GES traffic, we assume each GES has assigned a proportional part of the total number of AES, N_{AES}/N_{GES} users, then we can obtain $\overline{R_{b,GES}}$ and σ_{GES} by doing:

$$\overline{R_{b,GES}} = \frac{N_{AES}}{N_{GES}} \cdot \overline{R_{b,AES}}$$

$$\sigma_{GES} = \frac{N_{AES}}{N_{GES}} \sigma_{AES}$$

So for each of the possible GES values we get the traffic demands in Table 1.6. Histograms per each case are shown in Figure 1.6.

N_{GES}	$R_{b,GES}$	σ_{GES}	$\overline{R_{b,GES}} + 3 \cdot \sigma_{GES}$	$\overline{R_{b,GES}} + 3 \cdot \sigma_{GES}$
1	6.084Mbps	1.385Mbps	10.2Mbps	1.92Mbps
3	2.02Mbps	461.85kbps	3.40Mbps	634.4kbps
5	1.217Mbps	277.140kbps	2.04Mbps	385.5kbps
30	202.82kbps	46.190kbps	341.3kbps	64.25kbps

Table 1.6: Bitrate demanded per GES

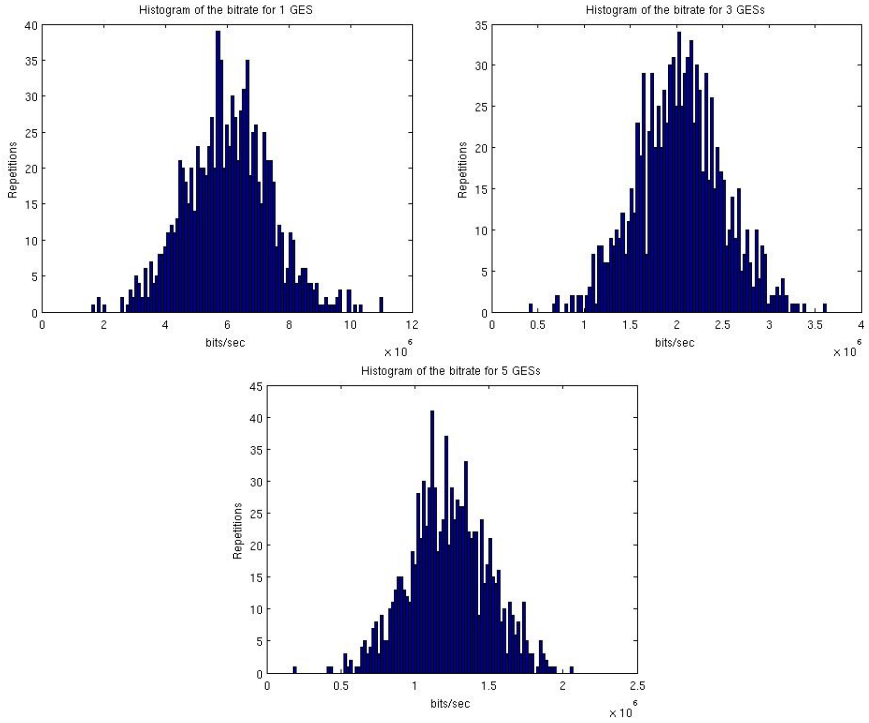

Figure 1.6: Histograms of the bitrate demanded per 1, 3, or 5

Air Traffic Management (ATM) applications send many different messages with different delay requirements. These requirements must be strongly accomplished since its information is very important, e.g. distance to other airplanes, alarm collisions, landing instructions etc. As it is impossible to establish a different criterion for each of the messages, they have been grouped into different Classes of Service (CoS) that must meet some QoS requirements. The QoS specification for each CoS is given in Table 1.7 for unicast traffic and in Table 1.8 for multicast traffic. The definition of each requirement is given here below:

- Time Delay 95% (TD_{95}): 95-th percentile of the transit delay one-way latency. This means a 95% of the messages sent must be received within

this delay.

- Expiration Time (ET): Maximum time beyond which a service interruption is declared. This means that the packets not received within the TD_{95} delay must be received in this time. As an approximation $ET \geq 2TD_{95}$.
- Continuity (C): Probability that a transaction will be completed having met specified performance. Possible anomalous behaviors include late transactions, lost messages or transactions that cannot be recovered within the expiration time, duplicate messages and uncorrected detected message errors.

CoS	TD_{95}(s)	ET (s)	C (%)
DG-C	1.4	5	0.996
DG-D	2.4	7.8	0.996
DG-F	4.7	12.0	0.996
DG-G	9.2	24.0	0.996
DG-H	13.6	32.0	0.996
DG-J	13.6	not available	not available
DG-K	26.5		
DG-L	51.7		

Table 1.7: Unicast QoS requirements per CoS

CoS	TD_{95} (s)	ET (s)	C(%)
DG-C	2.4	7.8	0.996

Table 1.8: Multicast QoS requirements

These QoS requirements will affect on further design decisions we will take for the ANTARES system specification. Message mean sizes and message arrival rates per CoS will also be necessary for further design decisions.

CoS	Message size (bytes)
DG-C	91.01
DG-D	489.47
DG-F	466.89
DG-G	293.16
DG-H	85.06
DG-J	3322.24
DG-K	116.45
DG-L	102.83
Mean size	1390

Table 1.9: Message sizes per CoS

CoS	Message arrival rate per CoS per AES	Arrival Rate per CoS
DG-C	0.0076	42.49
DG-D	0.0188	105.63
DG-F	0.0039	1.51
DG-G	0.0031	1.18
DG-H	0.0003	0.10
DG-J	0.0086	48.44
DG-K	0.0080	44.83
DG-L	0.0068	2.62

Table 1.10: Unicast Messages arrival rates per CoS (messages/s)

CoS	Message arrival rate per CoS per AES	Arrival Rate per CoS
DG-D	2.5097	489.47

Table 1.11: Multicast Messages arrival rates per CoS (messages/s)

Besides UT located in the AESs must also follow a certain structure:

- Each UT must be able to decode simultaneously the three different types of traffic an AES can receive which are carriers for unicast traffic, carriers for multicast traffic and carriers for signaling traffic.
- To this aim UTs are capable of receiving a N_{UT} subset of different carrier frequencies (the fewer, the better) that must include all the types of traffic listed in the point above.

A scheme to depict this issue considering a MF-TDMA Super Frame can be seen in Figure 1.7. Of course carriers need not be distributed uniformly (as depicted in the figure) but assign less carriers to signaling traffic or multicast traffic than to unicast traffic.

A secondary option for the UT design is assume a dynamically configurable terminal, i.e. the UT can be assigned any subset of the available carriers in the system before transmission starts. This can be done by sending a RAT from the GESs to AESs UT. This option is preferable since it does not add any restriction to the resource allocation process and **it is the assumed UT model in our simulations**.

1.3 Problem statement

The specific purposes of this work, always with regard to the **forward link**, are listed here below:

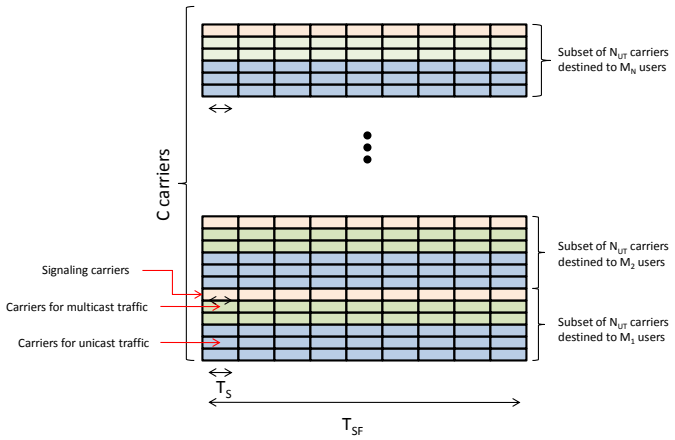

Figure 1.7: UT allocation

- Analysis of the architecture of the ANTARES system and its requirements to being able to design the required parts of the system (done in the current chapter).
- Designing the Radio Resource Management (RRM) for the selected Medium Access Control (MAC) (Chapter 2).
- Analyze whether or not is necessary to use Link Layer Forward Error Correction (LL-FEC) in the system and in case its necessary choose a suitable code and design a preliminary coding option (Chapter 3).
- Analysis of the co-channel interference of the system (Chapter 5), to this aim are studied first the elements that influence on this effect, which are the satellite payloads (Chapter 4).

Chapter 2

Design of the Radio Resource Management for the ANTARES system

In this chapter is carried out the RRM design of the ANTARES system. The tasks involving this design are listed here below:

- Definition of the types of link between AESs, GESs and NCC in section 2.1.
- Definition at MAC level of the entities forming the system and the operations that must perform. Related section is 2.2.
- Design of the MF-TDMA frame and its allocation algorithm explained in section 2.3.

2.1 System Level Architecture Design

Within this section is specified at system level, the different available options for the architecture design, taking into account its advantages and disadvantages. Note that the elements constituting the system were specified in Figure 1.2 but not the interfaces between them. Considerations made for the architecture design are listed here below:

- The link between GESs and AESs is always a satellite link.
- The link between the NCC and the GESs can either be a satellite or a terrestrial link.

These leads to two basic different architectures, an architecture with a satellite based Wide Area Network (WAN), and an architecture with a terrestrial based WAN. Besides for the delay estimation in each of the architectures the following notation is used:

- $t_{GES,NCC}$ stands for the propagation time between the GESs and the NCC and can take values either for a satellite or terrestrial link.
- $t_{NCC,GES}$ stands for the propagation time between the NCC and the GESs and can take values either for a terrestrial or a satellite link.
- $t_{GES,AES}$ stands for the propagation time between the GES and the AES and takes the value for a satellite end-to-end travel (0.25 seconds).
- t_{SCH} stands for the total time a packet is being scheduled which includes the amount of time the packet is queued and elapsed in the buffer waiting for being transmitted.
- t_a stands for the amount of time needed to transmit a packet using a certain modulation and codification (MODCOD).

It is of course important to reduce the quantity of satellite hops between the NCC and GESs as well as the information sent over these hops. The amount of time introduced in these links is relatively high when compared with any other delay and can not be reduced or optimized, so it will considerably affect to accomplish the QoS delay requirements.

2.1.1 Satellite Based Wide Area Network (SATBASED-WAN) Architecture

2.1.1.1 Distributed scheduling and resource allocation process

The basic characteristics of this option, which is depicted in Figure 2.1, are the following:

- The communication between the GESs and the NCC is carried out over a satellite link.
- Scheduling process is performed at each GES while the resource allocation process is performed in the NCC leading to a distributed architecture.

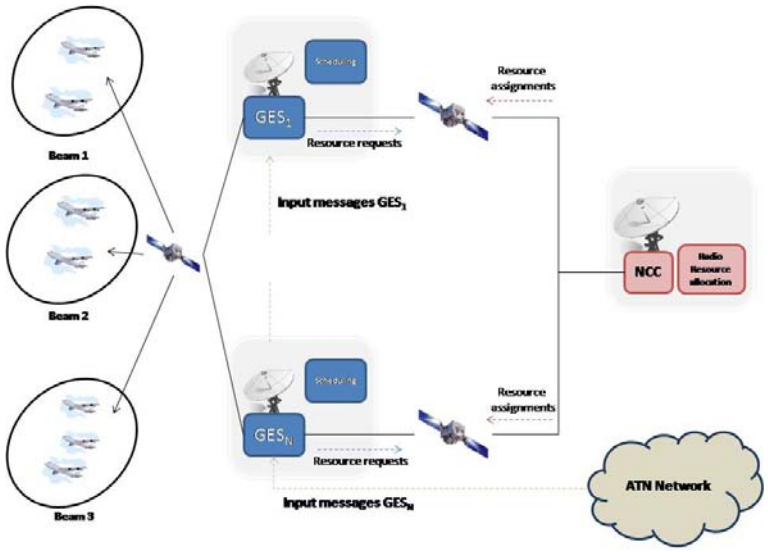

Figure 2.1: Satellite based distributed architecture

Therefore the top level process to send information to the AESs is as explained next:

- Based on the incoming messages, each GES requests resources to the NCC.
- The NCC performs the radio resource allocation and sends the assigned resources to each GES in a Resource Allocation Table (RAT).
- Each GES perform a scheduling policy in order to send the most priority packets to its assigned AESs by using the assigned resources.

A delay estimation for sending a packet can be performed as follows:

$$d(s) = max\{t_{SCH}, t_{GES,NCC} + t_{NCC,GES}\} + t_a + t_{GES,AES} \qquad (2.1)$$

The term $max\{t_{SCH}, t_{GES,NCC} + t_{NCC,GES}\}$ stands for the minimum time a packet will be scheduled, which is the time for a GES demanding resources and the NCC assign it to the GES. As under this option all links are satellite based air hops are delayed 0.25 seconds, the total delay estimation turns into:

$$d(s) = max\{t_{SCH}, 0.5s\} + t_a + 0.25s$$

Hence there is always a minimum 0.75 seconds delay introduced by the satellite links.

2.1.1.2 Centralized scheduling and resource allocation process

The basic characteristics of this option, which is depicted in Figure 2.2, are the following:

- The communication between the GESs and the NCC is carried out over a satellite link.
- Scheduling process and resource allocation process are both performed in the NCC leading to a centralized architecture.

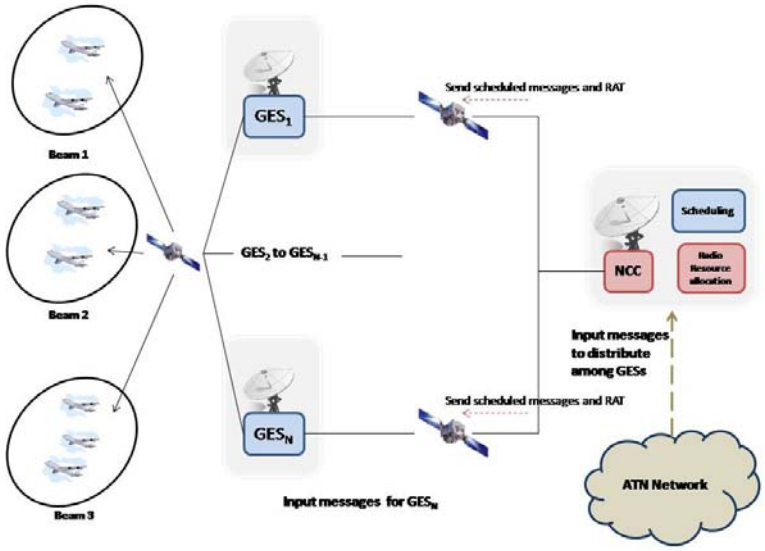

Figure 2.2: Satellite based centralized architecture

Therefore the process for sending information to the AESs is as follows:

- NCC receives messages from the ATN and performs the radio resource allocation process and the scheduling.
- The NCC sends the scheduled messages and the RATs to the GESs that retransmit it to the corresponding AESs by using the assigned resources from the NCC.

Again we can do delay estimation for sending a packet, which result as follows:

$$d(s) = t_{SCH} + (t_a + t_{NCC,GES}) + (t_a + t_{GES,AES}) \tag{2.2}$$

Where the terms $t_a + t_{x,y}$ stand for the transmission time of a packet plus the delay of the link from x to y. As we are assuming all links are satellite based, this options leads to a minimum end-to-end delay of:

$$d(s) = 2(t_a + 0.25s) + t_{SCH}$$

Hence there is always 0.5 seconds delay because of the satellite links.

2.1.2 Terrestrial Based Wide Area Network (TERRBASED-WAN) Architecture

2.1.2.1 Distributed scheduling and resource allocation process

Under this design we assume the same architecture as in subsection 2.1.1.1; however the GESs-NCC path considered is terrestrial. Proposed architecture can be seen in Figure 2.3.

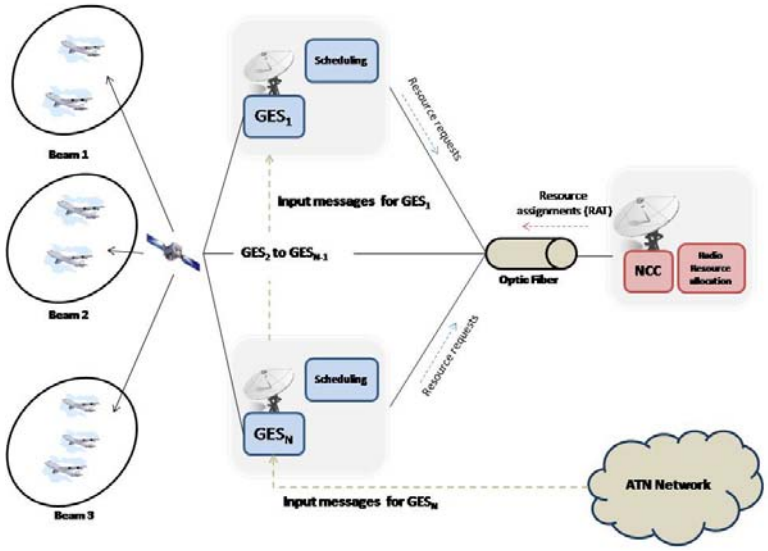

Figure 2.3: Terrestrial based distributed architecture

The top-level process to send the information is the same than in the mentioned section, however delays can be highly reduced because of the use of terrestrial links. Now the total delay can be simplified to:

$$d(s) = max\{t_{SCH}, t_{GES,NCC} + t_{NCC,GES}\} + t_a + t_{GES,AES} = \quad (2.3)$$

$$= t_a + t_{SCH} + t_{GES,AES}$$

Where the term $t_{GES,NCC} + t_{NCC,GES}$ has been neglected since in a terrestrial link these delays are considerably small compared with the rest of the delays. Considering $t_{GES,AES}$ equal to 0.25 seconds we get $d(s) = t_a + t_{SCH} + 0.25s$. **Hence the delay introduced because of satellite links is 0.25 seconds.**

2.1.2.2 Centralized scheduling and resource allocation process

Under this design we assume the same architecture as in section 2.1.1.2; however the GESs-NCC path considered is terrestrial. Proposed architecture is shown in Figure 2.4.

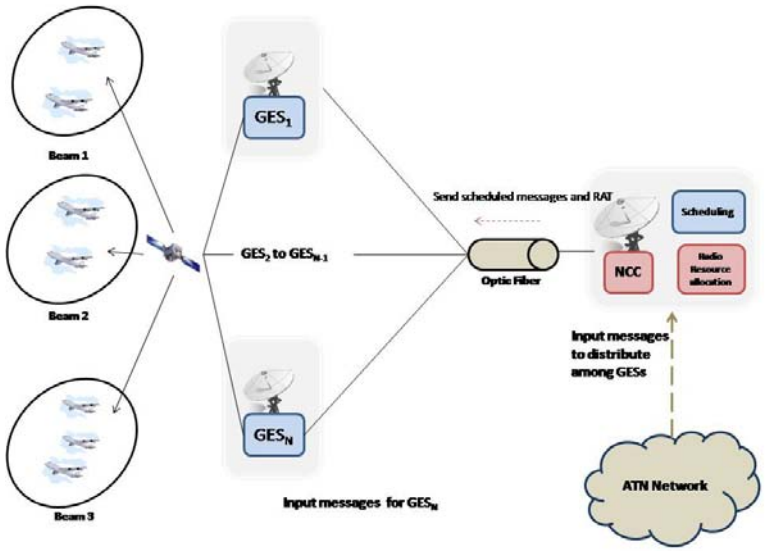

Figure 2.4: Terrestrial based centralized architecture

The top-level process is the same than in the mentioned section, however delays can be highly reduced because of the use of terrestrial links. Now the end-to-end delay can be simplified to:

$$d(s) = t_{SCH} + (t_a + t_{NCC,GES}) + (t_a + t_{GES,AES}) = \tag{2.4}$$

$$= t_{SCH} + t_a + t_{GES,AES}$$

Where the term and $t_a + t_{NCC,GES}$ have been neglected since in terrestrial links these delays are considerably small compared with the rest of delays. Considering $t_{GES,AES}$ equal to 0.25 seconds we get $d(s) = t_{SCH} + t_a + t_{GES;AES}$. **Hence the delay introduced by the satellite links is just 0.25 seconds.**

2.2 MAC-level Architecture

In this section we specify at MAC level the blocks that form each of the architectures, the centralized and distributed architectures, whether based on satellite or terrestrial links.

2.2.1 MAC-level architecture for distributed system level architectures

The MAC-level scheme for both distributed architectures can be seen here below in Figure 2.5.

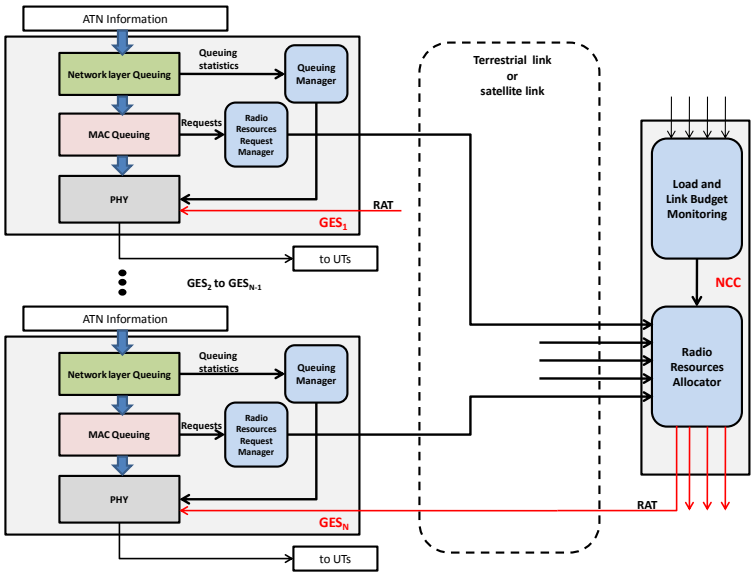

Figure 2.5: MAC level architecture for distributed option

A detailed scheme of how queuing is performed in the three different levels, Network, MAC and PHY can be seen in Figure 2.6 here after:

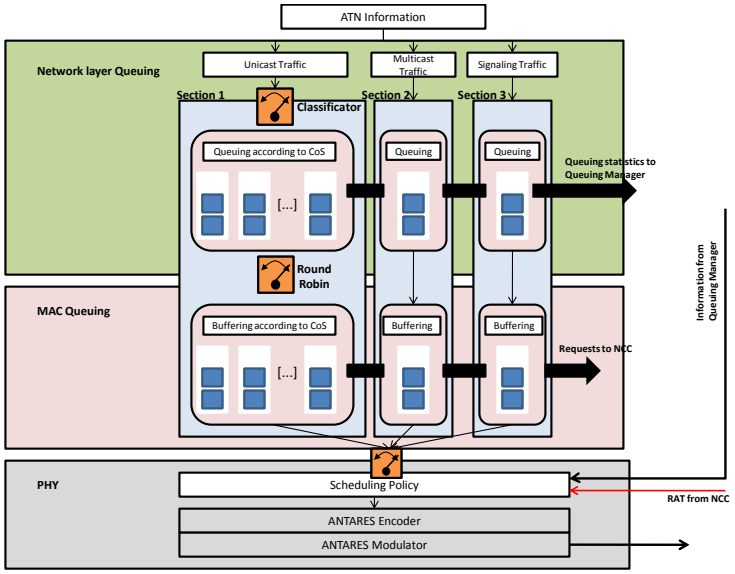

Figure 2.6: Detailed scheme of queuing performance

In the list below the entities belonging to the GES and its functions are specified:

- Incoming traffic is divided in three sections, one for unicast traffic, one for multicast traffic and another one for signaling traffic. Regarding to unicast section, traffic is divided into eight queues; one per the CoS specified in Table 1.7 and then buffered also into eight different buffers before the scheduler polls them. In multicast and signaling section just one queue and buffer is used.
- The Queuing Manager gathers information from the queues and communicates this information to the scheduler in order to "adapt" the scheduling policy.
- The Radio Resource Request Manager extracts information from the buffers within each section and based on that sends requests to the NCC Radio Resource Allocator.
- The scheduler polls the messages from the different sections and from the different buffers within each section by following a scheduling policy. The scheduling policy can be adaptive and vary in function of the information send by the Radio Resource Allocator in the NCC or the Queuing Manager in the GES.
- The ANTARES Encoder/Modulator shapes the signal with the correct MODCOD indicated by the Radio Resource Allocator in order to send it to the AESs.

In the list here below the entities belonging to the NCC and its functions are specified:

- The Load and Link Budget Monitoring block gathers information in order to indicate to the Radio Resource Allocator information regarding to Adaptive Coding and Modulation (ACM).
- The Radio Resource Allocator receives the resource requests from the Radio Resource Requests Manager in each of the GESs of the system and receives information from the Load and Link Budget Monitoring block. Then performs an algorithm to assign the different carriers and timeslots to all GESs in a fair way and communicate it through the RAT to each GESs. This RAT is received by GESs at the PHY level.

Note that communication between the NCC and the GES can be done either by a satellite or a terrestrial link leading to different delays for the same architecture.

2.2.2 MAC-level architecture for centralized system level architectures

The MAC-level scheme for both centralized architectures can be seen here below in Figure 2.7. The queuing scheme is the same seen in Figure 2.6 with the only difference that after scheduling information is sent to each GES where it is modulated and encoded to send to the UTs in the AESs.

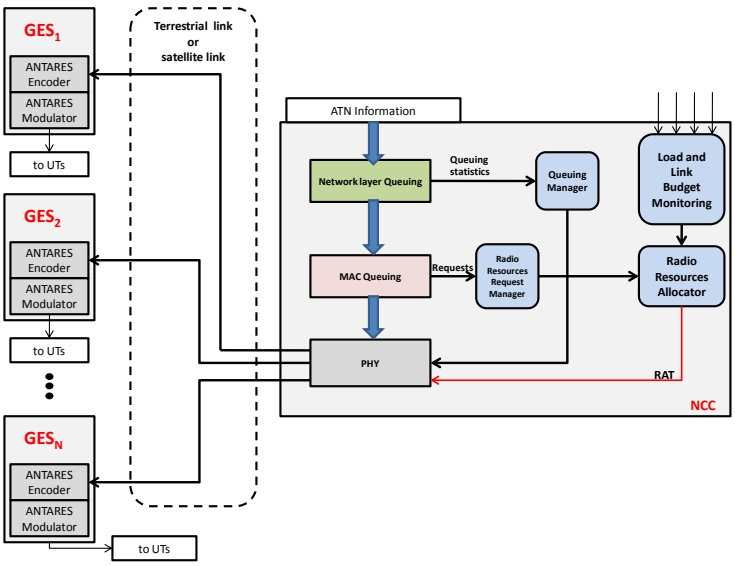

Figure 2.7: MAC level architecture for centralized option

In the list here below the entities belonging to the GES and its functions are specified:

- The ANTARES Encoder/Modulator receives scheduled messages from the NCC ready to encapsulate them with the right MODCOD and send it to the AESs.

In the list here below are specified the entities belonging to the NCC and its functions:

- Incoming traffic from GESs is divided in three sections, one for unicast traffic, one for multicast traffic and another one for signaling traffic. Regarding to unicast section, traffic is divided into eight queues; one per the CoS specified in Table 1.7 and then buffered also into eight different buffers before the scheduler polls them. In multicast and signaling sections just one queue and buffer are used.
- The Queuing Manager gathers information from the queues and communicates this information to the scheduler in order to "adapt" the scheduling policy.
- The Load and Link Budget Monitoring block gathers information in order to indicate to the Radio Resource Allocator information regarding to ACM.
- The Radio Resource Requests Manager extracts information from the buffers within each section and based on that sends requests to the Radio Resource Allocator.
- The Radio Resource Allocator receives the resource requests from the Radio Resource Requests Manager in the NCC and receives information from the Load and Link Budget Monitoring block. Then performs an algorithm to assign the different carriers and timeslots to all GESs in a fair way and communicate it through the RAT to each GESs.
- The scheduler polls the messages from the different sections and from the different buffers within each section by following a scheduling policy and then distributes the scheduled messages to the corresponding GESs. The scheduling policy can be adaptive and vary in function of the RAT send by the Radio Resource Allocator or the Queuing Manager. Polled messages are sent to the GES ANTARES Encapsulator/Modulator.

Note again that the link between the NCC and the GESs can either be over satellite or terrestrial.

Conclusions and delay estimation results on architecture design can be seen in Chapter 6 section 6.1.1.

2.3 MF-TDMA SF Design

The chosen option for the MAC in the ANTARES forward link is Multi Frequency Time Division Multiple Access (MF-TDMA). Under this scheme GESs are placed into a two-dimensional, frequency and time, space in order to meet their resources request. Resource requests are obtained from section 1.2.5. MF-TDMA allows a lot of possibilities in terms of bandwidth and timeslots configuration. Two basic options are possible, MF-TDMA structure with the timeslot duration (T_S) fixed or structure with the T_S optimized.

2.3.1 General MF-TDMA SF structure

The MF-TDMA Super Frame (SF) is divided into N_f frames of C carriers sharing all the bandwidth, where each of the frames has a different carrier bandwidth to meet different Service Level Agreements (SLAs). In the ANTARES traffic case just one frame will be used since all GESs have the same SLA. Within each frame timeslots are organized in a way that GES using the same MODCOD are placed together in areas. This is done for reducing the amount of signaling information. Each SF has a T_{SF} duration.

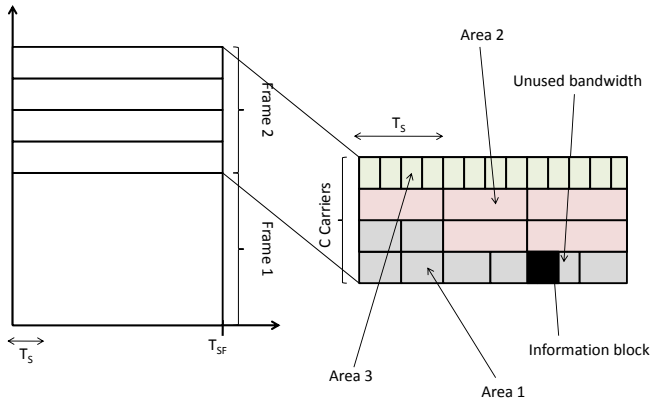

Figure 2.8: General MF-TDMA SF structure

One important issue in the MF-TDMA SF is the timeslot duration. As a first approach it could seem that a good design is to set the timeslot duration, T_S, to lowest MODCOD transmitting rate, so GESs with higher transmitting rates would transmit more than one information block in one timeslot. However it can be easily seen that some of the bandwidth of the timeslot could be unused depending on the assigned MODCOD to the GES, which leads to a loss of efficiency in the system. For this reason we present to options for the MF-TDMA SF resource allocation, one with a fixed timeslot structure and a second

one that optimizes the duration of the timeslot in order to improve the efficiency of the system.

In Table 2.1 are summarized the supposed parameters for the ANTARES MF-TDMA SF configuration taking into account the characteristics of the traffic.

Parameter	Value
T_{SF}	1s
N_f	1
C (number of carriers of 200kHz)	71
T_S (timeslot for fixed structure)	46ms

Table 2.1: MF-TDMA SF parameters

In Table 2.2 is calculated the transmission time of one frame, t_a, for each of the MODCODS, taking into account the following values specified in Table 1.2, BW, B_{guard}, OV L1/L2, N bits used in each modulation, BS, α and the coderate r. The formula applied is as follows:

$$\frac{1}{t_a} = \frac{BW \cdot N}{(1+B_{guard})\cdot(1+\alpha)\cdot(1+OV\ L1/L2)} \cdot \frac{1}{r} \cdot \frac{1}{BS}$$

It is also calculated in Table 2.2 the transmitted blocks, K, per timeslot for each MODCOD (only for the fixed timeslot structure). This value is calculated by applying:

$$K = \left\lfloor \frac{T_S}{t_a} \right\rfloor$$

Note that if K is not an integer number, the down rounding means not all the timeslot is used to transmit which leads to the loss of efficiency mentioned above.

MODCOD	t_a for 4096 bit frame	t_a for 8192 bit frame	K per T_S
(1) QPSK 1/3	46ms	92ms	1
(2) QPSK 1/2	31ms	62ms	1
(3) QPSK 2/3	23ms	46ms	1
(4) 8PSK 1/2	20.7ms	41.4ms	2
(5) 8PSK 2/3	15.5ms	31ms	2
(6) 16APSK 2/3	11.6ms	23ms	3

Table 2.2: Transmission time, t_a for each MODCOD

The parameters of the MF-TDMA SF in Table 2.1 have been deduced from the following information:

- T_{SF} is set to the RAT update time which is 1 second.
- N_f is set to 1 since all GES are expected to have the SLA. Hence there is no need for having different carrier bandwidths.
- For the fixed structure T_S is set to 46ms the lowest MODCOD transmission rate. GESs with higher transmission rate will be able to transmit more than one information block in one timeslot, e.g. MODCOD 6 can transmit 3 information blocks in one timeslot.
- The number of carriers C is calculated to cope $\overline{R_{b,GES}}$ traffic demand with any of the QPSK modes. (Note that for the chosen T_S all QPSK modes transmit just one information block per timeslot). This value is extracted from the RRM requirements for the ANTARES system specified in Table 1.6.

2.3.2 Fixed T_S MF-TDMA

Under this structure we assume the timeslots of each of the areas are fixed to a value. Then the problem lies in allocating the GESs in an efficient way to satisfy its demands. The Dynamic Bandwidth Allocation (DBA) algorithm for the fixed timeslot structure is as shown in equation (2.5):

$$\begin{aligned} &\underset{\{x_{i,j}\}}{max} \prod_{i,j}(x_{i,j}\cdot K_i)^{p_{i,j}} \\ &\qquad s.t. \qquad \sum_{i,j} x_{i,j} \leq P \\ &\qquad\qquad \left\lceil \frac{m_{i,j}}{K_i} \right\rceil \leq x_{i,j} \leq \left\lceil \frac{d_{i,j}}{K_i} \right\rceil \end{aligned} \tag{2.5}$$

Where P is the total number of timeslots in the frame, $x_{i,j}$ stands for the number of timeslots assigned to GES i with request j and $p_{i,j}$ stands for the priority of GES i with request j (this value should be one in our case since all GESs have the same priority). Besides $d_{i,j}$ and $m_{i,j}$ stands for the demanded and minimum guaranteed blocks and K_i the number of blocks a GES transmit in one timeslot which depends on the MODCOD used. It is demonstrated that this problem is analytically solvable using the Karush Kuhn Tucker (KKT) conditions which impose the following solutions (when $p_{i,j}$=1, $\forall i, j$ as it is the case).

$$x_i = \begin{cases} \frac{1}{\lambda}, & \frac{m_{i,j}}{K_i} \leq \frac{1}{\lambda} \leq \frac{d_{i,j}}{K_i} \\ \frac{m_{i,j}}{K_i}, & \frac{1}{\lambda} \leq \frac{m_{i,j}}{K_i} \\ \frac{d_{i,j}}{K_i}, & \frac{1}{\lambda} \geq \frac{d_{i,j}}{K_i} \end{cases} \tag{2.6}$$

Where λ is a positive value such that $\sum_{i,j} x_{i,j} = P$. Note that to impose the real solution with an scalar number of timeslots we must down round the results and redistribute the sparing resources to users. Although this is an easy-computing

solution and allows sending more than one information block per timeslot, it is not a completely optimal solution since some of the bandwidth in the timeslot could remain unused as it can be seen in Figure 2.8. This happens because the transmission time of an information block for each of the MODCOD does not need to be multiple of the T_S time. [16, 17]

2.3.3 Dynamic T_S MF-TDMA

Under this structure we suppose the timeslots for each of the areas are optimized in order to maximize the GESs resource allocation. Thus the problem lies in finding the most suitable T_S for each of the areas of the frame and allocating the GESs requests in an efficient way to satisfy its demand. The DBA algorithm for the optimization of the timeslot structure is as shown in equation (2.7).

$$\begin{aligned} \max_{T_s, x_{i,j}} & \prod_{i,j} \left(x_{i,j} \cdot \left\lfloor \frac{T_s}{t_a(i)} \right\rfloor \right)^{p_{i,j}} \\ s.t. \quad & \sum_{i,j} x_{i,j} \leq C \cdot \left\lfloor \frac{T_{SF}}{T_S} \right\rfloor \\ & 0 \leq x_{i,j} \leq \left\lceil \frac{d_{i,j}}{\left\lfloor \frac{T_S}{t_a(i)} \right\rfloor} \right\rceil \\ & T_{min} \leq T_S \leq T_{max} \end{aligned} \tag{2.7}$$

Where $t_a(i)$ is the duration of transmitting an information block by GES i which depends on the used MODCOD. Note that the total number of timeslots P has been substituted by $C \cdot \left\lfloor \frac{T_{SF}}{T_S} \right\rfloor$ and the number of blocks, K_i, a GES transmit in one timeslot has been substituted by $\frac{T_s}{t_a(i)}$. Besides we do not consider a minimum guaranteed resources to GES i. Again $p_{i,j}$ can be considered equal to 1 since all GESs have the same transmitting priority. This non-convex optimization problem can be solved knowing that departing from a feasible value of T_S and increasing it can only reduce its objective value unless a multiple value of some of the $t_a(i)$ is reached. This mean we can solve the problem by finding the $t_a(i)$ multiples inside the range [Tmin,Tmax] optimizing the $x_{i,j}$ resource for each of the values using (2.6) and getting the best $\{T_S, x_{i,j}\}$ pair of values.[16, 17]

2.3.4 Figures of Merit for the MF-TDMA SF performance

In order to compare the obtained results the following figures of merit are used, Bandwidth Occupation (BO) and Transported Capacity (TC):

$$BO = \frac{\sum_{i=1}^{N_{GES}} x_{i,j} \cdot K_i \cdot t_a(i)}{C \cdot T_{SF}} \tag{2.8}$$

$$TC = \frac{\sum_{i=1}^{N_{GES}} x_{i,j} \cdot K_i}{ASD_{REF}} \tag{2.9}$$

Where ASD_{REF}, or reference Aggregated System Demand corresponds to the maximum possible transported capacity obtained when using the most efficient bitrate (16APSK 2/3). The figure of merit BO can be seen as the amount of data sent in the MF-TDMA SF with respect to the amount of data that can be sent. TC can be seen as the capacity in blocks with respect to the maximum achievable capacity in blocks by using the most efficient MODCOD.

Graphics with regard to these figures of merit and graphics with the mean of resources demand over the allocated resources in function of the requested bitrate for the fixed T_S and dynamic T_S algorithms are provided in section 6.1.2. Also in the mentioned section are taken conclusions on the results.[16, 17]

Chapter 3

Analysis of the Erasure Channel and Proposed Solution

3.1 Introduction to LL-FEC

3.1.1 LL-FEC concept

Forward Error Correction (FEC) solutions above the physical layer are proposed any time it is necessary to overcome the losses resilient to physical layer FEC mechanisms (and link layer retransmission schemes, if any). The concept is as follows. At the receiver side, each packet is considered by the link layers either completely received or completely lost usually based on a CRC (Cyclic Redundancy Check). This way, it can be considered as if there is a virtual erasure channel. Different upper layer FEC solutions are available in several specifications for different applications. Current standards include solutions that are partly integrated in the application layer above the Network level, then referred to as Application Layer FEC (AL-FEC), or in the link layer (LL) below the Network level, then referred to as Link Layer FEC (LL-FEC) which will be the case under study.

3.1.2 From Information Theory

In digital communications the transmitter sends one out of a finite set of codewords and the receiver would like to know which codeword has been transmitted. A general scheme of an end to end communication system can be seen just in Figure 3.1.

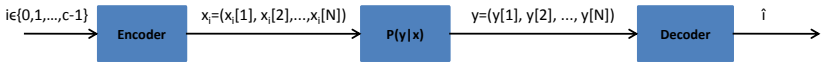

Figure 3.1: End to end communications system

The input and output, $x[m]$ and $y[m]$, respectively lie in a finite set which are called the input and output alphabets, $x \in X$ and $y \in Y$. The Binary Erasure Channel (BEC) has a binary input $x = 0, 1$, and a ternary output, $y = 0, 1, e$, where e denotes the erasure. The transition probabilities, $p(j|i)\ |_{j\in Y, i\in X}$, are depicted in Figure 3.2. As we can see the bits cannot be flipped as in the Binary Symmetric Channel (BSC), but can be lost or erased.

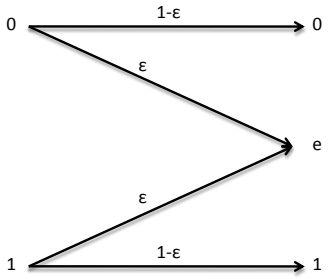

Figure 3.2: Probability transitions of the BEC

We can calculate the maximum capacity of the BEC channel as follows:

$$C = max_{p(x)} I(X;Y) = max_{p(x)} H(Y) - H(\varepsilon)$$

Letting E be the event Y=e and using the expansion:

$$H(Y) = H(Y,E) = H(E) + H(Y|E)$$

And letting p(x=1)=π, we have:

$$H(Y) = ((1-\pi)\cdot(1-\varepsilon), \varepsilon, \pi(1-\varepsilon) = H(\varepsilon) + (1-\varepsilon)H(\pi)$$

Hence:

$$C = max_{p(x)} H(Y) - H(\varepsilon) = max_{\pi}(1-\varepsilon)H(\pi) + H(\varepsilon) - H(\varepsilon) =$$

$$= max_{\pi}(1-\varepsilon)H(\pi) = 1-\varepsilon$$

This maximum is achieved when $\pi = 1/2$. Intuitively we can see that as an epsilon proportion of the bits are lost in the channel (the erased ones), we can only recover up to one minus epsilon bits, hence the capacity is one minus epsilon.[20]

3.2 Justification of the LL-FEC use in ANTARES

3.2.1 Link Layer channel vs Physical Layer Channel

As it is mentioned in the introduction, FEC can be used at different levels, normally at the physical layer, link layer or application layer. The use of FEC at a certain level does not exclude to use it at another level since its purposes are different. Therefore in this section we identify what type of errors LL-FEC codes can deal with in front of physical layer-FEC (PHY-FEC). In further subsections within this section we analyze whether in any of the ANTARES scenarios is given a situation for the LL-FEC use.

So PHY-FEC is intended for correcting errors at bit level produced within a physical layer frame:

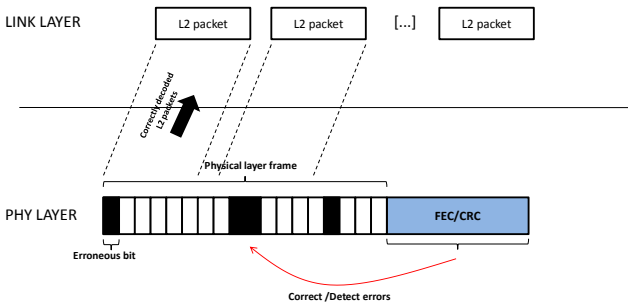

Figure 3.3: PHY-FEC correcting/detecting errors idea

Those errors can be produced by fast/medium term variations of the channels such it can be Rayleigh or Rice effects. However it is possible that under certain conditions a channel produced the effect shown in Figure 3.4, where we obtain a burst of erroneous bits so as several LL packets are lost.

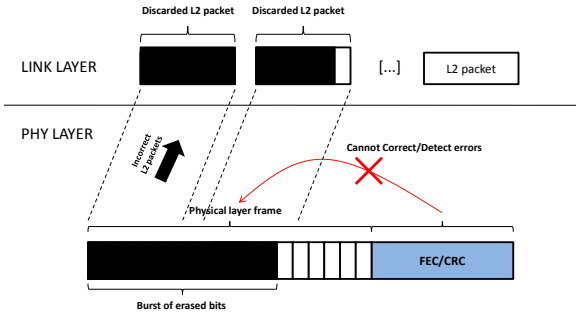

Figure 3.4: Burst erasure scenario

Such burst of erroneous bits makes the PHY-FEC/CRC correction or detection useless and those frames would be simply discarded by the decoder. To overcome this problem FEC is used at link layer level as follows:

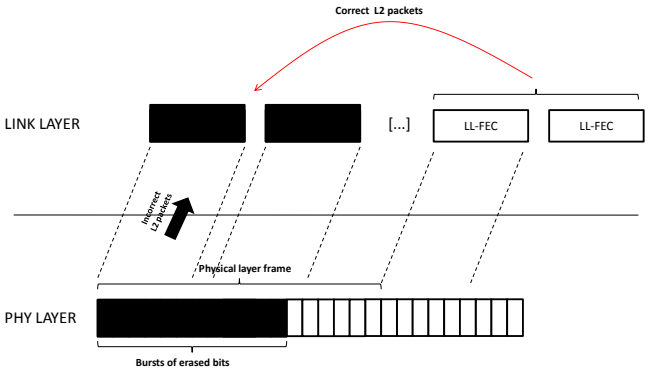

Figure 3.5: LL-FEC idea

Where the fact that each of the FEC packets are calculated from different L2 packets makes possible to correct the burst of erasures. The specific way this is done is explained in subsection 3.5.3. Hence **if we demonstrate the ANTARES aeronautical channel behaves as an erasure channel, the use of LL-FEC** to correct errors **is almost straightforward**. The only drawback for the LL-FEC is the delay it introduces which must be under the ANTARES QoS requirements specified in Table 1.7. The purpose of the following subsections is:

- Analyze if the ANTARES aeronautical channel behaves as a burst erasure channel and under which cases.

- Characterize these cases in order to design properly the LL-FEC codes to use.

3.2.2 Aeronautical Erasure Channel Models

In this section we analyze two potential link layer erasure aeronautical channel models, one for commercial aviation and another one for helicopters. The erasures for each scenario are generated as follows:

- For commercial aviation erasures can be produced due to:
  - Other airplanes in the line of sight between the satellite and the airplane intending to receive the communication.
  - By the airplane itself when maneuvering.

For the first case no statistics have been found on the literature. For the second case it is demonstrated in the literature that it may so happen that maneuvers of the airplane make the elevation angle with the satellite negative. First order statistics are available on the literature, but not second order statistics.

- For the helicopter scenario erasures can be produced basically by two effects:
  - The blades of the helicopter when rotating over the antenna
  - When the helicopter is flying along a building located between the line of sight with the satellite.

3.2.2.1 Erasure Model for Commercial Aviation

In this section two cases of erasure channel models with airplanes are explained, in the first case the erasures are produced by an airplane blocking the satellite signal to another airplane and in the second case the erasures are produced because of the airplane itself.

Erasures produced by airplanes in the same line of sight with the satellite The first example of erasure channel model with airplanes is depicted in this section. Understanding the aeronautical channel as a mobile multiuser environment we find feasible that burst erasures could be produced by another airplane positioned in the same line of sight with the satellite during certain time as shown in Figure 3.6. Due to the fast increase of air traffic, the congestion in some aerial routes and airports this effect is reliable to happen in airplanes in en route phase and in airplanes maneuvering or landing. In Figure 3.7 we can see

an image of the aerial routes in a zone of Spain, extracted from the national air navigation service provider, AENA, and see how routes cross each other often.

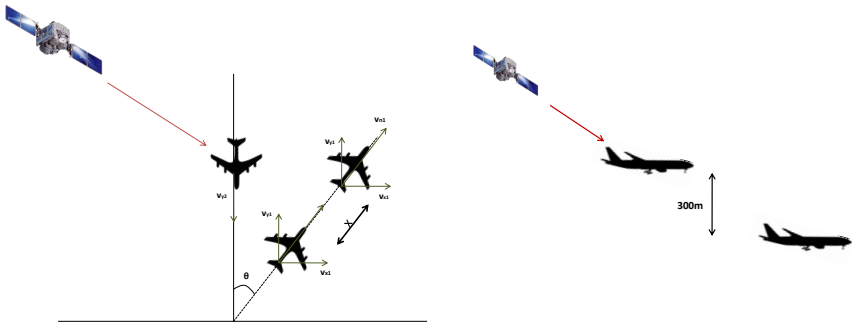

Figure 3.6: Burst erasure channel scenario

There are an infinite number of possibilities for the way an airplane could block the signal to another airplane, depending on the relative speed of both planes, the angle between them and the position of the satellite. The minimum regulated distance between the two airplanes traveling at different heights is 300m.

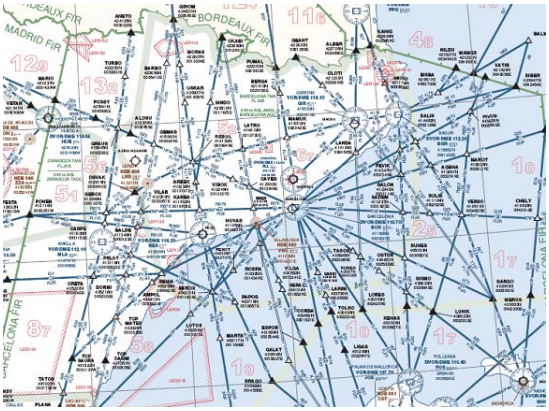

Figure 3.7: Catalonia aerial routes

As shown in Figure 3.6, we consider the distance the airplane travels with its line of sight with the satellite blocked by another airplane, x, as a function of θ. Airplanes can travel in the same or in different directions. In the same figure v_n indicates the nominal speed of the airplane, and v_x and v_y the x and y speed components respectively. All speeds are expressed in m/s.

Note that this is a very specific case since we are assuming both planes are

traveling without any change on its altitude flight, without maneuvering, at constant speed and no variations in the angle θ are produced.

Airplane	Length (m)	Landing/Maneuvering speed (m/s)	En route speed (m/s)
Airbus	60	83.3	245
Boeing	50	83.3	245
Regional	30	83.3	240
Cargo plane	20	83.3	240

Table 3.1: Standard airplane lengths

As it is shown in Table 3.1 we have considered some different speeds that lead to two different cases:

- One landing or maneuvering airplane at 83.3m/s is having the satellite signal blocked by an en route airplane at 240m/s-345m/s at a higher altitude.
- One en route airplane at 240m/s is having the satellite signal blocked by another en route airplane traveling higher and at a 245m/s.

We can find the relative speed, $v_{relative}$, in m/s between the two airplanes by doing:

$$v_{x1} = v_{n1} \cdot \sin(\theta), v_{y1} = v_{n1} \cdot \cos(\theta)$$

$$v_{x2} = 0, v_{y2} = v_{n2}$$

$$v_{relative} = \sqrt{(v_{y1} \pm v_{y2})^2 + (v_{x1} \pm v_{x2})^2}$$

Where the operator "+" is applied when the airplanes travel in the same direction and the operator "-" is applied when travel in opposite directions. Then we can find the time in seconds one airplane blocks the other one by:

$$t(s) = \frac{x(m)}{v(m/s)} = \frac{x}{\cos(\theta) \cdot v_{relative}} \tag{3.1}$$

Where x is the length of the aircraft. Signal blockage produces erasures consisting of bursts of packets. Minimum, mean and maximum values of duration of the erasure are given in Table 3.2. As a first approach, Table 3.3 and Table 3.4 below show packets lost in the worst, mean and best case erasure for different

Minimum duration	Mean duration	Maximum duration
0.04	0.3	1.15

Table 3.2: Minimum, mean and maximum values of erasure duration

bitrates (16kbps, 32kbps and 64kbps) and for different packet sizes (4096 and 8192 bits) in the forward downlink.

Packet Size	Packet Loss Case	R_b@16kbps	R_b@32kbps	R_b@64kbps
4096 bits	PL_{min}	1	1	1
	PL_{mean}	2	3	6
	PL_{max}	5	10	18

Table 3.3: Number of packets lost at each bitrate 4096 bit frame length

Packet Size	Packet Loss Case	R_b@16kbps	R_b@32kbps	R_b@64kbps
8192 bits	PL_{min}	1	1	1
	PL_{mean}	1	2	3
	PL_{max}	3	5	9

Table 3.4: Number of packets lost at each bitrate 8192 bit frame length

Erasures produced by the airplane itself when maneuvering View angle statistics to an Immarsat I-4 GEO satellite have been obtained in reference [12] from simulated flights using a database of 8 thousand scheduled flights. The Cumulative Density Function (CDF) of the elevation angle in the Terminal Maneuvering Area (TMA) showed the results in Figure 3.8.

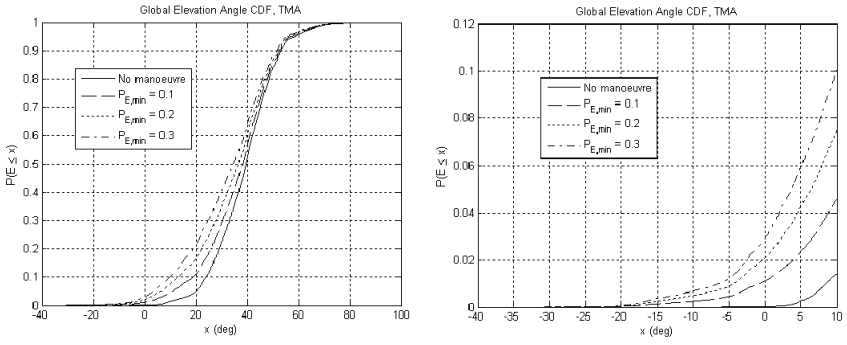

Figure 3.8: Elevation angle CDF and zoomed region respectively

The negative elevation angles show the case where the satellite view falls under the aircraft horizontal plane, these would cause blockage of the satellite signal.

As we can see in the figure in the TMA zone this can happen with an approximate probability of 2%. The $P_{E,min}$ values mean the probability of the aircraft to perform a maneuver resulting into a minimum elevation angle E_{min}. This E_{min} is computed from some pitch and roll angles of the airplane. $P_{E,min}$ is taken as a known parameter. As said, the literature does not provide second order statistics and we would need realistic data on maneuvering erasures to obtain how many packets would be erased.

3.2.2.2 Erasure Model for Helicopters

Another example of erasure channel model happens in an helicopter aeronautical scenario. Here, we can distinguish two cases:

- Erasures produced by the helicopter blades when rotating over the antenna.
- Erasures produced when the receiving signal could be blocked by a building in the Line of Sight (LOS) of the helicopter.

Both scenarios are illustrated in Figure 3.9. Standard helicopter blade measures have been chosen, 0.5 meters width and 6 meters length, while the revolution speed of the blades can be comprehend between 300-500 Revolutions Per Minute (RPM) and the speed of the helicopter can be comprehend between 150km/h and 250km/h.

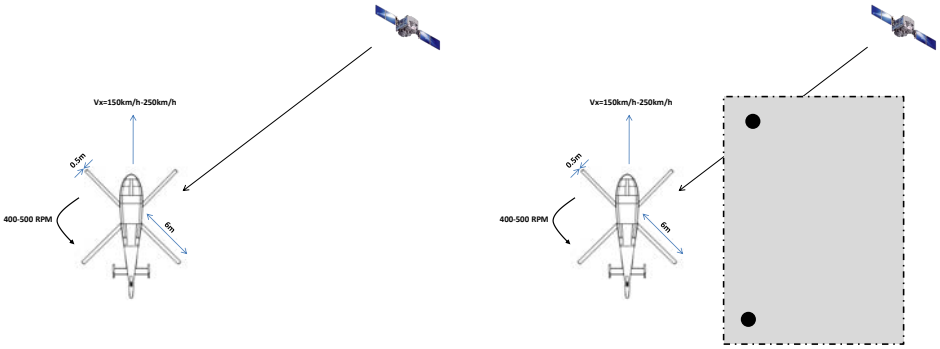

Figure 3.9: Helicopter scenarios, erasures produced because of the blades an erasures produced because of a building respectively

Erasures produced by the blades of the helicopters Under this scenario we assume the antenna is under the helicopter blades and the RPM of the blades can be between 300RPM and 500RPM. The amount of time in seconds the blades block the LOS signal is shown in Table 3.5.

RPM	Time (s)
300	0.160
400	0.0751
500	0.061

Table 3.5: Time in seconds the signal is blocked by helicopter blades

We can trace an imaginary route of a helicopter between two points without any buildings blocking the signal, then the erasures produced only depend on the RPM of the blades. In Figure 3.10 and Figure 3.11 we can observe how many packets per per blade blockage (each time a blade rotates over the antenna) would be erased for 4096 bit and 8192 bit packet length and for three different bitrates (16kbps, 32kbps and 64kbps).

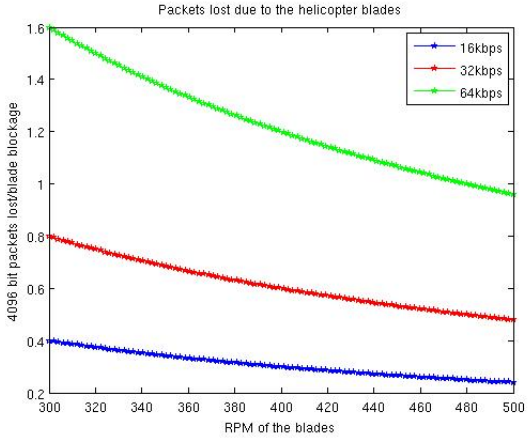

Figure 3.10: 4096 bit length packets lost in function of the RPM of the blades for different bitrates

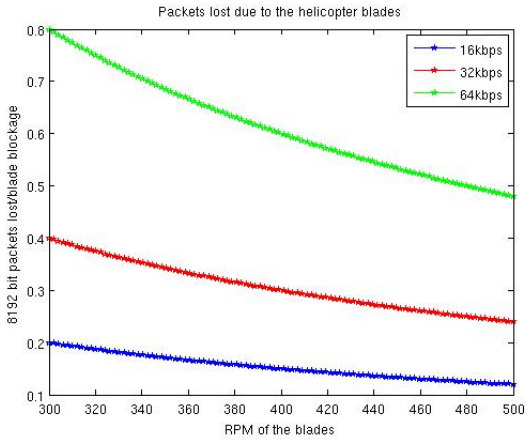

Figure 3.11: 8192 bit length packets lost in function of the RPM of the blades for different bitrates

For the worst case 4096 bit packet length at 64kbps bitrate we would need to recover up to 1.6 packets in each blockage. The erasure model in time at three different RPM can be seen here after, where '0' indicates an erasure is produced and '1' that the signal is received correctly.

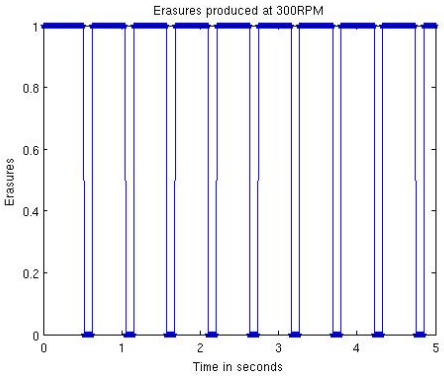

Figure 3.12: Erasure channel model in time produced at 300RPM

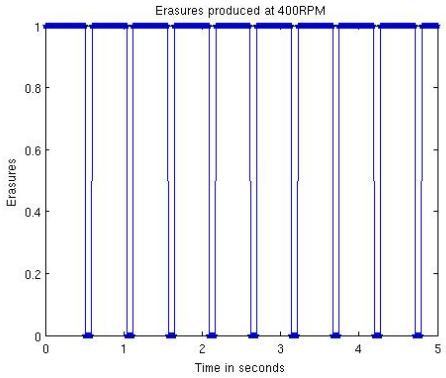

Figure 3.13: Erasure channel model in time produced at 400RPM

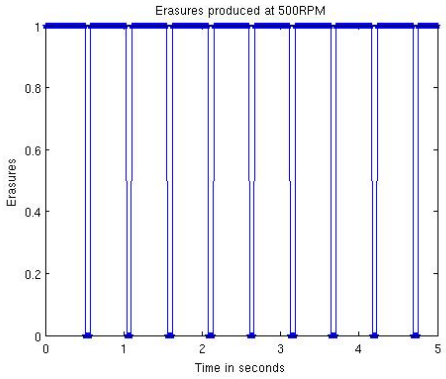

Figure 3.14: Erasure channel model in time produced at 500RPM

We can observe a periodic behavior of the erasures. As the RPM of the blades increase less packets ares lost in the erasures, but the erasures are produced more often. However not significant difference can be seen in the figures above since the differences are very small in time, but not in packets loss as we have seen in Figure 3.10 and Figure 3.11. The duty cycles of the erasures in each case are as shown in Table 3.6.

RPM	300	400	500
Duty Cycle	33%	26%	23%

Table 3.6: Duty cycle of the erasures

Since we have not considered any building blocking the satellite signal, this is a best case scenario, however it is possible that the helicopter travels through

high buildings that could block the satellite signal. This scenario is explained here after.

Erasures produced by buildings In this scenario we assume that the helicopter is crossing high buildings or skyscrapers that block the satellite signal during a certain amount of time. We can compute the time the signal is blocked considering different helicopter speeds and buildings widths. To model this scenario we have chosen a realistic route between two points in Madrid City using real building heights and widths. In Figure 3.15 is traced the route followed by the helicopter.

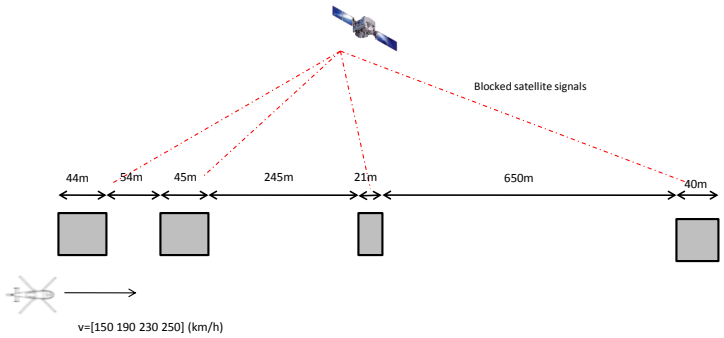

Figure 3.15: Helicopter route

Each time the helicopter crosses one of these building that block the satellite signal burst of packets are lost. In the figures below, 3.16 and 3.17, we can see the packets erased each time the helicopter crosses one of the 4 buildings (index of building from 1 to 4). Four different helicopter speeds are considered (150km/h, 190km/h, 230km/h and 250 km/h), three different bitrates (16kbps, 32kbps and 64kbps) and two different packet lengths (4096 bits and 8192 bits).

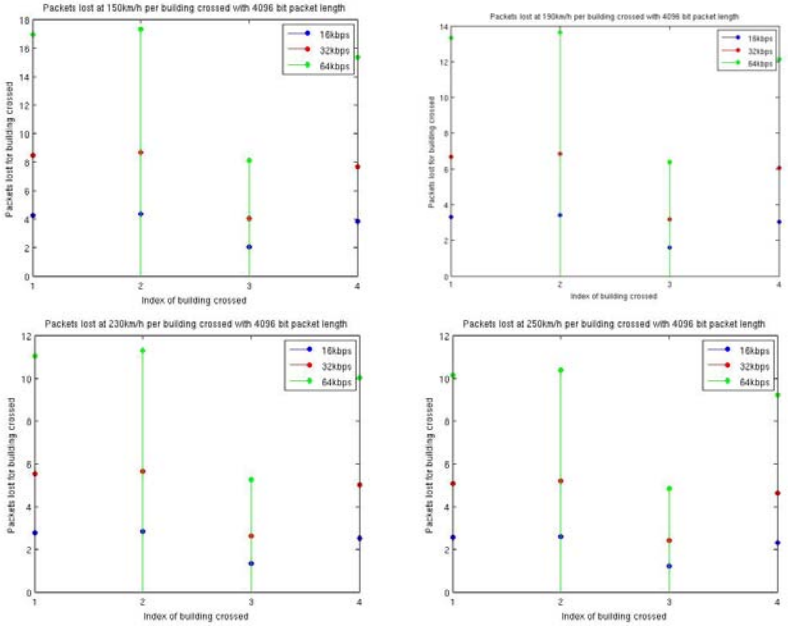

Figure 3.16: Packets lost at different speeds for the 4096 bit packet length

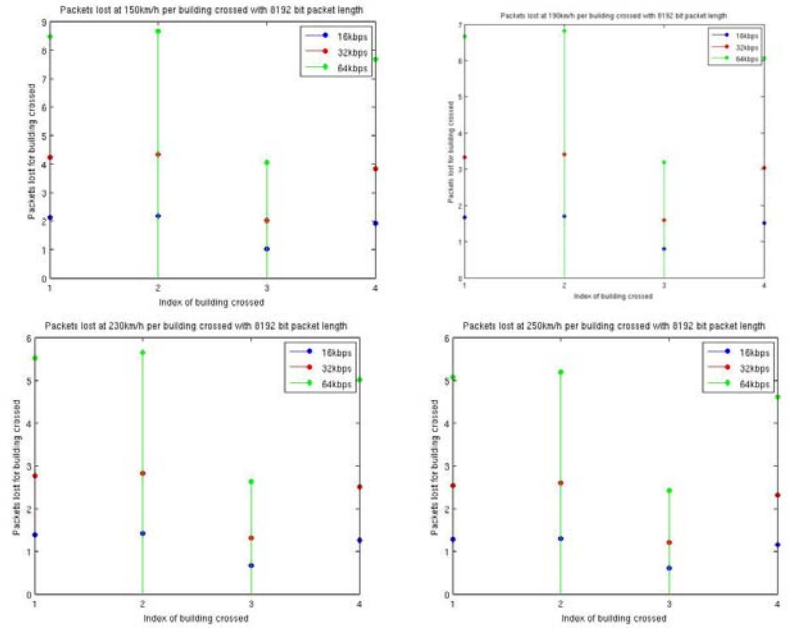

Figure 3.17: Packets lost at different speeds for the 8192 bit packet length

Observing the figures we can see that in the worst case, 4096 bit frame at 64kbps we need to recover up to 17 packets and for the 8192 bit frame at 64kbps up to 7.4 packets. The erasure model in time for the traced route at the four different speeds can be seen in Figure 3.18 , where '1' denotes no erasure and '0' that the helicopter is under an erasure.

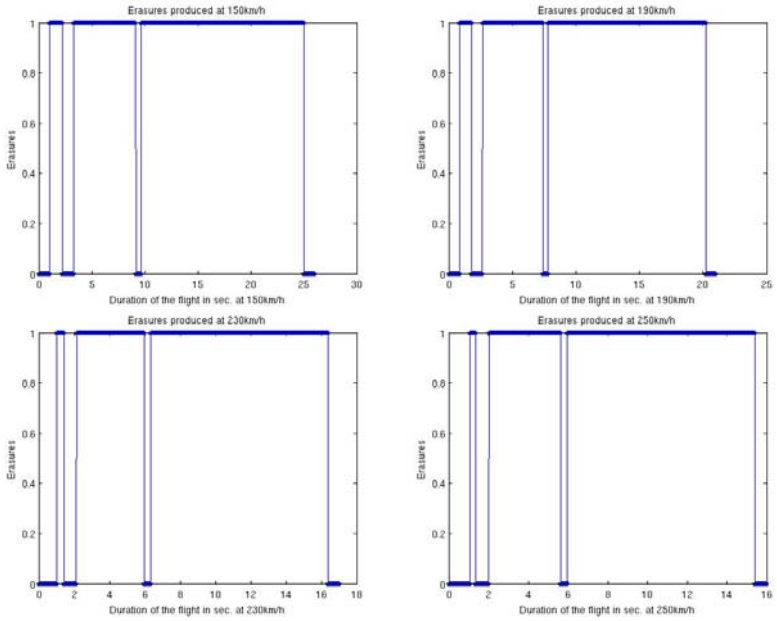

Figure 3.18: Erasure channel model in time at the four different speeds produced by the buildings

As we can see at higher speeds, the duration of the erasures produced by the buildings decrease, hence less packets are lost.

Statistical Characterization of the helicopter scenario Combining the erasure produced by the blades of the helicopter with the erasures produced by the buildings, we can build a general erasure model for a given flight route. We can express the total erasures produced in packets as follows:

$$E_T = E_{blades} + E_{buildings} \quad [packets]$$

Where E_{blades}can be expressed as:

$$E_{blades} = \frac{r}{bits/packet} \cdot t_h \Big]_{t=n \cdot t_r}$$

Where r is the bitrate of the signal in bits per seconds, t_h is the amount of time the antenna is blocked by the blade which depends on the RPM of the blades and its width, and t_r is the periodicity which what the blades overlap the antenna that depends on the distance of the antenna to the rotation center and the RPM of the blades. This term is only applied when there are no buildings blocking the LOS signal.

The term $E_{buildings}$ can be obtained by:

$$E_{buildings} = \sum_{i=1}^{K} \left(\frac{r}{bits/packet} \cdot \frac{l_i}{v} \right)$$

Where K are the number of buildings in the trajectory, l the length of these buildings and v the speed of the helicopter. We can apply this formula to our designed route. We will assume that lower speeds are achieved at lower RPM and high speeds at a higher RPM. Therefore 150km/h are achieved at 300RPM, 190km/h and 230km/h are achieved at 400RPM and 250km/h are achieved at 500RPM. This leads to the following erasure models in Figure 3.18 where '1' denotes no erasures and '0' that an erasure is produced.

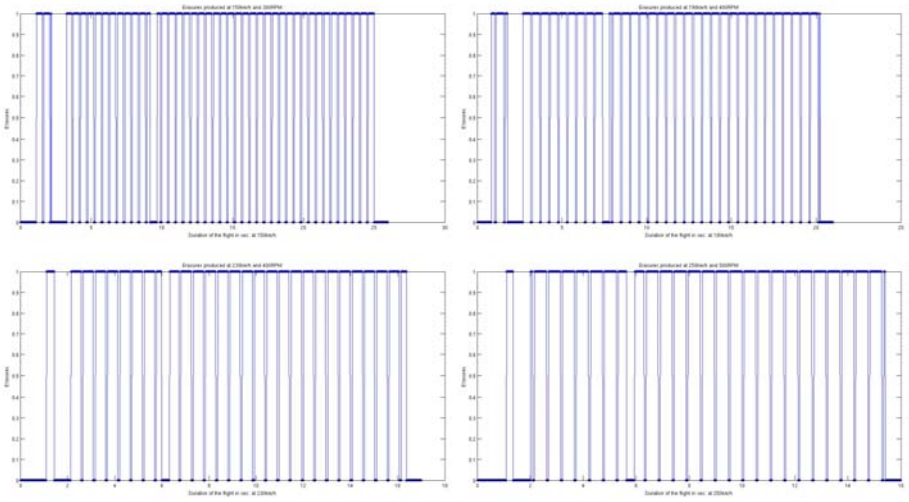

Figure 3.19: Erasure channel models due to blades and buildings in the flight route

Longer erasures belong to buildings, while shorter erasures belong to the blades of the helicopter. Thus we can obtain the first and second order statistics of our erasure channel model as it is shown in Figure 3.20 and Figure 3.21. In Figure 3.20 we can see an interesting result: that, the erasures probability remains approximately constant for the different speeds. The reason being that

although at higher RPM the erasures are produced more often, its duration is lower.

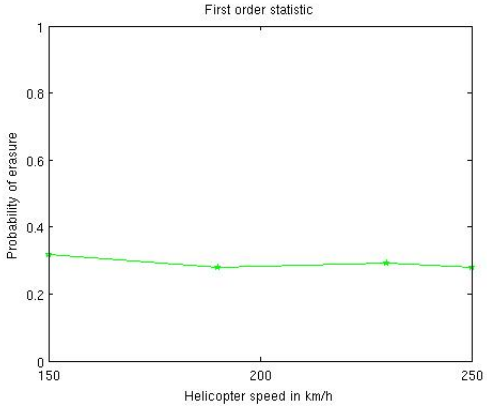

Figure 3.20: First order statistic: Probability of erasure

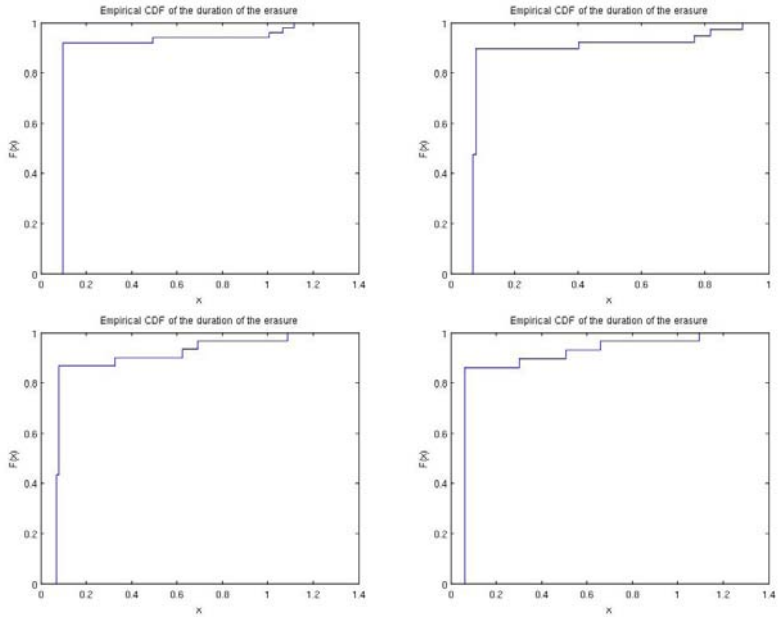

Figure 3.21: Second order statistics: CDF of the duration of the erasure for the 150km/h 300RPM, 190km/h 400RPM, 230km/h 400RPM and 250km/h 500RPM from top to bottom and right to left

In Figure 3.21 we can observe the probability that the duration of the erasure,

x, is lower than a certain level, F(x), this is the empirical CDF of the duration of the erasure. The figure shows that short erasures are produced almost always because while long erasure are barely produced. This happens because short erasures are produced because of the rotation of the blades which are a periodical effect while long erasure are produced by buildings which is a low-probability effect. This is also the reason why the graphic is so abrupt. No big differences are noticed between the different pairs of speeds/blade rotation.

3.3 Design Options

The basic idea in LL-FEC codes is that K blocks of source data are encoded at the transmission to produce N blocks of encoded data, such code is called an *(N,K)* code. An *(N,K)* code is able to correct up to N-K losses in a group of N encoded blocks. Several codes exist for this purpose, here below we list some of them together with a brief description and we give performance results on real applications for each of them.

3.3.1 Reed Solomon (RS) Codes

The basic characteristic of RS codes is that they are MDS codes. Despite of its simplicity and attractiveness RS codes have some disadvantages; the encoding/decoding complexity grows up exponentially with the codeword size. To keep this complexity manageable several restrictions to the codeword length must be imposed [3]. RS codes have been adopted as the standard codes for the first DVB generation. Simulation in reference [6] for a typical Rayleigh channel and in [9] for a burst noise channel shows that RS standalone codes are outperformed by both Raptor and LDPC codes respectively. However this result is not directly extrapolable to the ANTARES case because the channel it is not demonstrated to be an erasure+noise channel.

3.3.2 RS+Channel Interleaver

This solution is proposed to mitigate the fact that the encoding/decoding complexity of RS codes with long codewords is unmanageable. It is shown in [4] that for a pure long burst erasure channel without added noise the optimal solution is using block interleaved RS codes, moreover this optimality does only depend on the length of the block interleaver. The basic idea scheme is shown in Figure 3.22.

Several comparisons on the long burst erasure channel are carried out in this reference with the following summarized results:

- For a fixed N and K, the efficiency can be made as close to one as desired by simply increasing the interleaving length sufficiently.

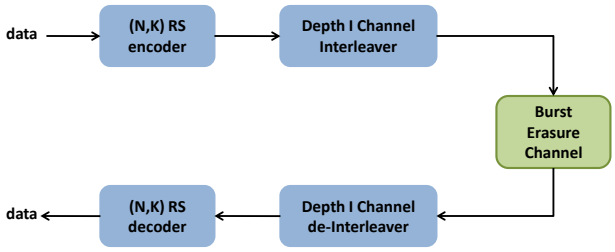

Figure 3.22: Basic idea of channel interleaved RS codes

- Very short RS codes are less than 1% inefficient at many lengths of practical interest.
- In channels modeled as erasure+noise (not our assumed case), RS interleaved codes are outperformed by LDPC codes.

3.3.3 Low Density Parity Check (LDPC) codes

LDPC are linear error correcting codes, although they are not MDS codes permit the use of longer codewords lengths than in RS with linear complexity increasing, providing much better performance. If well designed LDPC codes can be asymptotically (in N) MDS and can provide protection to long burst erasures if interleaved [3]. In references [8] and [9] it is proved that LDPC codes outperform RS and interleaved RS codes for burst erasures channels with added noise, however in pure burst erasure channels interleaved RS codes are the best option. As said before is still not clear if the ANTARES channel behaves as an erasure plus noise channel.

3.3.4 Raptor Codes

Raptor codes are a class of Fountain codes based on the Luby Transform. Compared with RS codes provide more flexibility, larger code dimensions, and lower decoding flexibility. Another advantage is that show linear time encoding/decoding with N, however Raptor codes are not MDS. Raptor codes have been lately introduced in the DVB standards [6]. Also in [6] a comparison between RS codes and Raptor codes is carried out. The study was made for a typical correlated Rayleigh channel using both Multi Protocol Encapsulation-Forward Error Correction (MPE-FEC) and MPE-Interburst FEC (MPE-IFEC) and for different modulations and codifications (MODCODs). The obtained results are summarized in Table 3.7.

	Raptor outperformance over RS	
MODCOD	MPE-FEC	MPE-IFEC
QPSK, 1/2	0.7dB	1.5dB
8PSK, 3/4	0.1dB	2.7dB

Table 3.7: Raptor over RS outperformance for a PER@1e-4 at v=100km/h

The results also showed that the best framework is MPE-IFEC which outperforms MPE-FEC for every MODCOD in RS and Raptor codes. The best overall result is the MPE-IFEC framework with Raptor codes.

3.3.5 Other Codes

Also more variants for packet level coding exists like Irregular Repeat and Accumulate (IRA), Generalized IRA (GeIRA), Tornado and Protograph codes shortly explained in [3].

3.4 Comparative Performance Analysis

Under this section is carried out a comparative between the LL-FEC design options depicted in 3.3 in order to choose the most suitable code for the LL-FEC implementation in ANTARES. To this aim we will compare the capacity of the codes to solve a burst of erasures (efficiency) and the difficulty to encode/decode the information of each of them (complexity in arithmetic operations).

3.4.1 Information from literature review

3.4.1.1 Efficiency

Regarding to code efficiency, in reference [4] a thorough study is presented to compare the efficiency in burst erasure channels of several types of codes. This efficiency is measured as the ratio of the maximum resolvable length burst, L_{max}, divided by *N-K*, being N the encoded bits and K the original source bits. *N-K* is the maximum resolvable erasure length indicated by the Singleton bound. For an RS code, interleaved or virtual interleaved the efficiency can be measured as:

$$\eta = \frac{(N-K)\cdot I\cdot m - m + 1}{(N-K)\cdot I\cdot m} = 1 - \frac{m-1}{m\cdot I\cdot N(1-r)} \tag{3.2}$$

Where r is the code rate *K/N*, m is the number of bits per symbol that in RS must accomplish that 2^m*-1=N* and I is the block interleaving depth. From the

expression above in the form $\eta = 1 - \mu$ it can be seen that $\mu = \frac{m-1}{m \cdot I \cdot N(1-r)}$ is the inefficiency of the code. For RS we can also define the total transmission length in bits of an interleaved code as:

$$Tranmission\,length = N \cdot I \cdot m \tag{3.3}$$

This is the total number of bits sent during all the interleaving. Note that if I is set to one we obtain the number of encoded bits of the code.

For LDPC codes finding L_{max} must be done by applying the algorithm in reference [7] to the parity check matrix of the LDPC codes. In this same reference and in [13] are provided results for different types of LDPC codes such as MacKay, extended Irregular Repeat and Accumulate (eIRA), array, Euclidean Geometry (EG) or Progressive Geometry (PG), under the burst erasure channel. These results will be used for an efficiency code comparison.

For Raptor codes efficiency no results in the literature have been found for the burst erasure channel.

3.4.1.2 Complexity

With reference to the complexity issue, it is well-known that the major drawback of RS codes is the exponential encoding and decoding complexity increase in terms of operations. The complexity on RS encoding/decoding can be expressed in terms of Galois Field Multiply and Accumulate (GFMAC) operations that the encoder/decoder performs for computing the RS codeword. Complexity performance is written in function of *N*, *K*, and *T=(N-K)/2*. For the encoding process just one option is possible, while for the decoding process several algorithms are available.

Encoding algorithm	Operations
-	*O(N·2T)*

Table 3.8: RS encoding algorithm complexity

Decoding algorithm	Operations
Syndrome computation	*O(N·2T)*
Berlekamp-Massey	*O(2T·T)*
Chien Search	*O(N·T)*
Forney Algorithm	*O(T·T/2)*

Table 3.9: RS decoding algorithm complexity

As we can see in Table 3.8 and 3.9, complexity is basically a function of *T=(N-K)/2*, i.e. a function of the redundancy added to the code. The lower the term T is, for a fixed N,the bigger is K; and lower is the encoding/decoding complexity.

For LDPC codes also exist several encoding/decoding algorithms, which in general require less arithmetic operation than in RS. Some of those algorithms are listed in Table 3.10 and in Table 3.11 and extracted from references [14] and [15].

Encoding algorithm	Operations
$LDPC_1$	*O(2q)*
$LDPC_2$	*O(2(K·(K-q)))*

Table 3.10: LDPC encoding algorithm complexity

Decoding Algorithm	Operations
Belief Propagation	*O(2·q)*
Extended Mini Sum	*O(q·log(q))*

Table 3.11: LDPC decoding algorithm complexity

Being q the number of codewords of the LDPC code, i.e. for an LDPC code (N,K), q is *N-1*.

With regard to Raptor codes the most common used encoding/ decoding algorithms are shown in Table 3.12 and in Table 3.13 and extracted from reference [5].

Encoding algorithm	Operations
-	*O(K)*

Table 3.12: Raptor encoding algorithm complexity

Decoding algorithm	Operations
-	*O(K)*

Table 3.13: Raptor decoding algorithm complexity

3.4.2 Simulations on comparative analysis

3.4.2.1 Efficiency simulations

To obtain comparison between LDPC, Raptor and RS codes regarding to the figure of merit of the efficiency, the codes listed in Table 3.14 have been used. Note that several types of LDPC codes have been simulated, as well as several $r=K/N$ ratios and lengths of the encoded block N in order to obtain a fair comparison with the RS codes. In order to show the results in a more understandable way,

in the graphics are plotted the inefficiencies of the codes in function of the total transmission length defined as in equation (3.2) and equation (3.3) respectively.

Code	(N,K)	L_{max} (bits)
LDPC MacKay	4095,3358	515
LDPC EG1	4095,3367	376
LDPC eIRA1	4095,3367	507
LDPC eIRA2	4550,4096	300
LDPC Array1	4095,3367	500
LDPC Array2	4550,4096	299
LDPC EG2	255,175	70
LDPC EG3	1023,781	157
LDPC PG1	273,191	75
LDPC PG2	1057,813	124
RS	255,85	Dependent on I
RS	255,127	Dependent on I
RS	15,5	Dependent on I
RS	15,7	Dependent on I

Table 3.14: Simulated codes

From the curves in Figure 3.23 we can extract the following conclusions:

- Note that for any interleaving length of an RS code, including non-interleaving (*I=1*) RS codes are less inefficient that any of the LDPC codes in the graphics. Hence in terms of solving errors **in burst erasure channels; RS codes are more efficient than LDPC codes**.
- We can observe that for a same interleaving length, a shorter RS code is less inefficient.
- Codes with lower coderate, r, are less inefficient for the same N length.

3.4.2.2 Complexity simulations

In order to show the encoding complexity two length N codes have been chosen, *N=15* and *N=255*. For each of these lengths the encoding complexity is plotted for the several algorithms available per code in function of *T=(N-K)/2*. This allows us to see the dependence of the complexity algorithm with T and K.

The following conclusions can be extracted from Figure 3.24:

- Raptor and LDPC encoding algorithms present the lowest encoding complexity. Besides, $LDPC_1$ algorithm presents a linear encoding complexity increase with N, which is desirable.

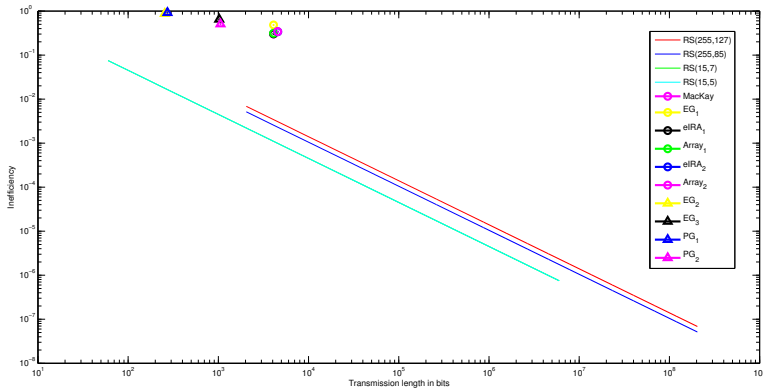

Figure 3.23: Inefficiency comparison vs total transmission lengths in bits for pure burst erasure channels

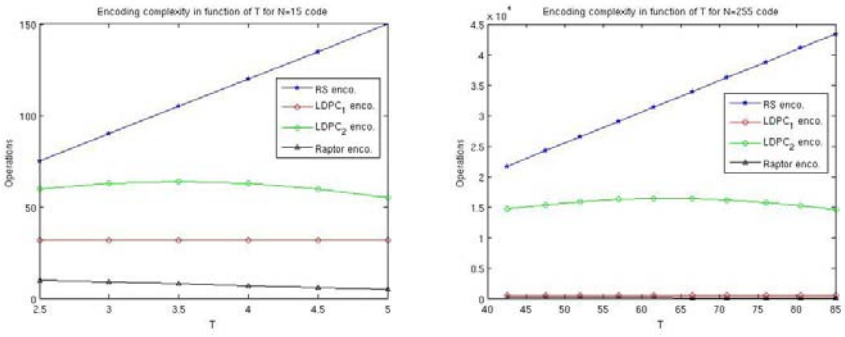

Figure 3.24: Encoding complexity at N=15 and N=255 respectively for several algorithms

- RS codes present two drawbacks when encoding, complexity increases when increasing T, i.e. the redundancy of the code. Complexity increases exponentially when increasing N as we can see when comparing both graphics, the increase in N from 15 to 255 is not the same increase in number of operations.

For the decoding complexity we will compare first the different available algorithms for the RS codes at *N=15* and *N=255* as a function of T. After that we will compare the least complex algorithms.

From Figure 3.25 the following conclusions can be observed:

- Forney algorithm presents the best performance, since its complexity increase with T is very slow and its complexity increase with N it is no as

abrupt as the other algorithms (although it is still exponential).

- Berlekamp Massey algorithm presents a similar performance to Forney algorithm however its complexity increase with T is higher.

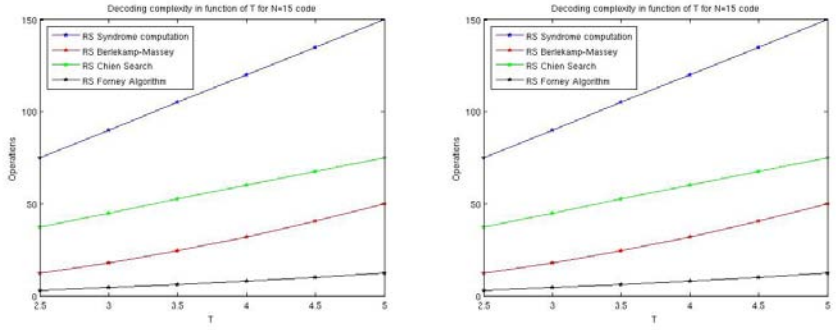

Figure 3.25: Decoding complexity for several RS algorithms at N=15 and N=255 respectively

So, in order to compare the RS decoding complexity with the complexity of other codes we will take as reference the Forney algorithm.

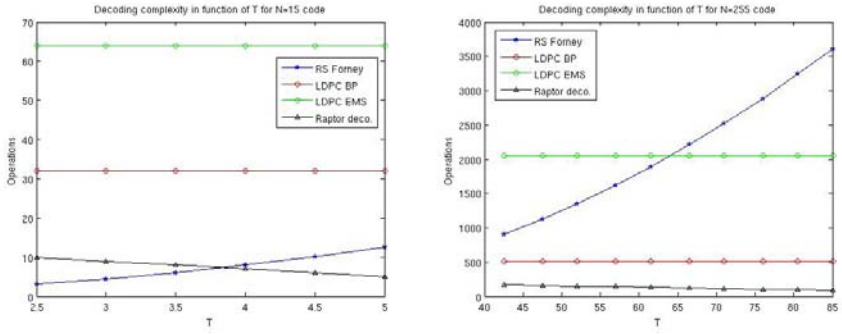

Figure 3.26: Decoding complexity at N=15 and N=255 for several algorithms

So a similar behavior to the encoding can be observed in Figure 3.26, specifically:

- LDPC BP and EMS algorithms present very low complexity and almost a linear increase with N and remain constant when only K varies.
- We can see that for short lengths of the code, Forney algorithm has very low decoding complexity (lower than LDPC codes).
- Raptor codes present low complexity.

3.4.3 Conclusions on code comparative

- In terms of efficiency, as it can be seen in Figure 3.23, RS codes, whether interleaved or not, clearly outperform the rest of the codes.
- From the complexity point of view LDPC are the best codes, however it is shown in Figure 3.25 that some some RS decoding algorithms such as Forney algorithm reduce considerably the number of operations to perform and in Figure 3.26 that for short lengths have a similar performance to LDPC algorithms.

Being known that, if the channel behaves as a pure erasure channel, we recommend using interleaved/virtual interleaved short length RS codes. The major drawback would only rely on the encoding complexity. Figure 3.27 helps to clear out this issue where we can see the RS decoding complexity for a short code (N=15) is very low while the major drawback relies on the encoding.

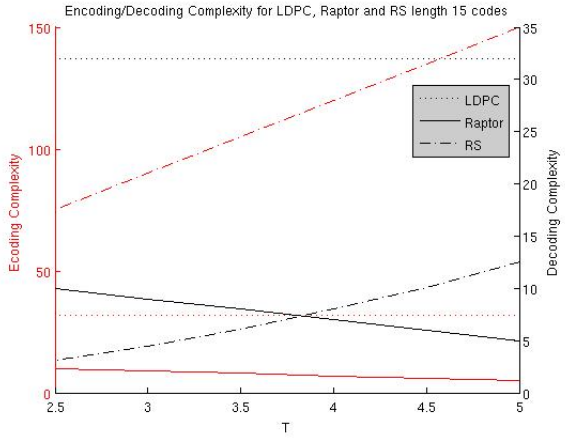

Figure 3.27: Encoding/Decoding comparison for short LDPC, Raptor and RS codes

However in Figure 3.28 we can see this drawback is compensated by much higher efficiency of the code, two order difference, for the range of total transmitted bits, from 1e3 to 1e4 depending on the delay-aware introduced. The region is marked with a red ellipse.

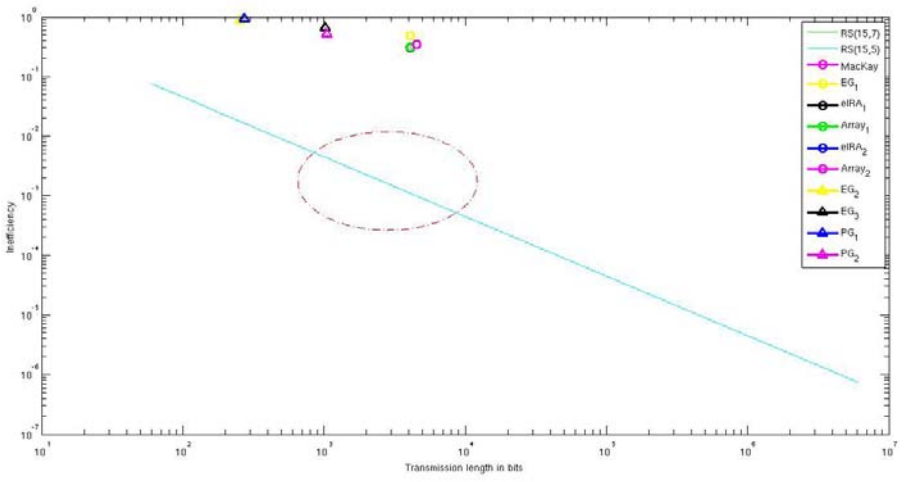

Figure 3.28: Inefficiency comparison for short RS codes

3.5 Code Choice and Performance results

3.5.1 Code Choice

From conclusions in section 3.4 our choice is to use RS codes using a delay-aware link-level packet interleaving. The reason is that Reed-Solomon codes belong to the class of Maximum Distance Separable (MDS) codes, i.e. they enable a receiver to recover the K source symbols from any set of K received symbols. Further, in order to increase the effectiveness of packet-level FEC, it is sensible to apply it across an interleaved group of packets, because in that way consecutive packets within the error burst are separated out. Effectiveness of this is also demonstrated in section 3.4. We propose the design of a delay-aware link layer packet interleaving design, i.e. the level of interleaving can be adapted so as LL-FEC can be applied with different depths across the different traffic types and/or QoS.

RS+ channel interleaver codes could perform better under the type of channels developed, however it would introduce even a higher delay that would not allow to meet the QoS requirements.

3.5.2 Discussion on the use of GSE

As it has been mentioned in subsection 1.2.3, GSE standard does not specify a fixed size for the link layer frames. According to the messages sizes in Table 1.9 and to the base band frame sizes, two suitable lengths could be 256 or 512 bytes including the GSE header in order to do not partition messages excessively.

Another issue regarding to the use of GSE is the number of errors the RS code will be able to correct. It is demonstrated that knowing where the erasures are located, i.e. using CRC, an RS code is able to correct $T = N - K$ erasures. However GSE standard specifies that CRC is only added at the last frame of a partitioned message in order to increase the encapsulation efficiency, hence the number of erasures we will be able to correct is $T = {}^{(N-K)}/_{2}$. Another commonly used standard in satellite communications is Multi Protocol Encapsulation (MPE) which specifies a 14 bytes header, a variable payload and a 4 bytes CRC in each frame. Therefore although MPE is less efficient encapsulating it allows to correct twice the number of errors than using GSE. As the ANTARES project specifies the use of GSE, all simulation have been carried out with this standard.

3.5.3 Simulator Construction

The Reed Solomon encoding process for a RS(N,K,T) code used in the simulations is as follows:

- A matrix consisting of two separated parts, the Application Data Table (ADT) and the Reed Solomon Data Table (RSDT) is created with the dimensions indicated in Figure 3.29. This is also the terminology used in the DVB standards. The number of columns of the ADT matrix is the number of input source symbols of the RS code, *N*. The number of columns of the RSDT matrix is the number of redundancy generated symbols, *T*. Each symbol is defined a group of m bits forming a codeword that must accomplish that:

$$N = 2^m - 1$$

- The ADT part of the matrix is column-wise filled with data from the upper layers, in our case different ATN messages as it can be seen in Figure 3.29. We start filling the matrix by the upper left corner to down, if the message does not fit in one column it is continued in the next column. If it is not possible to fill an entire number of messages the remaining space at the end of the matrix is filled with zeros.

- The RSDT part of the matrix contains information of the RS LL-FEC code, for each of the rows containing information of different messages, are generated T columns of parity information.

Once the entire matrix is filled the messages are extracted in the same order they arrived, starting by the upper left corner to down. The parity information in the RSDT is extracted last. An encapsulation process as the shown in Figure 1.4 is followed. For simulation purposes the BBH, Start of Frame and pilots are computed as an overhead of the 10%.

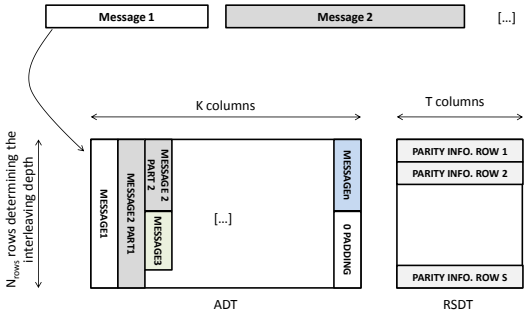

Figure 3.29: ADT and RSDT tables for the LL-FEC encoding

When physical layer frames are sent through the channel, they may be affected by erasures. In reception ADT part and RSDT part of the matrix, is filled again with the received. The idea is shown in Figure 3.30.

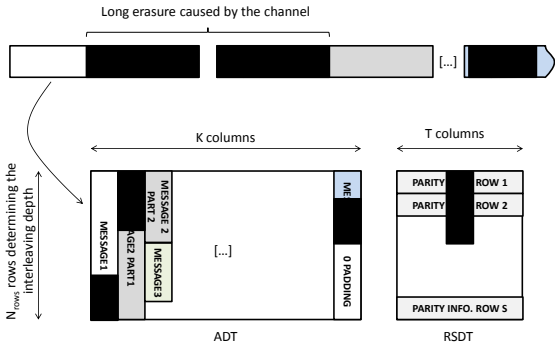

Figure 3.30: RS decoding scheme

Physical layer packets are de-encapsulated to obtain the link layer frames of 256 or 512 bytes, the GSE header is extracted and the information within the frame is plugged again together with the FEC sent in the ADT and RSDT tables in the same way it was done in transmission. For each row if less than T erasures are present we can correct the errors in the row. After the correction, the Frame Error Rate is calculated taking into account that information is column wise ordered. We consider that within a frame one erroneous received symbol corrupts the entire link layer frame. In the end:

$$FER = \frac{\#\ erroneus\ frames}{\#\ sent\ frames}$$

Then we express the results in terms of Correct Frame Rate (CFR), computed as:

$$CFR = 1 - FER$$

The LL-FEC delay-aware introduced t_{delay} is computed taking into account that the last of the FEC frames must be received to start decoding the RS, hence it is related with the size of the code, N, the depth of the table, N_{rows}, the number of bits per symbol m, OH (bits) the overhead in bits due to encapsulation (link layer and physical layer headers) and R_b the bitrate.

$$t_{delay} = \frac{m \cdot N \cdot N_{rows} + OH\,(bits)}{R_b}$$

In our case we will fix the delay-aware and N values to $t_{delay} \in \{0.68, 1.5\}$, $N \in \{15, 255\}$, and vary the number of rows, N_{rows}, of the table to match this parameters. Delay-aware have been set in order to satisfy the most stringent TD_{95} requirements of the messages 1.4s as shown in Table 1.7. There is a worst case the erasure is 1.15 seconds long, the delay for this case has been set to 1.5 seconds. Although in this case, for one CoS, the TD_{95} would not accomplished we assume this worst case is within the 5% of margin in TD_{95}.

Simulation results and conclusions are shown in section 6.2, also brief guidelines for LL-FEC design in ANTARES are included in Appendix B.

Chapter 4

Payload Dependent System Model

The study of different payload models is necessary for a further study of the co-channel interference in multibeam satellite systems. Each payload will lead to a different link budget computation and therefore to different interference levels. Three different types of payload models are studied here in, the conventional payload model, the flexible payload model and the beam-hopping payload model. Related with the ANTARES system, which is a multibeam scenario, this study can give us an idea of which payload is more suitable since satellite configuration has not been decided yet. It could also be possible that for the characteristics of the system all payloads had a similar behavior in terms of interference.

The conventional payload is used for the typical MF-TDM/MF-TDMA air interfaces using the classical frequency and time division, while the flexible payload is used in Non Orthogonal Frequency Reuse (NOFR) systems , where a ground cell can allocate a variable number of carriers depending on the traffic request, carriers can be re-used throughout the coverage without any restrictions. Beam-Hopping (BH) payload is used when the air interface is "beam-hopped", this means the total bandwidth is used in some specific beams during a time slot. Figure 4.1 shows the basic difference between the air interfaces. Different air interfaces in the different payloads will also affect on the further interference analysis.

All payload configurations will obviously depend on the designed frequency plan for the system, but explanations in here are done in a generalized way.

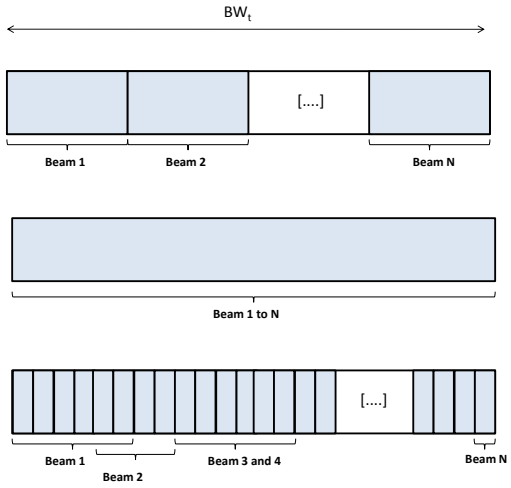

Figure 4.1: MF-TDM beam-hopped and NOFR air interfaces respectively

4.1 Conventional Payload Model

4.1.1 Payload Elements

The conventional payload elements for both forward (FWD) and return (RTN) links are referred in Table 4.1.

Forward Link	Return Link
Low Noise Amplifiers (LNAs)	LNAs
Down-Converters (DOCONs)	DOCONs
Input Demultiplexers (IDMUXES)	Input Multiplexers (IMUXES)
Linear Traveling Wave Tube Amplifiers (LTWTAs)	LTWTAs
Output Filters (OFLTRs)	OFLTRs

Table 4.1: Conventional payload elements

4.1.2 Antenna Design

In the conventional payload combined transmission and reception antennas are used in the satellite, with a Single Feed per Beam Network (SFBN) antenna configuration. The number of apertures on the antenna will depend on the beam configuration.

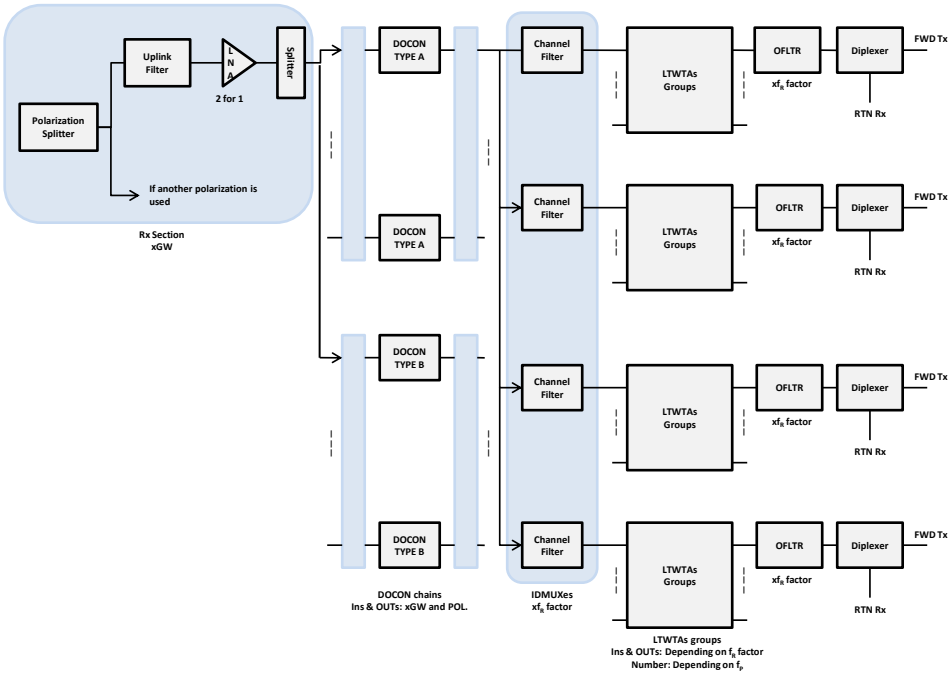

Figure 4.2: Conventional forward link payload

4.1.3 Payload Architecture

4.1.3.1 Forward Link Architecture

After uplink signal filtering of each polarization output, the antenna elements are connected to a 2 for 1 redundant LNA to amplify the signal introducing as less noise as possible. Depending on the frequency plan, f_P, more than one type of DOCON could be needed, so the splitter performs the action of sending the signal to the correct DOCON. Then the DOCONs down converts each of the frequency segments of each polarization FWD uplink to the frequency segments of the FWD downlink. Depending on the number of gateways and the number of polarizations the number of inputs and outputs for the DOCONs changes.

After the frequency down-conversion the IDMUXes separates the channels assigned to each user link beam, at least are needed as many IDMUXes as the frequency reuse factor, f_R factor. Groups of LTWTAs are used to provide the final amplification of the channels and OFLTRs are used to limit the intermodulation and harmonics high amplification effects. An scheme of this payload can be seen in Figure 4.2.

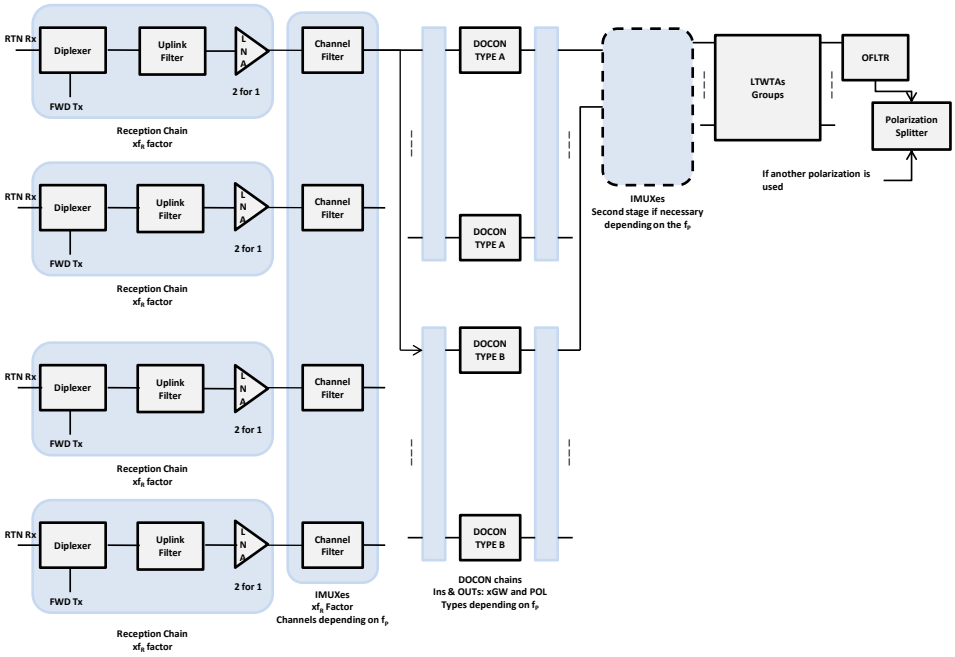

Figure 4.3: Conventional return link payload

4.1.3.2 Return Link Architecture

In the RTN link after uplink filtering, each output of the receive elements is connected to a 2 for 1 redundant LNA, then the IMUXes combine the channels in order to accomplish the frequency plan for the RTN downlink, as many IMUXes as the frequency reuse factor are needed. Then the DOCON down-converts the frequency RTN uplink segments into the RTN downlink frequency segments. Depending on the frequency plan the DOCONS chains needed could vary and a second stage of IMUXes could be needed. Also depending on the frequency plan more than one type of DOCON could be needed.

LTWTAs are used to high amplify several channels and OFLTRs are used to limit the effect of intermodulation in the adjacent channels and to limit the harmonics. At last the filters can be connected to two polarization transmit ports if needed. An scheme of this payload can be seen in Figure 4.3.

4.2 Flexible Payload Model

4.2.1 Payload Elements

The conventional payload elements for both forward FWD and return RTN links are referred in Table 4.2.

Forward Link	Return Link
LNAs	LNAs
DOCONs	DOCONs
Intermediate Frequency Filters (IFLTRs)	IFLTRs
On Board Processor (OBP)	Return Link OBP
Up-Converters (UPCONs)	UPCONs
Channel Filters (CFLTRs)	CFLTRs
Hybrid Matrix Power Amplifier (HMPAs)	LTWTAs
OFLTRs	OFLTRs

Table 4.2: Flexible Payload Elements

4.2.2 Antenna Design

In the flexible payload are used separated transmission/reception antennas with antenna Array Fed Reflector (AFR) configuration, so each beam is generated using a determinate number of elements of the array. As the feed horns are too smalls one antenna for the transmission and one antenna for the reception is needed. The main advantage of AFR is that the number of apertures can be reduced with respect to the SFBN configuration.

4.2.3 Payload Architecture

4.2.3.1 Forward Link Architecture

In the forward link the signal follows the next process, first each polarization output is low noise amplified by the LNA, then the DOCONS down-convert the received signals to the C-band frequency used by the OBP, the IFLTRs after the DOCONs limit the out of band spurious emissions.

The signals inputs into the OBP, which performs the following actions:

- Spectral isolation of the individual modulated user channels that compose each FDM multiplexed, multicarrier, gateway signal.
- Routing and steering of the complex samples that compose the uplink carriers signals received on FWD uplink to the destined FWD downlink

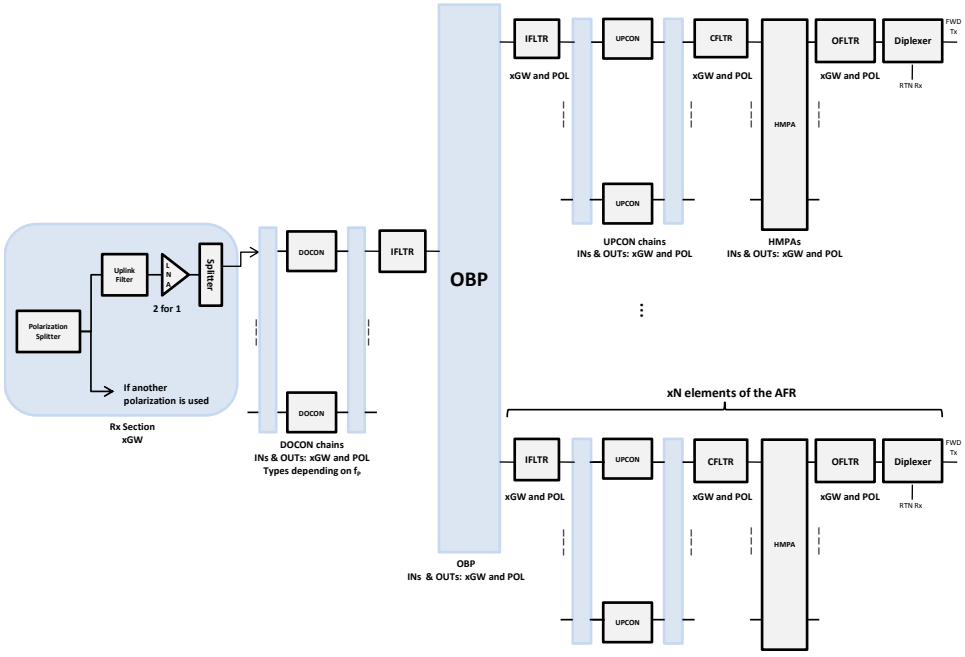

Figure 4.4: Flexible forward link payload

Digital Beam Forming Network (DBFN) in order to generate the subsequent FWD downlinks.

- Spatial filtering of the complex samples that compose the uplink carriers signals to generate the subsequent constituent beam signals to be applied to the antenna elements.
- Frequency synthesis of the spatially filtered element beam signals to generate the FDM multiplexed, multicarrier element signal to be applied to each of the antenna elements that compose the transmission antenna array.

The signals from the output of the OBP are then upconverted with the UPCONs to the downlink frequencies and channel filtered to limit the out of band spurious emissions with the CFLTRs. HMPAs composed of LTWTA are used to amplify the signals that feed the antenna elements and before are transmitted the signals are filtered to limit the noise in the receive frequency band and to limit the spurious emissions with the OFLTRs. An scheme of the FWD link flexible payload can be seen in Figure 4.4.

4.2.3.2 Return Link Architecture

In the return link the following process is performed, first the uplink output of each receive element is connected to a 2 for 1 LNA to low noise amplify, then this signal is down-converted through the DOCONs to get the C-band used by the return link OBP and filtered with IFLTRs to limit the out of band spurious emissions.

The OBP for the return link performs the following actions on the signal:

- Spectral isolation of the frequency segments that compose the FDM multiplexed, multicarrier, co-channel RTN uplink signal derived from the output of each of antenna elements.
- Spatial filtering of each spectrally isolated frequency sub-band to generate the corresponding constituent beam signals.
- Spectral isolation of the individual user or channel bands assigned to each RTN downlink beam.
- Routing and steering the complex samples that compose each individual user channel received on the RTN uplink to the RTN downlink.
- Frequency synthesis of the spatially filtered user beam to generate the FDM multiplexed multicarrier gateway signals.

The signal from the output of the OBP is up-converted with the UPCONs to get the RTN downlink frequency and CFLTRs are used to limit out of band spurious. In this case LTWTAs are used to amplify the full frequency band of one polarization and output filtered with OFLTRs and then ready to be sent to the antenna feed elements. An scheme of this payload can be seen in Figure 4.5.

4.3 Beam Hopping Payload Model

4.3.1 Payload Elements

The elements of the beam hopping payload for the FWD and RTN link are listed in Table 4.3.

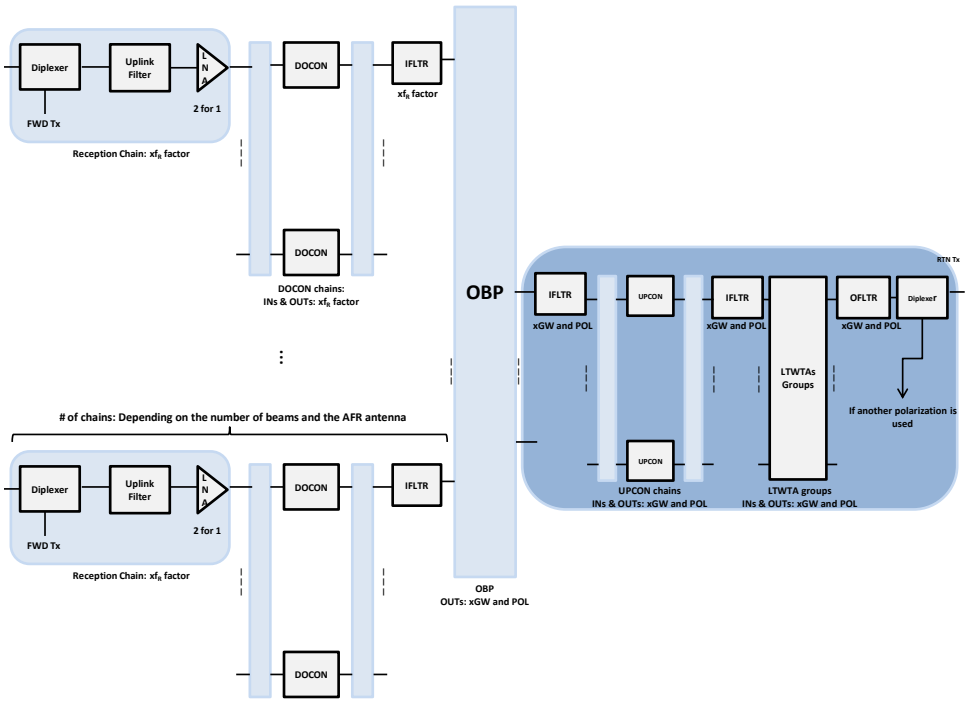

Figure 4.5: Flexible return link payload

Forward Link	Return Link
LNAs	LNAs
DOCONs	DOCONs
IFLTRs	IMUXes
OBP	
UPCONs	
CFLTRs	
HMPAs	LTWTAs
OFLTRs	OFLTRs

Table 4.3: Beam-hopping payload elements

4.3.2 Antenna Design

The antenna used in this payload is the same used in the conventional one, combined transmission and reception antennas are used in the satellite, with a SFBN antenna configuration using 4 apertures.

4.3.3 Payload Architecture

4.3.3.1 Forward Link Architecture

In the forward link the process is as follows, the signals goes through the 2 for 1 LNAs to amplify it, then is down-converted with the DOCONs to the OBP C-band and the IFLTRs limit the out of band spurious emissions.

In the OBP the following actions are performed:

- Spectral isolation of the individual, phase modulated carriers signals that constitute each FDM multiplexed, multicarrier gateway signal.
- Grouping the carriers received on the FWD uplink into FWD downlink sets.
- Frequency synthesis of the FWD downlink carrier sets to generate the sub-sequent FDM multiplexed, multicarrier signals. These synthesized multicarrier signals are identified as beam-hopping signals.
- Application of the beam hopping signals to the antenna elements.

The signal at the output of the OBP is upconverted with the UPCONs from the OBP C-band to the FWD downlink frequency, channel filtered and amplified with the HMPA matrix. At last before sent to the antenna feed elements is filtered to limit noise in the receive frequency and to limit harmonic distortion with OFLTRs. The scheme of the FWD link beam-hopping payload can be seen in Figure 4.6.

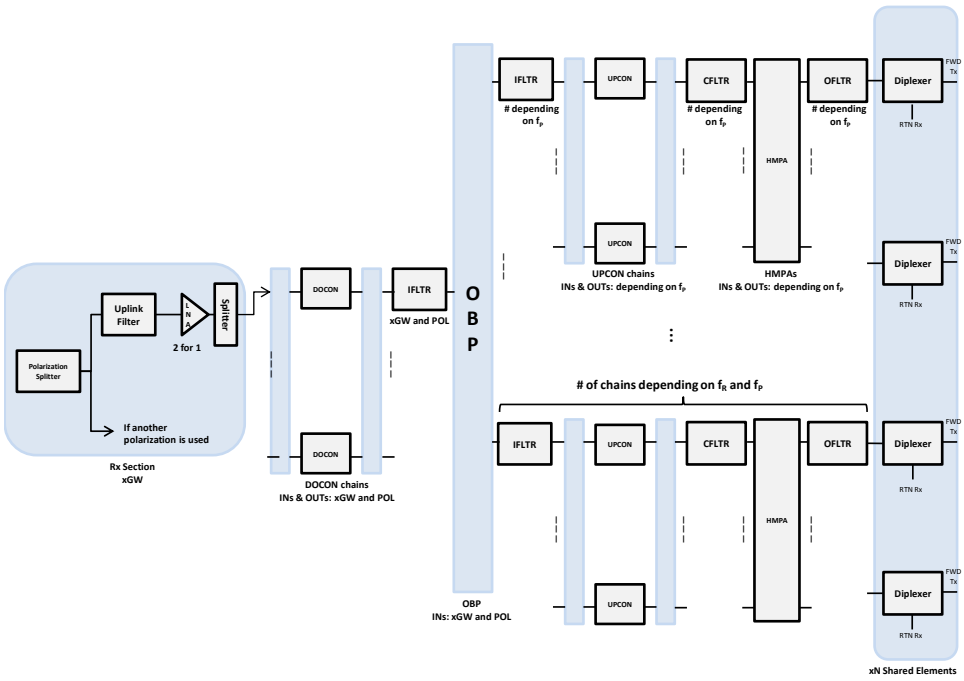

Figure 4.6: Beam-hopping forward link payload

4.3.3.2 Return Link Architecture

For the return link the process followed is the same than in the conventional payload in section 1.1 and the payload scheme can be seen in Figure 4.3.

Chapter 5

Analysis of co-Channel Interference

The purpose of this chapter is obtain analytic expressions for the co-channel interference at beam level for the forward downlink of satellite systems. To this aim is obtained the received signal in the form $\mathbf{y} = \mathbf{Hx} + \mathbf{n}$, where $\mathbf{H}$ is a matrix compound of the satellite antenna gains matrix $\mathbf{G}$, which depend on the angle θ defined in section A.1, and the rest of the link budgets contributions in matrix $\mathbf{A}$. To perform the analysis in a systematic way we will first analyze a two beam model to extract at the end a general expression for a variable number of beams. Considered geometric aspects, antenna models and link budget computations are extracted from Appendix A.

Besides, as we have seen in Chapter 4, the computation of the link budget depends on the payload model used, and this will affect to matrix $\mathbf{A}$. So for different payloads we will obtain different levels of interference. The notation used within this chapter for the system model definition is described here below:

- Vectors are set in bold lowercase letters.
- Matrix are set in bold uppercase letters.
- Subindex $(.)^T$ denotes the transpose.

5.1 Two beam model

Consider the following scenario, a satellite is transmitting information using a determinate number of antennas, *1* to *N*, to a determinate number of beams, *1* to *N*. Two of these beams are using the same frequency, hence because of the

antenna side lobes they interfere each other. The scenario is depicted in Figure 5.1.

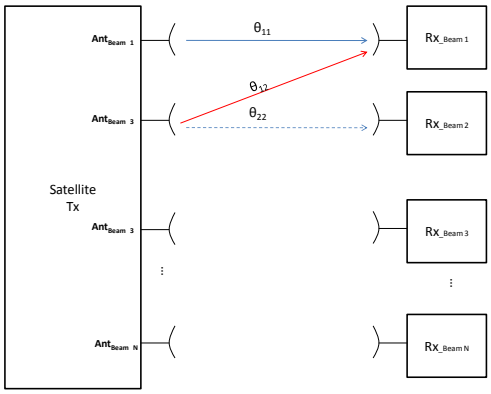

Figure 5.1: Forward downlink two interfering beam scenario

In this Figure 5.1 we can observe how the received power of the user in the beam of interest (continuous blue line) is a function of its angle θ_{11} towards the spot beam center and is getting and interference from another beam with which it forms an angle θ_{12} to its beam center. We could have considered the interfering beam as the one of interest so the effect would have been viceversa produced. Therefore we can model the system channel of this two beams, $\mathbf{H}$, as 2x2 matrix with a constant contribution part and a varying part due to the angles towards the beam center.

Let the symbols transmitted to user i inside the coverage of beam i, be defined as $\mathbf{x}_i = [x_{i1}, x_{i2}, ..., x_{iM}]^T \in \mathbb{C}^{M\times 1}$. Lets also define two matrixes $\mathbf{A} \in \mathbb{C}^{k\times k}$and $\mathbf{G} \in \mathbb{C}^{k\times k}$, with $k = 2$, where $\mathbf{A}$ comprehends all the gains and attenuation terms involved in the forward downlink link budget except for the satellite antenna gain defined in $\mathbf{G}$ which depends on the angle θ.

$$\mathbf{A} = \begin{pmatrix} \sqrt{\beta}_1 & 0 \\ 0 & \sqrt{\beta}_2 \end{pmatrix} \tag{5.1}$$

$$\mathbf{G} = \begin{pmatrix} g_{11} & g_{12} \\ g_{21} & g_{22} \end{pmatrix} \tag{5.2}$$

Where:

- $\beta_i = OBO_{hpa} \cdot L_{sat} \cdot L_{down} \cdot G_{gt}$ are the gain and losses terms that do not depend on the angle θ. This expression is extracted from subsection A.2.2.

- $g_{ij} := \sqrt{g(\theta_{ij})}$ is the square root of the gain, g, of the satellite transmitter antenna for beam j towards beam i being θ_{ij} is the angle that forms the receiver in beam i towards the spot beam center j as seen from the satellite.

So now we can compute the channel matrix $\mathbf{H} = \mathbf{AG} \in \mathbb{C}^{\mathbf{2\times 2}}$ which models the system:

$$\mathbf{H} = \begin{pmatrix} \sqrt{\beta_1}\sqrt{\mathrm{g}(\theta_{11})} & \sqrt{\beta_1}\sqrt{\mathrm{g}(\theta_{12})} \\ \sqrt{\beta_2}\sqrt{\mathrm{g}(\theta_{21})} & \sqrt{\beta_2}\sqrt{\mathrm{g}(\theta_{22})} \end{pmatrix} \tag{5.3}$$

Hence we can express the received signal $y(\theta)_i \in \mathbb{C}^{M\times 1}$ for a user in a beam i as desired and non-desired contributions as:

$$\mathbf{y}(\theta)_i = \sqrt{P_{sat}} \cdot h_{ii} \cdot \mathbf{x}_i + \Big(\sum_{j=1, j\neq i}^{j=2} \sqrt{P_{sat}} \cdot h_{ij}\mathbf{x}_j \Big) + \mathbf{n}_i \tag{5.4}$$

Where the term $\sqrt{P_{sat}} \cdot h_{ii} \cdot \mathbf{x}_i$ is our desired signal, the term $\sum_{j=1,j\neq i}^{j=2} \sqrt{P_{sat}} \cdot h_{ij}\mathbf{x}_j$ is the co-channel interference and the term $\mathbf{n}_i \in \mathbb{C}^{M\times 1}$ is a column vector of zero mean and complex circular noise with variance N introducing the thermal noise in the receiver.

Developing in equation (5.4) we get the following solutions for our two beams:

$$\mathbf{y}(\theta)_1 = \sqrt{P_{sat}} \cdot \sqrt{\beta}_1 \cdot \sqrt{g(\theta_{11})}\mathbf{x}_1 + \sqrt{P_{sat}} \cdot \sqrt{\beta_1} \cdot \sqrt{g(\theta_{12})}\mathbf{x}_2 + \mathbf{n_i}$$

$$\mathbf{y}(\theta)_2 = \sqrt{P_{sat}} \cdot \sqrt{\beta_2} \cdot \sqrt{g(\theta_{22})}\mathbf{x}_2 + \sqrt{P_{sat}} \cdot \sqrt{\beta_2} \cdot \sqrt{g(\theta_{21})}\mathbf{x}_1 + \mathbf{n_i}$$

Besides it is possible to extract the Signal to Interference plus Noise Ratio (SINR) expressions from equation (5.4) assuming the power of the transmitted symbols to user i is normalized, $E[|x_i|^2] = 1$.

$$SINR_i(\theta) = \frac{P_{sat} \cdot |h_{ii}|^2}{\sum_{j=1, j\neq i}^{j=2} (P_{sat} \cdot |h_{ij}|^2) + N_i} \tag{5.5}$$

Developing and substituting we get:

$$SINR_1(\theta) = \frac{P_{sat} \cdot \beta_1 \cdot g(\theta_{11})}{\beta_1 \cdot g(\theta_{12}) + N_1}$$

$$SINR_2(\theta) = \frac{P_{sat} \cdot \beta_2 \cdot g(\theta_{22})}{\beta_2 \cdot g(\theta_{21}) + N_2}$$

5.2 General model

For the general model we consider that the user in the beam of interest is being interfered by any number of beams comprehend between 1 and N-1. The scenario is depicted in Figure 5.2.

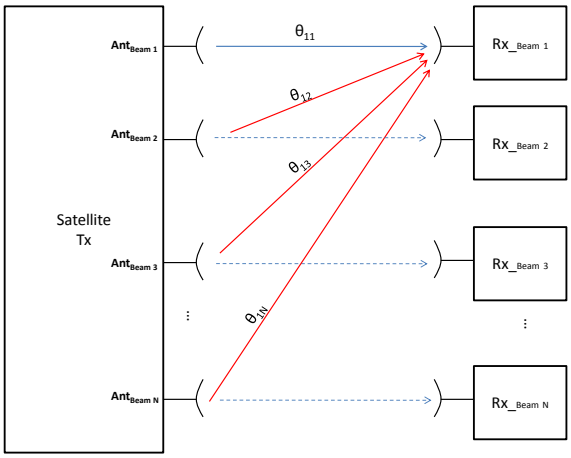

Figure 5.2: Forward downlink general interference scenario

Where we can see our beam of interest is being interfered by a general number of beams k which are using the same frequency. So now, matrix $\mathbf{A} \in \mathbb{C}^{\mathbf{k}\times\mathbf{k}}$ turns into:

$$\mathbf{A} = \begin{pmatrix} \sqrt{\beta_1} & 0 & \cdots & 0 \\ 0 & \sqrt{\beta_2} & \cdots & 0 \\ \vdots & \vdots & \ddots & \vdots \\ 0 & 0 & \cdots & \sqrt{\beta_k} \end{pmatrix} \tag{5.6}$$

Moreover matrix $\mathbf{G} \in \mathbb{C}^{\mathbf{k}\times\mathbf{k}}$ turns into:

$$\mathbf{G} = \begin{pmatrix} g_{11} & g_{12} & \cdots & g_{1k} \\ g_{21} & g_{22} & & g_{2k} \\ \vdots & \vdots & \ddots & \vdots \\ g_{k1} & g_{k2} & \cdots & g_{kk} \end{pmatrix} \tag{5.7}$$

Where as before:

- $\beta_i = OBO_{hpa} \cdot L_{sat} \cdot L_{down} \cdot G_{gt}$ are the gain and losses terms that do not depend on the angle θ.

- $g_{ij} := \sqrt{g(\theta_{ij})}$ is the square root of the gain, g, of the satellite transmitter antenna for beam j towards beam i being θ_{ij} is the angle that forms the receiver in beam i towards the spot beam center j as seen from the satellite.

And $\mathbf{H}$=$\mathbf{AG}$$\in \mathbb{C}^{k\times k}$ the matrix that models the system channel:

$$\mathbf{H} = \begin{pmatrix} \sqrt{\beta_1}\cdot\sqrt{g(\theta_{11})} & \sqrt{\beta_1}\cdot\sqrt{g(\theta_{12})} & \cdots & \sqrt{\beta_1}\cdot\sqrt{g(\theta_{1k})} \\ \sqrt{\beta_2}\cdot\sqrt{g(\theta_{21})} & \sqrt{\beta_2}\cdot\sqrt{g(\theta_{22})} & \cdots & \sqrt{\beta_2}\cdot\sqrt{g(\theta_{2k})} \\ \vdots & \vdots & \ddots & \vdots \\ \sqrt{\beta_k}\cdot\sqrt{g(\theta_{k1})} & \sqrt{\beta_k}\cdot\sqrt{g(\theta_{k2})} & \cdots & \sqrt{\beta_k}\cdot\sqrt{g(\theta_{kk})} \end{pmatrix} \tag{5.8}$$

Hence we can express the received signal $\mathbf{y}(\theta)_i \in \mathbb{C}^{M\times 1}$ for a user in a beam i separating the received signal from non-desired signal as follows:

$$\mathbf{y}_i(\theta) = \sqrt{P_{sat}}\cdot h_{ii}\cdot\mathbf{x}_i + (\sum_{j=1,j\neq i}^{j=k} \sqrt{P_{sat}}\cdot h_{ij}\cdot\mathbf{x}_j) + \mathbf{n}_i \tag{5.9}$$

Being the term $\sqrt{P_{sat}}\cdot h_{ii}\cdot\mathbf{x}_i$ is our desired signal, the term $\sum_{j=1,j\neq i}^{j=k}\sqrt{P_{sat}}\cdot h_{ij}\mathbf{x}_j$ is the co-channel interference and the term $\mathbf{n}_i \in \mathbb{C}^{M\times 1}$ is a column vector of zero mean and complex circular noise with variance N.

Developing and replacing in h_{ii} the following expression is obtained:

$$\mathbf{y}_i(\theta) = \sqrt{P_{sat}}\cdot\sqrt{\beta_i}\cdot\sqrt{g(\theta_{ii})}\mathbf{x}_i + \sum_{j=1,j\neq i}^{j=k}\left(\sqrt{P_{sat}}\cdot\sqrt{\beta_i}\cdot\sqrt{g(\theta_{ij})}\mathbf{x}_j\right) + \mathbf{n_i}$$

As before it is possible to obtain an expression for the SINR of a beam i, as before assuming the power of the transmitted symbols is normalized:

$$SINR_i(\theta) = \frac{P_{sat}\cdot|h_{ii}|^2}{\sum_{j=1,j\neq i}^{j=k}(P_{sat}\cdot|h_{ij}|^2) + N_i} \tag{5.10}$$

And developing in h_{ii} again:

$$SINR_i(\theta) = \frac{P_{sat}\cdot\beta_i\cdot g(\theta_{ii})}{\sum_{j=1,j\neq i}^{j=k}(P_{sat}\cdot\beta_i\cdot g(\theta_{ij})) + N_i}$$

Taking the obtained β results in Table A.5, the noise density levels per unit bandwidth in equation (A.15) and (A.16) we can obtain expressions for each of the different payloads:

$$SINR(\theta)_i^{conv,Ka} = \frac{P_{sat} \cdot \beta_i^{conv,Ka} \cdot g(\theta_{ii})}{\sum_{j=1,j\neq i}^{j=k} (P_{sat} \cdot \beta_i^{conv,Ka} \cdot g(\theta_{ij})) + N_i^{conv,Ka}}$$

$$SINR(\theta)_i^{flex,Ka} = \frac{P_{sat} \cdot \beta_i^{flex,Ka} \cdot g(\theta_{ii})}{\sum_{j=1,j\neq i}^{j=k} (P_{sat} \cdot \beta_i^{flex,Ka} \cdot g(\theta_{ij})) + N_i^{flex,Ka}}$$

$$SINR(\theta)_i^{bh,Ka} = \frac{P_{sat} \cdot \beta_i^{bh,Ka} \cdot g(\theta_{ii})}{\cdot \sum_{j=1,j\neq i}^{j=k} (P_{sat} \cdot \beta_i^{bh,Ka} \cdot g(\theta_{ij})) + N_i^{bh,Ka}}$$

$$SINR(\theta)_i^{conv,ANT} = \frac{P_{sat} \cdot \beta_i^{conv,ANT} \cdot g(\theta_{ii})}{\sum_{j=1,j\neq i}^{j=k} (P_{sat} \cdot \beta_i^{conv,ANT} \cdot g(\theta_{ij})) + N_i^{conv,ANT}}$$

$$SINR(\theta)_i^{flex,ANT} = \frac{P_{sat} \cdot \beta^{flex,ANT} \cdot g(\theta_{ii})}{\sum_{j=1,j\neq i}^{j=k} (P_{sat} \cdot \beta_i^{flex,ANT} \cdot g(\theta_{ij})) + N_i^{flex,ANT}}$$

$$SINR(\theta)_i^{bh,ka} = \frac{P_{sat} \cdot \beta_i^{bh,ANT} \cdot g(\theta_{ii})}{\sum_{j=1,j\neq i}^{j=k} (P_{sat} \cdot \beta_i^{bh,ANT} \cdot g(\theta_{ij})) + N_i^{bh,ANT}}$$

Where the sub-index a and b in $SINR_i^{a,b}$ and ${\beta_i}^{a,b}$ make reference to the a payload used (conventional, flexible or beam-hopping) for the b system (Ka band system or Antares system) in the *i-th* beam, $N^{a,b}$ denotes the power noise level in the a payload for system b.

P_{sat} values are extracted from Table A.2, A.3 and A.4, $\beta^{a,b}$ values are extracted from Table A.5.

Chapter 6

Overall Performance

6.1 Simulations and Performance for the RRM design

In this section are presented the results related to the RRM design, whether they are related to the architecture design or to the MF-TDMA design.

6.1.1 Conclusions and delay estimation for the architecture design

In Table 6.1 we can see a comparison of the proposed architecture options in terms of delays and entities complexity.

Type of Architecture	Delays (s) for a packet	GES complexity	NCC complexity
Distributed SATBASED	$max\{t_{SCH},0.5\} + t_a + 0.25$	The complexity is distributed among the NCC and the GES since each of them performs one of the processes	
Distributed TERRBASED	$t_{SCH} + t_a + 0.25$		
Centralized SATBASED	$2(ta + 0.25) + t_{SCH}$	GESs complexity is highly reduced and almost act like repeaters	NCC complexity is very high since it has to perform the scheduling and resource allocation for the GESs
Centralized TERRBASED	$t_{SCH} + t_a + 0.25$		

Table 6.1: Design options comparison

From this general information of the architectures we can compute important data regarding to the delays for sending a packet:

- Lower delay bounds for sending a packet can be extracted by assuming t_{SCH} is close to zero and that t_a is going to be the transmission time of the most efficient MODCOD. This number gives us an idea of which would be the minimum delay for each of the architectures.
- As upper delay bounds are fixed by the CoS imposed delays, we will take the most restricting TD_{95} delay (from Table 1.7, DG-C=1.4s) and suppose t_a is going to be the transmission time of the less efficient MODCOD and obtain t_{SCH}. This number will give us an idea of the maximum time a packet must be in queues, i.e: how good must be the scheduling we design in each of the architectures for the most restricting CoS. As higher is the t_{SCH} number, more relaxed is the constraint while if negative it is impossible to achieve.

To these aim, the system parameters in Table 1.2 have been taken and obtained the transmission times (t_a, for a 4096 bits block) specified in Table 6.2. Although messages are smaller they must be encapsulated within a block of this size and we assume the entire block must be received to start decoding.

MODCOD	t_a
(1) QPSK 1/3	46ms
(2) QPSK 1/2	31ms
(3) QPSK 2/3	23ms
(4) 8PSK 1/2	20.7ms
(5) 8PSK 2/3	15.5ms
(6) 16APSK 2/3	11.6ms

Table 6.2: Obtained transmission time for a packet t_a

For extracting lower delay bounds 16APSK t_a will be used, while for knowing how good must be the scheduling QPSK 1/3 t_a will be used.

Type of architecture	Type of WAN	Lower delay for a packet d_{min}
Distributed	SATBASED	$d_{min}(s) = 0.7616$
	TERRBASED	$d_{min}(s) = 0.2616$
Centralized	SATBASED	$d_{min}(s) = 0.5232$
	TERRBASED	$d_{min}(s) = 0.2616$

Table 6.3: Lower delay bounds

Type of architecture	Type of WAN	t_{SCH}(s)
Distributed	SATBASED	1.104
	TERRBASED	1.104
Centralized	SATBASED	0.408
	TERRBASED	1.104

Table 6.4: Scheduling complexity

From Table 6.3 and Table 6.4 the following conclusions can be extracted:

- Both architectures using TERRBASED-WAN, whether it is centralized or distributed get the minimum lower bounds in end-to-end delay.
- The worst lower bound is achieved by the distributed SATBASED-WAN since three satellite hops are introduced, one for requesting resources, another to receive the allocation of the resources and the last one to send the information.
- Centralized SATBASED-WAN offers a mid value lower bound delay.
- Although lower delay bounds, the time in which the scheduling must be performed is very similar for all the architectures. Particularly the distributed SATBASED-WAN architecture can start the scheduling process while the GESs and the NCC are exchanging resources information (requests petitions and allocation assignments) to minimize this time.

Being known this the architecture that would achieve the best trade-off between delay bounds and scheduling complexity are the distributed and centralized architectures with the a terrestrial based WAN.

6.1.2 Simulations and Performance for MF-TDMA design

In this section are presented the simulation and performance results for the MF-TDMA design done in Chapter 2 section 2.3. As it is explained in the related chapter, two allocation algorithms are compared, the fixed T_S algorithm and the dynamic T_S algorithm. As the baseline options for the number of GES in the system is 1, 3, 5 these will be the cases simulated. The process used for evaluating the MF-TDMA SF allocation algorithms is described next:

- Choose a number of GES for the system (1 GES case is obviated since is straightforward to see all resources would be allocated to the unique GES).
- Choose a MODCOD per GES supposing a real distribution of the AES per GES, as it can be seen in the table below:

Number of GES	MODCOD distribution	Users assigned per GES
3	[6 2 2]	[6000 2000 2000]
5	[6 4 2 2 1]	[3500 2500 1334 1333 1333]

Table 6.5: Table of MODCODs and users distributions used in the simulations (MODCOD indexes are extracted from Table 2.2)

- Obtain a vector of possible demands between a minimum and a maximum per GES using the characteristics of the ANTARES traffic shown in subsection 1.2.5.
- Compute the fixed timeslot allocation algorithm and the dynamic timeslot allocation algorithm.
- Plot the obtained figures of merit using both algorithms in function of the global requested bitrate and plot the total allocated timeslots vs the total demanded timeslots.

6.1.2.1 Simulations for a system with 3 GES

The obtained system performance with 3 GES is as shown in Figure 6.1 and 6.2.

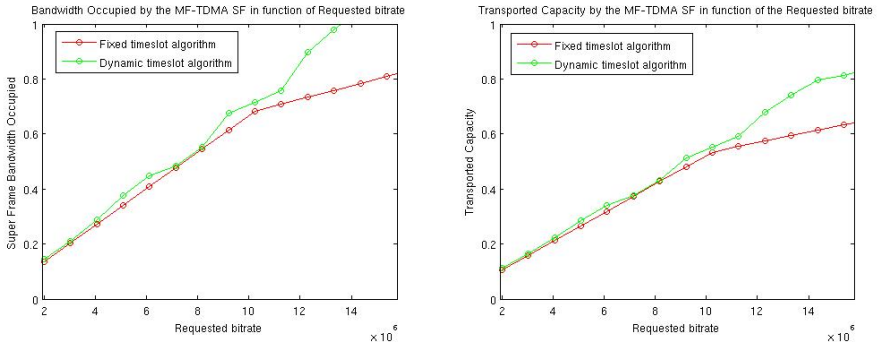

Figure 6.1: BO and TC performance

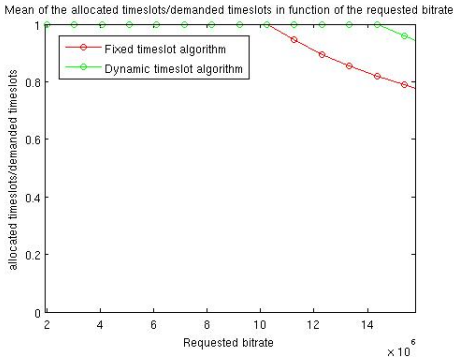

Figure 6.2: Mean of Allocated timeslots vs Demanded timeslots

6.1.2.2 Simulations for a system with 5 GES

The obtained system performance with 5 GES is as shown in Figure 6.3 and 6.4.

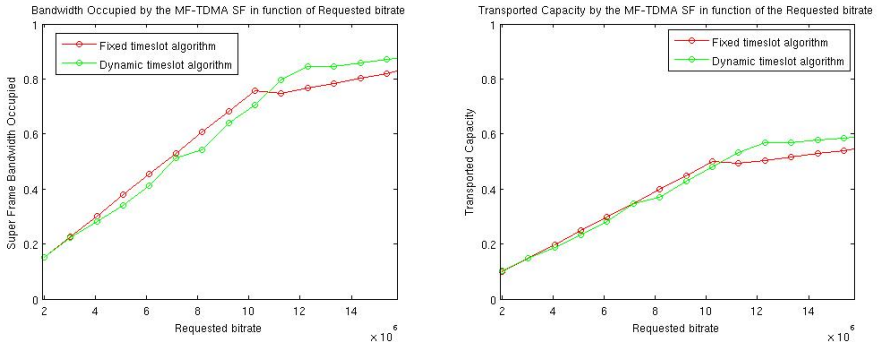

Figure 6.3: BO and TC performance

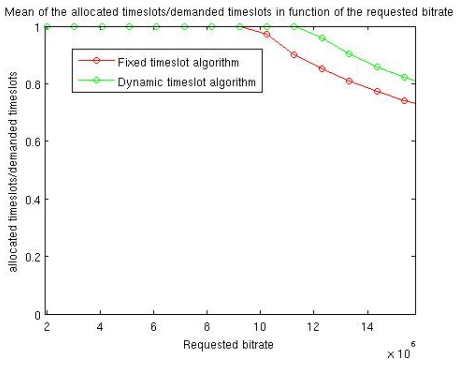

Figure 6.4: Mean of Allocated timeslots vs Demanded timeslots

6.1.2.3 Conclusions on simulation results

The following conclusions can be extracted from the graphics in sections 6.1.2.1 and 6.1.2.2 above.

- For a system with 3 GES:
  - When bitrates requests are under the mean (around 6Mbps), both algorithms perform very similar, the results for the BO and TC figures of merit are very similar and both algorithms achieve to allocate all the demanded timeslots.
  - When bitrates requests are over the mean the dynamic timeslot algorithm performs clearly better than the fixed timeslot algorithm. The improve on the BO and TC figures of merit is at least of the 10%. Besides it also gets to allocate at least 10% more demanded timeslots than in the fixed timeslot algorithm.
- For a system with 5 GES:
  - When bitrates requests are under the mean, both algorithms perform very similar, the results for the BO and TC figures of merit are very similar and both algorithms achieve to allocate all the demanded timeslots.
  - When bitrates requests are over the mean the dynamic timeslot algorithm performs slightly better than the fixed timeslot algorithm. The improve on the BO and TC figures of merit is around 5%. It also gets to allocate 5% more demanded timeslots than the fixed timeslots algorithm.

Being known this, we propose to use the dynamic timeslot algorithm since for high bitrate requests it performs clearly better than the fixed timeslot algorithm.

Besides as it is explained in the introduction to this work, it is expected than in the following years air traffic is going to increase exponentially and therefore control communications. Hence the need of an algorithm to allocate traffic demands properly when requests are elevated.

The major drawback of this algorithm is its computational complexity, however in the literature are explained several methods to reduce this computational complexity, such as the one in reference [18].

6.2 Simulations and Performance for LL-FEC design

Within this section are presented the simulations and performance results for the LL-FEC design. The chosen scenarios in the following subsections correspond to each of the erasure models detailed in Chapter 3, section 3.2.2. Results are plot as the CFR using RS vs the CFR without using RS. CFR figure of merit is defined in subsection 3.5.3.

6.2.1 Simulations for the "Erasures produced by airplanes in the same line of sight with the satellite" scenario

The duration of the erasures for this scenario have been extracted from Table 3.2, minimum, mean and maximum values. However the probability of having an erasure, i.e. of one airplane being in the same line of sight with the satellite and blocking the signal, is taken as an input since no information to obtain this value has been found in the literature. Simulation parameters are summarized in Table 6.6.

Duration of the erasure (s)	LL-FEC delay aware(s)	Probability of erasure	RS(N,K) codes
0.04	0.68	[1e^{-4},1e^{-2}]	RS(255,127), RS(255,85), RS(15,7), RS(15,5)
0.3	0.68	[1e^{-4},1e^{-2}]	RS(255,127), RS(255,85), RS(15,7), RS(15,5)
1.15	1.5	[1e^{-4},1e^{-2}]	RS(255,127), RS(255,85), RS(15,7), RS(15,5)

Table 6.6: Simulation parameters for the current scenario

The results for the different erasure durations can be seen in Figure 6.5. The conclusions that can be extracted are:

- Erasure durations of 0.04 have not been simulated since if the RS code is able to overcome with CFR=1 the 0.3 seconds erasure a shorter with same probability can too.
- Codes with N=255 perform slightly better than codes with N=15 for both link layer frame sizes.
- Codes using bigger link layer frame sizes perform better. However it must be taken into account that for some bitrates the ADT table is not big enough to fit one link layer frame accomplishing the delay requirement then it is impossible to use this mode, i.e. for 0.6s delay at 16kbps ADT size is 3200 bits and link layer frame size is 8192 bits.

- Codes with coderate 1/3 get 1 or close to one CFR in all the cases, while codes using coderate 1/2 does not perform so well with long erasures.

It is possible to achieve even better performance if the LL-FEC delay-aware is increased, however, if done this, some of the CoS delay requirements could not be met.

6.2.2 Simulations for the "Erasures produced by the airplane itself when maneuvering" scenario

The simulation parameters for this scenario are extracted from section 3.2.2.2. The probability of performing a maneuver, δ, and the probability of the elevation angle with the satellite, ε, being lower than zero are extracted from Figure 3.8 and resumed in Table 6.7. As no duration for the erasure has been obtained in the literature, as an approximation it will be considered 0.5 seconds erasure.

Duration of erasure (s)	LL-FEC delay aware	Prob. of δ	Prob. of $\varepsilon < 0$	Flight Duration (s)	RS (N,K) Codes
0.5	0.68	0.1-0.3	0.2	7200	RS(255,127), RS(255,85), RS(15,7), RS(15,5)

Table 6.7: Simulation parameters for the current scenario

As we can observe from the values in the Table 6.7, this effect is really unreliable to happen since the probability of erasure is under $1e^{-9}$. Simulations showed that no erasures occurred during the simulation time. However if that happened the performance should be similar than in the case above for mean erasure duration since the erasure duration values are similar.

6.2.3 Simulations for the "Erasures produced by the blades" scenario

Although this is not a general case, in the helicopter scenario, as it can be seen in Figure 3.19, most of the erasures are produced because of the blades (any probability interferes in the process). When the erasures are produced by the blades the case is deterministic since the probability of the signal being blocked is always constant. The parameters used in the simulations are shown in Table 6.8 and extracted from section 3.2.2.2.

Duration of the erasure (s)	LL-FEC delay aware (s)	Duration no erasure	Duty cycle (%)	RS(N,K) codes
0.078	0.68	0.2	30%	RS(255,127), RS(255,85), RS(15,7), RS(15,5)

Table 6.8: Simulation parameters for the current scenario

Results for this scenario in terms of CFR using RS vs CFR without using RS are shown in Figure 6.6. The conclusions that can be extracted are:

- Both RS codes with N=255 and N=15 are able to correct all the errors for the different bitrates.
- 512 bytes link layer frame with link layer FEC delay 0.6 seconds it is not possible since the ADT table is too small to fit a frame.

6.2.4 Simulations for the "Erasures produced by blades and buildings" scenario

This scenario takes as a base the scenario where erasures are produced because of the blades, and adds the probability of finding a building during the flight, high enough to block the signal from the satellite. The parameters used in the simulations and extracted from section 3.2.2.2 are listed in Table 6.9.

Duration of buildings erasure (s)	LL-FEC delay-aware (s)	Probability of building	RS(N,K) codes
0.9	1.5	$1e^{-4}$-$1e^{-2}$	RS(255,127), RS(255,85), RS(15,7), RS(15,5)

Table 6.9: Simulation parameters for the current scenario

Results for this scenario are shown in Figure 6.6. The conclusions that can be extracted are the following:

- RS codes with N=255 perform slightly better than codes with N=15.
- RS codes with bigger link layer frame size (512 bytes) perform better than those with 256 bytes frame size. However as it has been said it must taken into account that there are some cases where the link layer FEC delay is very low that results into a very small ADT table that can not fit even an entire frame, hence it is impossible to use this mode.

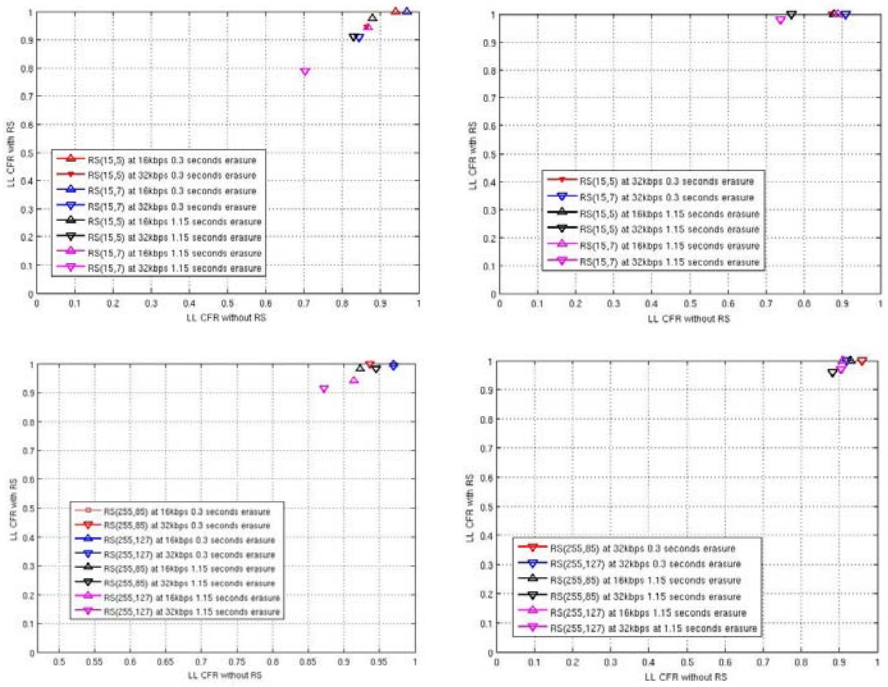

Figure 6.5: RS performance in commercial aviation scenario wit different erasure durations. Top row: RS(15,K) codes for 256 bytes and 512 bytes link layer frames. Bottom row: RS(255,K) codes for 256 bytes and 512 bytes link layer frames

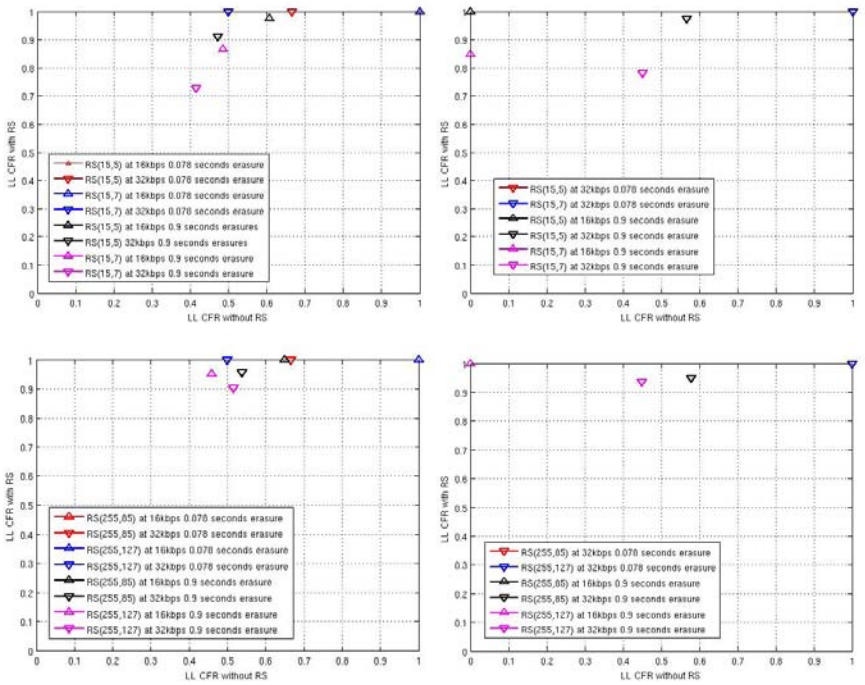

Figure 6.6: RS performance in Helicopter scenario with different erasure durations. Top row: RS(15,K) codes for 256 bytes and 512 bytes link layer frames. Bottom row: RS(255,K) codes for 256 bytes and 512 bytes link layer frames

	Helicopters 0.078s periodic erasure	Aviation 0.3s erasure	Aviation 1.15s erasure	Helicopters 0.9s erasure and periodic 0.078s erasure
LL-FEC delay-aware	0.68	0.68	1.5	1.5
$\text{CFR}_{RS(15,5)}$@16kbps	1	1	0.98	0.99
$\text{CFR}_{RS(15,5)}$@32kbps	1	0.95	0.9	0.9
$\text{CFR}_{RS(15,7)}$@16kbps	1	1	0.95	0.85
$\text{CFR}_{RS(15,7)}$@32kbps	1	0.9	0.8	0.72
$\text{CFR}_{RS(255,85)}$@16kbps	1	1	0.98	1
$\text{CFR}_{RS(255,85)}$@32kbps	1	1	0.98	0.95
$\text{CFR}_{RS(255,127)}$@16kbps	1	1	0.95	0.95
$\text{CFR}_{RS(255,127)}$@32kbps	1	0.99	0.92	0.9

Table 6.10: Summary of results for the carried out simulations for 256 bytes link layer frame size

	Helicopters 0.078s periodic erasure	Aviation 0.3s erasure	Aviation 1.15s erasure	Helicopters 0.9s erasure and periodic 0.078s erasure
LL-FEC delay-aware	0.68	0.68	1.5	1.5
$\text{CFR}_{RS(15,5)}$@16kbps	-	-	1	1
$\text{CFR}_{RS(15,5)}$@32kbps	1	1	1	0.99
$\text{CFR}_{RS(15,7)}$@16kbps	-	-	1	0.85
$\text{CFR}_{RS(15,7)}$@32kbps	1	1	0.98	0.79
$\text{CFR}_{RS(255,85)}$@16kbps	-	-	1	1
$\text{CFR}_{RS(255,85)}$@32kbps	1	1	0.95	0.95
$\text{CFR}_{RS(255,127)}$@16kbps	-	-	1	1
$\text{CFR}_{RS(255,127)}$@32kbps	1	1	0.98	0.94

Table 6.11: Summary of results for the carried out simulations for 512 bytes link layer frame size

In order to show in a more understandable way the performance of each code and the parameters used in the simulation, the following two tables,6.12 and 6.13 are presented:

RS (N,K) Code	PHY layer BBFRAME	LL layer frame	Type of scenario	Erasures generated (s)	Delay-aware introduced (s)	TD_{95} Accomplishment	CFR@16kbps	CFR@32kbps
RS(15,5)	4096 bits	256 bytes	Blades helicopter	0.078	0.68	Yes	1	1
			Aviation	0.3	0.68	Yes	1	1
			Aviation	1.15	1.5	No	0.98	0.95
			Blades helicopter plus buildings	0.9 +0.078	1.5	No	0.99	0.9
	8192 bits	512 bytes	Blades helicopter	0.078	0.68	Yes	-	1
			Aviation	0.3	0.68	Yes	-	1
			Aviation	1.15	1.5	No	1	1
			Blades helicopter plus buildings	0.9 +0.078	1.5	No	1	0.99
RS(15,7)	4096 bits	256 bytes	Blades helicopter	0.078	0.68	Yes	1	1
			Aviation	0.3	0.68	Yes	1	0.9
			Aviation	1.15	1.5	No	0.95	0.8
			Blades helicopter plus buildings	0.9 +0.078	1.5	No	0.85	0.72
	8192 bits	512 bytes	Blades helicopter	0.078	0.68	Yes	-	1
			Aviation	0.3	0.68	Yes	-	1
			Aviation	1.15	1.5	No	1	0.98
			Blades helicopter plus buildings	0.9 +0.078	1.5	No	0.85	0.79

Table 6.12: Simulation set 1, RS(15,5) and RS(15,7) codes

RS (N,K) Code	PHY layer BBFRAME	LL layer frame	Type of scenario	Erasures generated (s)	Delay-aware introduced (s)	TD_{95} Accomplishment	CFR@16kbps	CFR@32kbps
RS(255,85)	4096 bits	256 bytes	Blades helicopter	0.078	0.68	Yes	1	1
			Aviation	0.3	0.68	Yes	1	1
			Aviation	1.15	1.5	No	0.98	0.95
			Blades helicopter plus buildings	0.9 +0.078	1.5	No	1	0.95
	8192 bits	512 bytes	Blades helicopter	0.078	0.68	Yes	-	1
			Aviation	0.3	0.68	Yes	-	1
			Aviation	1.15	1.5	No	1	0.95
			Blades helicopter plus buildings	0.9 +0.078	1.5	No	1	0.95
RS(255,127)	4096 bits	256 bytes	Blades helicopter	0.078	0.68	Yes	1	1
			Aviation	0.3	0.68	Yes	1	0.99
			Aviation	1.15	1.5	No	0.95	0.92
			Blades helicopter plus buildings	0.9 +0.078	1.5	No	0.95	0.9
	8192 bits	512 bytes	Blades helicopter	0.078	0.68	Yes	-	1
			Aviation	0.3	0.68	Yes	-	1
			Aviation	1.15	1.5	No	1	0.98
			Blades helicopter plus buildings	0.9 +0.078	1.5	No	1	0.94

Table 6.13: Simulation set 2, RS(255,85) and RS(255,127) codes

As we can observe from Table 6.12 and Table 6.13 just above, better performances are achieved when using longer link layer frames (512 bytes in front of 256 bytes) and when using longer in N RS(N,K) codes. Regarding this latter issue it is deeply explained in section 3.4.1.2 and demonstrated in section 3.4.2.2 that RS codes with high N values are too complex. Hence we propose to use short in N RS(N,K) code such as the N=15 simulated code together with a long link layer frame e.g. 512 bytes.

It can also be noted that $TD_{95}$is not accomplished in all the cases since the delay-aware introduced is bigger. The reason beyond that is:

- Just one CoS has assigned a TD_{95} bigger than 1.5s, so we assume the combination of sending this type of message together with a worst case erasure is very small. If that happened we consider this would be in the 5% of the times we could overcome the TD_{95}.
- Of course there is a trade-off between performance and delay, final decisions will be taken on further stages on the project, however we demonstrate it is possible to improve the performance of the system by using LL-FEC, and that this performance for the considered channels is optimum when using RS delay-awared codes.

6.3 Simulations and Performance on the Interference Analysis study

In order to simulate the interference in multibeam satellite systems in function of the θ angle we have depicted two different scenarios.

- A first scenario composed of 70 beams covering Europe with a half angle beamwidth $\theta_{-3dB} = 0.245^{o}$, in the Ka band. Parameters for this system are listed in Tables A.1, A.2, A.3 and A.4. Beam lattice is depicted in the left part of Figure 6.7.
- A second scenario depicting the baseline option for the ANTARES system, using 3 beams which covers the entire ECAC flight area and with a beamwidth of $\theta_{-3dB} = 2.90^{o}$. Parameters for this system are listed in Tables A.1, A.2, A.3 and . Beam lattice is shown in the right part of Figure 6.7.

For both scenarios the satellite is located at 0^{o} Latitude, 0^{o} Longitude.

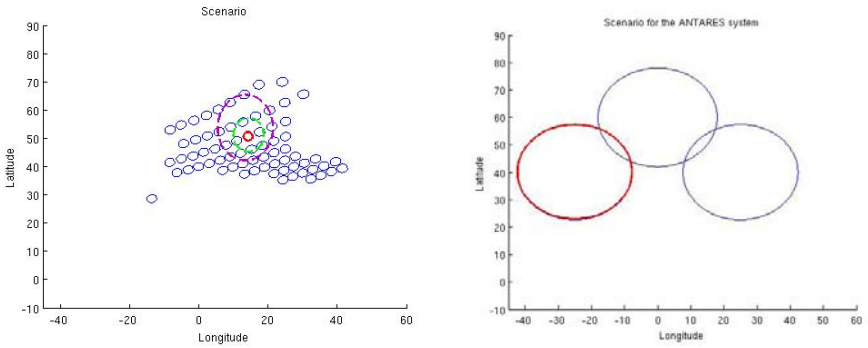

Figure 6.7: Beam lattice for 70 beam scenario and ANTARES scenario respectively

For each of the scenarios listed above we will analyze the received SINR within the beam of interest (red colored beam) changing the number and/or location of the interfering beams. Mention that the flexible payload has not been simulated since it has been impossible to implement an easy-computing AFR antenna model.

For the 70 beam scenario:

- We will analyze the SINR produced by an increasing number of adjacent interfering beams (dashed green ring) and the SINR produced by all non-adjacent beams (dashed lilac ring) in Figure 6.7, for each of the payloads.

For the ANTARES scenario:

- We will analyze the SINR received in the beam of interest supposing none, one or two interferers for the conventional and beam-hopping payload.

6.3.1 70 Beam system

Within this section we will analyze the effect of the interference in a 70 beam scenario, for the conventional and beam-hopping payloads. The following assumptions are made:

- For the conventional payload it is assumed a 4 colored bandwidth scheme, i.e. bandwidth is divided in four portions. This means interferers has assigned the same portion of bandwidth as the beam of interest.
- For beam-hopping payload, k-interferers mean that k beams are illuminated at the same time sharing the entire bandwidth.

Besides, figures from now on are plotted as follows:

- Marker shows the beam center of the beam of interest.
- First contour indicates the 3dB fall with respect to the maximum of the plotted variable.
- Green label shows the first 10dB with respect to plotted variable for the beam of interest.
- Grey points mark the original edge of the beam, i.e. 3dB fall without interferers.

6.3.1.1 Differences between payloads

The received SINR for a user in the beam of interest for each of the payloads and when there are no interferers, i.e. the SNR, is shown in Figure 6.8. In the mentioned figure it can be observed the following:

- Received SNR for the conventional payload is higher than in the beam-hopping payload since in the conventional payload the entire bandwidth is divided in parts while in beam-hopping the entire bandwidth is assigned to beams. Although this allows to receive more information it can make closing the link budget more difficult.

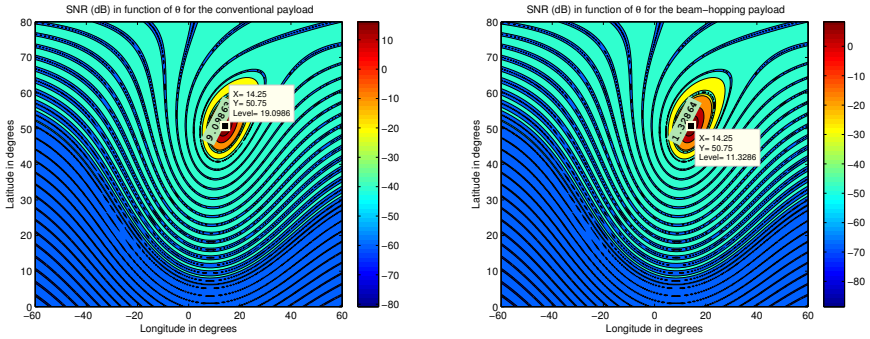

Figure 6.8: SINR received by the beam of interest for 0 interferers and for the conventional and beam-hopping payload respectively

6.3.1.2 Interference generated by adjacent beams

In this section we will study the effect of the interference generated by an increasing number of adjacent beams (green ring in Figure 6.7) for both payloads. To this aim we will plot the SINR as a function of the number of the adjacent interfering beams for both payloads as seen in Figure 6.9. The increase in the received SINR for the conventional payload with respect to the beam-hopping one is given in the rigth part of the figure.

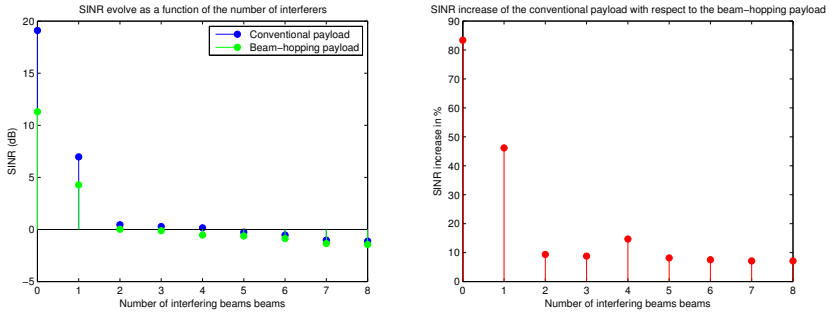

Figure 6.9: SINR as a function of the number of interferers

We can observe that as the number of adjacent interfering beams increase, the SINR decays very fast for both payloads, even for a small number of interferers. Moreover We the trend is that differences in the received SINR between both payload decrease when the number of interfering beams increase. Results lead to the following rules when designing:

- For the conventional payload it should be avoided to assign the same frequency bands to adjacent beams.

- For the beam-hopping payload it should be avoided to illuminate at the same time adjacent beams.

6.3.1.3 Interference generated by non-adjacent beams

In this section is plotted the SINR caused in the beam of interest by all the beams that cross the lilac dashed ring in Figure 6.7. This case is of special interest in the conventional payload because when using the typical algorithm for assigning frequencies these would be the beams with the same frequency band. Results for the beam-hopping payload will help us to compare performances.

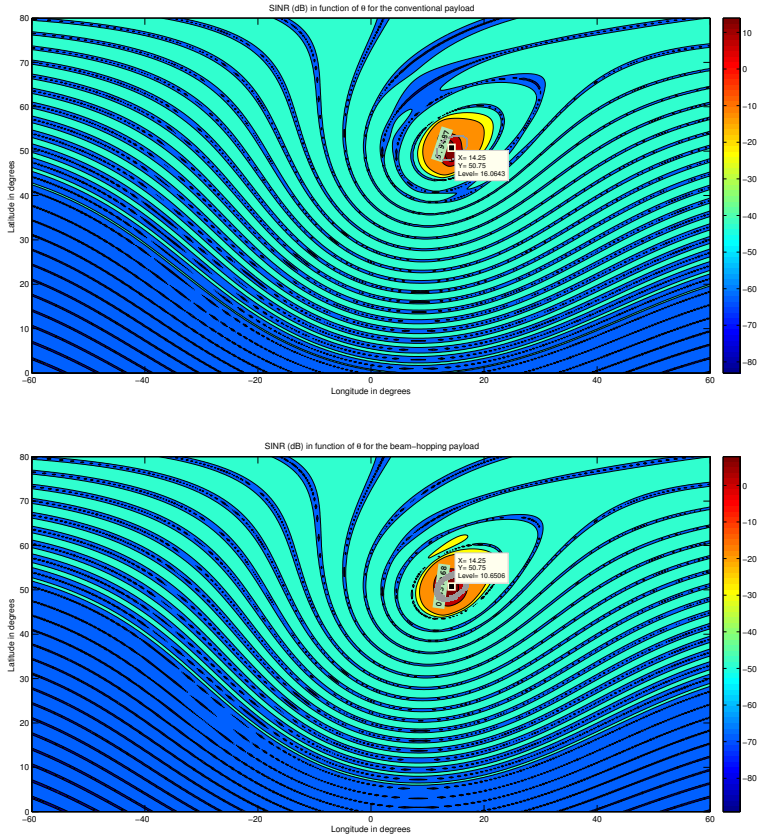

Figure 6.10: SINR in the beam of interest when all beams crossing the dashed lilac rings in Figure 6.7 interfere

As we expect other further beams using the same frequency band will not influence in the SINR, this can be a realistic example of the real received SINR

within a beam. In Figure 6.10 we can observe that all the interferers produce a 3dB fall in the the SINR for the conventional payload and a 1.3dB fall for the beam-hopping payload with respect to the case without interferers. Although differences in the received SINR are now smaller, conventional payload still receives a higher SINR than the beam-hopping payload. The increase in the SINR of the conventional payload with respect of the beam-hopping is of the 70%.

6.3.1.4 Interference generated by far away beams

Finally, we can observe which is the SINR decrease within the edge of coverage of the beam of interest, when the interfering beam is placed far-away from the beam of interest. The effect can be seen for both payloads in Figure 6.11.

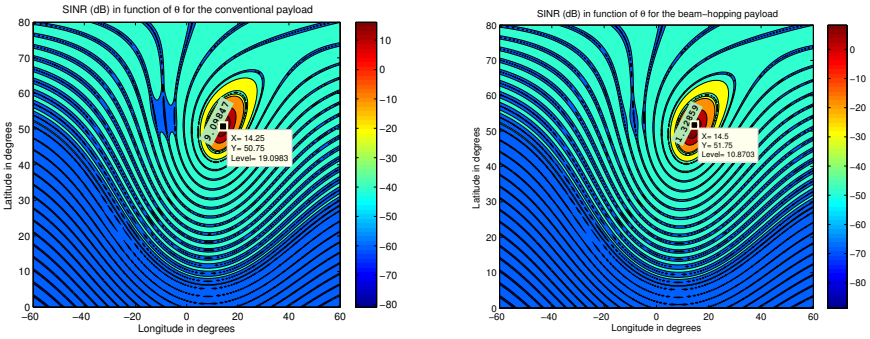

Figure 6.11: SINR decrease caused by far-way interfering beams

What can be observed for both payloads is that far-located interfering beams almost don't cause any decrease in the received SINR since the values obtained are similar than for no interferers (Figure 6.8).

6.3.1.5 Conclusions for the 70 beam system

Election between conventional payload or beam-hopping payload is a trade-off since:

- Conventional payload achieves much higher SINR values, increases reach the 80% in some cases. This makes closing the link budget easier than in the beam-hopping payload. The drawback of this scheme is that is not very flexible since we work with a fixed frequency reuse pattern.
- Beam-hopping payload assigns the entire bandwidth to each beam which in theory allows higher information fluxes, besides it is more flexible since we can decide which beams will be illuminated at a time. It is demonstrated

in reference [24] that beam-hopping payload adapts better to real traffic fluxes despite its lower SINR, specially under heavy loaded conditions. It achieves average increases on the Satisfaction Factor (defined as the ratio of served over demanded traffic) of the 10%. However closing the link budget under this case could be more difficult.

6.3.2 ANTARES system

Within this section we will analyze the effect of the interference in the ANTARES system for the conventional and beam-hopping payloads. Figures from now on are plotted as follows:

- Marker shows always the center of the beam of interest.
- First contour indicates the 3dB fall with respect of the maximum of the plotted variable.
- Successive contours indicate additional 10dB fall with respect of the maximum of the plotted variable and its values is indicated with a green label.
- Grey points mark the original edge of the beam, i.e. 3dB fall without interferers.

6.3.2.1 Analysis of the SINR

In Figure 6.8 is presented the received SINR in the beam of interest for the conventional and beam-hopping payloads when there are no interferers, i.e. the SNR of the system. It can be observed in the contour the characteristics of the antenna pattern,strong red contours are produced by the main lobe of the antenna while orange and yellow contours are produced by side lobes (such lobes cause the interference) finally dark and soft blue contours depict the zeros of the antenna.

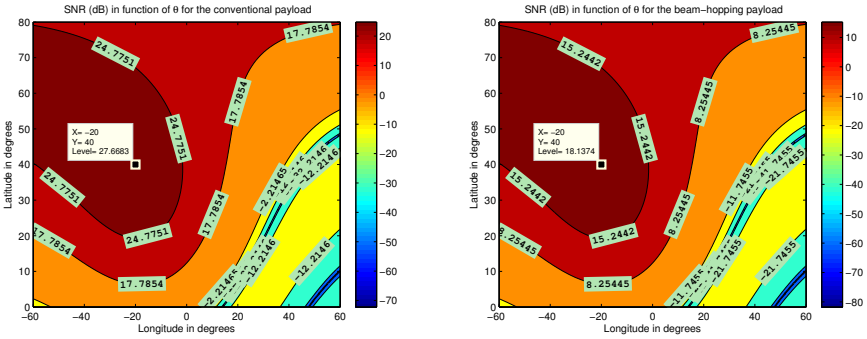

Figure 6.12: SINR received by the beam of interest for 0 interferers and for the conventional and beam-hopping payloads respectively

As we can observe there is a big difference in the received SNR between the conventional and the beam-hopping payload, the reason beyond that is:

- In the conventional payload the fact that there are no interferers means that bandwidth is shared among beams, hence noise bandwidth is reduced and the received SINR is bigger.
- In the beam-hopping payload the entire bandwidth is destined to each beam; the fact that there are no interferers means that only one beam is illuminated at a time. Hence for this case the noise bandwidth is bigger and the received SINR is lower.

Now, we will set one interfering beam in the system. In Figure 6.13 we can observe the received SINR for each of the payloads in the left part of the figure, while in the right part we can observe the power level of the interference.

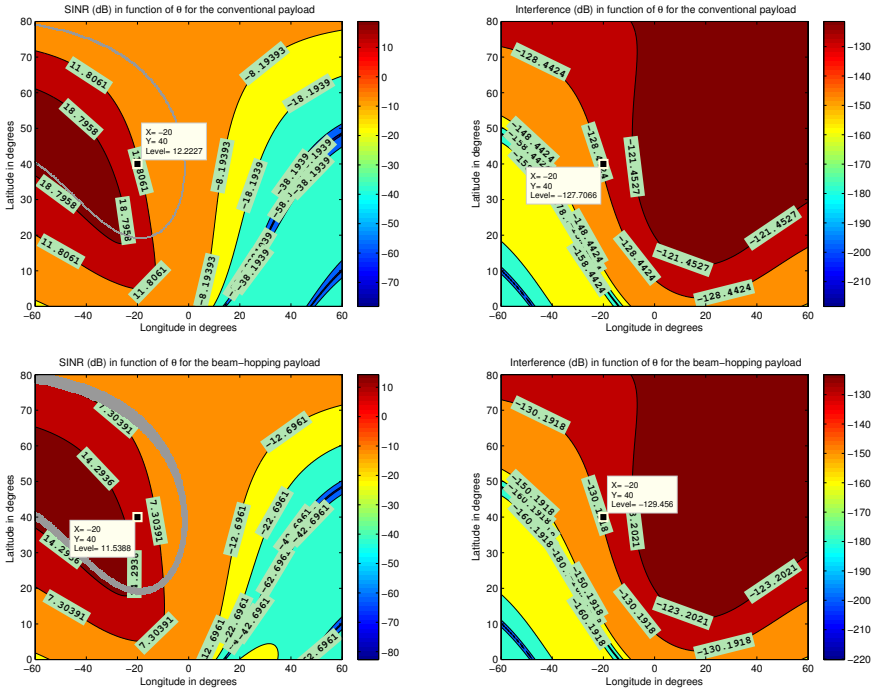

Figure 6.13: SINR received by the beam of interest for 1 interferer and for the conventional and beam-hopping payloads respectively

The following conclusions can be extracted:

- For the conventional payload one interfering beam means that the assigned bandwidth to each beam has increased, hence does it noise power level. Therefore besides of the interference power, noise power level has increased which leads to the big loss in the SINR level.

- For the beam-hopping payload one interfering beam means that the beam of interest and the interfering beam have assigned the entire frequency at the same time. Hence besides of the interference generated noise power level is maintained and the SINR loss is lower than in the conventional payload.

Although differences between the SINR level have been reduced, conventional payload achieves a mean higher value as we can deduce by the values of the contours.

Finally if we set that all beams interfere between them, we can see the pattern in Figure 6.14 for the beam of interest.Note that now conventional and beam-hopping payload have assigned the entire bandwidth to each of the beams, hence the noise power is the same for both of them. From there the similar SINR level obtained, conventional payload obtains a higher SINR value since its output power is higher.

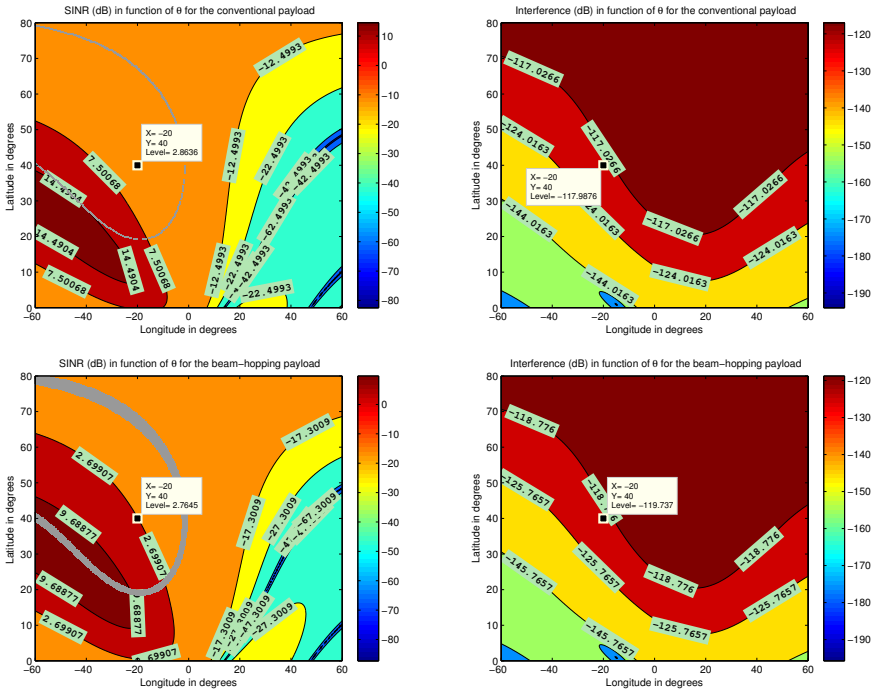

Figure 6.14: SINR received by the beam of interest for 2 interferer and for the conventional and beam-hopping payloads respectively

It can also be interesting to plot only the received SINR within the edge of the beam of interest and within the edge of the interfering beams and observe the results. Obtained SINR is shown in Figure 6.15 and results show the following:

- As the satellite is located at 0 latitude and 0 longitude it exists one case that the SINR of both considered beams is the same because beams are symmetrically located with respect the satellite.
- However as it can be seen in the two last images of Figure 6.15 the level of interference that a beam a causes to a beam b need not be the same as the one that beam b causes to beam a.

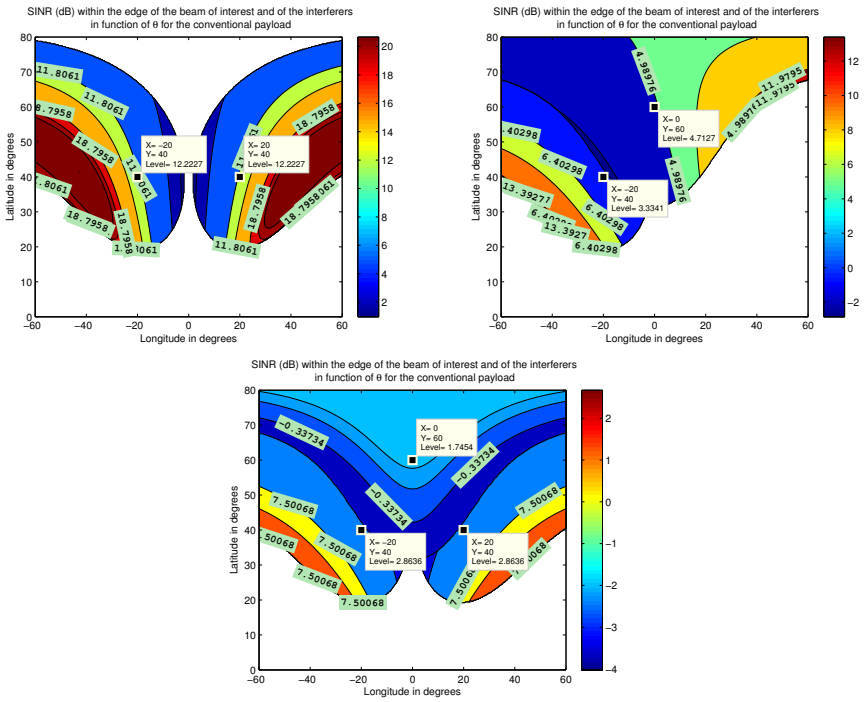

Figure 6.15: Received SINR within the edge of the beam of interest and within the edge of the interferers for conventional payload

This is produced because the θ from the interfering beam with the user is not the same for different beams of interest, it depends on the position of the satellite. As seen, if beams are symmetrically located from the satellite the interference is the same from a to b than from b to a, however, if not, generated interference levels are different. This must be taken into account when designing a system since we must consider worst cases for closing the link budget.

Figure 6.16 shows the mean received SINR in the beam of interest for each of the payloads as a function of the number of interferers. In the image we can observe how as the number of interfering beams increase differences between the received SINR in both payloads become smaller.

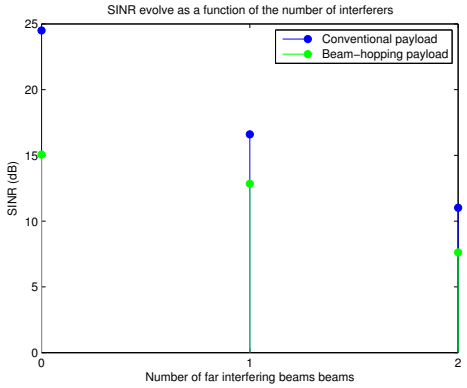

Figure 6.16: SINR evolution in the ANTARES system for the conventional and beam-hopping payloads

6.3.2.2 Conclusions on the ANTARES system

Conventional payload achieves higher SINR values for any number of interfering beams. However the beam-hopping payload assigns more bandwidth to each beam. Going back to subsection 1.2.5, where the mean traffic that an AES receive is $\overline{R_{b,AES}} = 608.47bps$ and for the entire system about $6Mbps$, we can note the traffic profile is very low compared with other satellite systems that support more than Gbps speeds. Hence for this specific case where we don't need do cope with high traffic volumes the conventional payload is more suitable than the beam-hopping payload.

Chapter 7

Conclusions and Further Work

In this project we have carried out a preliminary design work on the RRM, LL-FEC and Interference Analysis for the upcoming ANTARES system.

To this aim we have first analyzed the system-level architecture and operational functionalities. In addition, it was necessary to identify the basic design requirements established that we should achieve in the design of the RRM and LL-FEC modules.

During the work, quite some part of the necessary information that was relevant for our study was not available given the fact that the overall design of all modules was taking place simultaneously. Hence, in some cases we had to infer coherent and reasonable assumptions from related ones. This led most of the time to several possible options for the designs and trade-offs decisions to choose the most suitable options.

Our results have shown that it is possible to meet the technical requirements set forward by the official institutions in charge of aviation control (ECAC) if made a good design and improve the global performance of the system.

The MF-TDMA allocation and LL-FEC have been shown to be efficient to the trfficc requests and error correction requirements meeting the constraining delay imposed.

Further work on the ANTARES project mainly depend on future decisions that still must be taking in order to completely design the system modules and the overall system. This would allow to extract more and more accurate results regarding to the design issues obtained in this work.

We have also performed a system-level interference analysis and the preliminary conclusions obtained pave the way to further work for relevant comparisons to

parallel work results obtained within our group in which highly and asymmetric traffic requirements were considered. In addition, further work on the flexible payload has been left out of our current work as it needs a deeper insight on analytical models of AFR antennas.

Appendix A

Link Budget

In this chapter are explained the different contributions to the link budget for all the satellite links, forward uplink and forward downlink (complete path from the gateway to the user) and return uplink and return downlink (complete path from the user to the gateway or other users). The purpose is to separate the terms of the link budget in those which don't vary for a given payload and those that can change due to the payload. As we will specially focus on the forward downlink in the last section of the chapter will be given the values for the forward downlink link budget for each payload and for a given satellite system.

Previously to the link budget are explained some geometrical aspects in earth-satellite system that will be useful for a better understanding of the link budgets.

A.1 Geometrical Aspects

We consider the scenario shown in figure A.1 where the satellite radiates its maximum gain G_{max} towards the spot beam center and also radiates in different directions due to the its side lobes. We find a ground terminal in a point P. Known the position of the ground terminal point P, of the beam center BC, and of the satellite SL, we can compute the distances (P,BC), (P,SL) and (SL,BC) and hence extract the angle θ between (SL,P) and (SL,BC), the angle between the spot beam center and the receiver seen from the satellite.

Using the cosine theorem we obtain:

$$\theta = \arccos\left(\frac{(P,BC)^2 - (SL,BC)^2 - (SL,P)^2}{-(SL,BC)(SL,P)}\right) \tag{A.1}$$

This angle is important since we will compute the satellite antennas gains as a function of θ , besides the power level of the interference will also depend on this angle due to the power level of the side lobes.

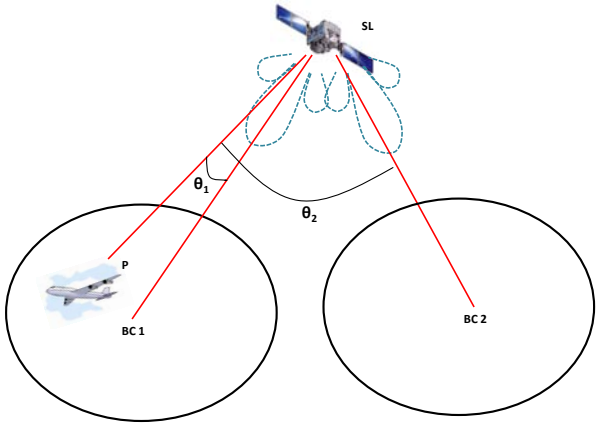

Figure A.1: Considered scenario

Equation (A.2) shows the antenna model for the conventional and beam-hopping payload:

$$G(\theta) = G_{max} \cdot \left(\frac{J_1(u)}{2u} + 36 \cdot \frac{J_3(u)}{u^3} \right)^2 \tag{A.2}$$

Where $u = 2.07123 \cdot \frac{\sin\theta}{\sin\theta_{-3dB}}$ being θ_{-3dB} the half angle half-power beamwidth, G_{max} is the antenna boresight gain and J_1, J_3 are the first and third order Bessel functions respectively.

The antenna patterns resulting of the formula in equation (A.2) for the conventional and beam-hopping payloads can be seen in Figure A.2.

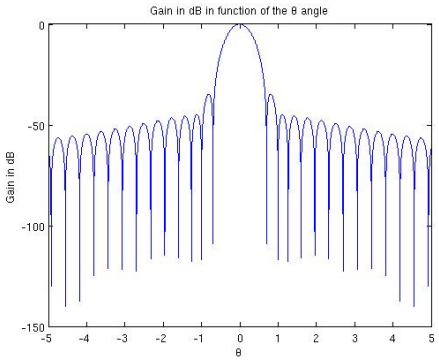

Figure A.2: Antenna pattern $G(\theta)$ with $\theta_{-3dB} = 0.245^{\text{o}}$ for the conventional/beam-hopping payloads

In the figure we can observe how side lobes are generated when θ is bigger than the specified θ_{-3dB}. These side lobes will introduce interference in our system. Besides as the main lobe gain does not turn to zero quickly after θ_{-3dB} it will introduce also interference in the system, specially when the interfering beam is adjacent or near by the beam of interest.

A.2 Link Budget Calculation in function of θ

Here in this section is explained the computation of the link budget for both gateway to satellite link and satellite to users link as C over N0, taking C as the satellite carrier power, and N0 as the noise density level in reception. Although normal formulation for link budgets is expressed in dB in this section are formulated in linear in order to do more understandable the extraction of the α, β, γ and δ parameters.

A.2.1 Forward Uplink

For the purpose of this section the following acronyms that make reference to link budget terms have been defined:

- $EIRP_{gw} = P_{gw} \cdot G_{gw} \cdot L_{gw}$ is the EIRP a gateway taking into account the gateway power, P_{gw}, the boresight gain, G_{gw}, and the depointing losses plus additional transmit losses, L_{gw}.
- L_{up} are the free space losses and the additional rain, polarization, atmospheric and scintillation losses for the uplink.
- G_{rx} is the gain of the antenna satellite in reception.
- T_{noise} is the noise temperature of the receiver considered, in this case the satellite.

The carrier power computation C and noise power per unit bandwidth N0 is given by the following equations:

$$C = P_{gw} \cdot G_{gw} \cdot L_{gw} \cdot L_{up} \cdot G_{rx}(\theta) \tag{A.3}$$

$$N0 = kT_{noise} \tag{A.4}$$

Since all the parameters in the C computation are fixed except for the gain in the satellite reception antenna, we can express C/N0 as:

$$\left.\frac{C}{N0}\right|_{FWD-UP} = \frac{P_{gw} \cdot \alpha \cdot G_{rx}(\theta)}{kT_{noise}} \qquad [dB \cdot Hz] \tag{A.5}$$

Where $\alpha = G_{gw} \cdot L_{gw} \cdot L_{up}$.

A.2.2 Forward Downlink

For the forward downlink the following acronyms have been defined:

- $EIRP_{sat} = P_{sat} \cdot OBO_{hpa} \cdot L_{sat} \cdot G_{tx}(\theta)$ is the satellite EIRP, with P_{sat} the on board saturated power, OBO_{hpa} is the Output Back-Off that applies to that satellite payload, L_{sat} are the satellite repeater output losses and G_{tx} is the antenna gain that depends on the angle formed between the satellite beam center for the considered ground terminal and the ground terminal position.
- L_{down} are are the free space losses and the additional rain, polarization, atmospheric and scintillation losses for the downlink.
- G_{gt} is the ground terminal antenna gain.
- T_{noise} is the noise temperature of the receiver considered, in this case the ground terminal.

The carrier power computation C and noise power per unit bandwidth N0 is given by the following equations:

$$C = P_{sat} \cdot OBO_{hpa} \cdot L_{sat} \cdot G_{tx}(\theta) \cdot L_{down} \cdot G_{gt} \tag{A.6}$$

$$N0 = kT_{noise} \tag{A.7}$$

So we can express the overall C/N0 for the forward downlink as:

$$\left.\frac{C}{N0}\right|_{FWD-DOWN} = \frac{P_{sat} \cdot \beta \cdot G_{tx}(\theta)}{kT_{noise}} \qquad [dB \cdot Hz] \tag{A.8}$$

Where $\beta = OBO_{hpa} \cdot L_{sat} \cdot L_{down} \cdot G_{gt}$.

A.2.3 Return Uplink

Besides we can substitute the subindex gw by the subindex gt in equations A.3 and A.4 to obtain the Return Uplink link budget, from ground terminal to satellite:

$$C = P_{gt} \cdot G_{gt} \cdot L_{gt} \cdot L_{up} \cdot G_{rx}(\theta) \tag{A.9}$$

$$N0 = kT_{noise} \tag{A.10}$$

And we can express the overall C/N0 as:

$$\left.\frac{C}{N0}\right|_{RTN-UP} = \frac{P_{gt} \cdot \gamma \cdot G_{rx}(\theta)}{kT_{noise}} \qquad [dB \cdot Hz] \tag{A.11}$$

Where $\gamma = G_{gt} \cdot L_{gt} \cdot L_{up}$

A.2.4 Return Downlink

If we substitute the subindex gt by the subindex gw in equation A.6 and A.7 we can obtain the computation of the Return Downlink link budget, from satellite to gateway where:

$$C = P_{sat} \cdot OBO_{hpa} \cdot L_{sat} \cdot G_{tx}(\theta) \cdot L_{down} \cdot G_{gw} \tag{A.12}$$

$$N0 = kT_{noise} \tag{A.13}$$

And we can express the overall C/N0 as:

$$\left.\frac{C}{N0}\right|_{RTN-DOWN} = \frac{P_{sat} \cdot \delta \cdot G_{tx}(\theta)}{kT_{noise}} \qquad [dB \cdot Hz] \tag{A.14}$$

Where $\delta = OBO_{hpa} \cdot L_{sat} \cdot L_{down} \cdot G_{gw}$.

A.3 Link Budget and Payload Values

The system and receiver parameters for the Ka band system and for the ANTARES system are given in the following Table (A.1).

	System and Receiver parameters	
Parameter	Ka band	ANTARES
Modulation	8PSK	QPSK, 8PSK, 16APSK
Downlink frequency	19.950GHz	1500MHz
Bandwidth	500MHz	14MHz
Half angle Beamwidth (θ_{-3dB})	0.245°	2.90°
G_{gt}	[21]	[23]
$T_{noise,gt}$	[21]	[23]

Table A.1: System and receiver parameters

Since we are strongly interested in the forward downlink, here below are given the references where the payload parameters for the forward downlink can be found, in Table A.2, A.3 and A.4.

	Conventional Payload	
Parameter	Ka band	ANTARES
P_{sat}	[21] Table 2-14	[21] Table 3-19
G_{max}	[21] Table 2-14	[22]
OBO_{hpa}	[21] Table 2-14	[21] Table 3-19
L_{sat}	[21] Table 2-14	[21] Table 3-19
L_{down}	211.1dB	188dB

Table A.2: Satellite parameters for conventional payload

	Flexible Payload	
Parameter	Ka band	ANTARES
P_{sat}	[21] Table 3-19	[21] Table 3-19
G_{max}	[21] Table 3-19	[22]
OBO_{hpa}	[21] Table 3-19	[21] Table 3-19
L_{sat}	[21] Table 3-19	[21] Table 3-19
L_{down}	211.1dB	188dB

Table A.3: Satellite parameters for flexible payload

	Beam-hopping Payload	
Parameter	Ka band	ANTARES
P_{sat}	[21] Table 4-9	[21] Table 4-9
G_{max}	[21] Table 4-9	[22]
OBO_{hpa}	[21] Table 4-9	[21] Table 4-9
L_{sat}	[21] Table 4-9	[21] Table 4-9
L_{down}	211.1dB	188dB

Table A.4: Satellite parameters for beam-hopping payload

The constant β for the system configuration chosen and for the three different payloads is detailed here after:

System	Conventional	Flexible	Beam-hopping
Ka band	$2.97e^{-22}$ (-215.2dB)	$3.58e^{-22}$ (-214.46)	$2.64e^{-22}$ (-215.77)
ANTARES	$5.92e^{-20}$ (-192.2)	$7.14e^{-20}$ (-191.46)	$5.28e^{-20}$ (-192.77)

Table A.5: β constant for the both systems and the three different payloads

The computed noise densities level per unit bandwidth, N0 for the Ka band system and the ANTARES system respectively is:

$$N0_{Ka} = 10\log_{10}(1.38e^{-23} \cdot 188.3K \cdot B) = -205.85dB \cdot Hz \tag{A.15}$$

$$N0_{ANT} = 10\log_{10}(1.38e^{-23} \cdot 164.3K \cdot B) = -206.4dB \cdot Hz \tag{A.16}$$

Appendix B

Guidelines for LL-FEC implementation in ANTARES

In this appendix is explained, for each of the scenarios found, the method used to implement and find the most suitable RS codes in function of the parameters defining each scenario. For the four different scenarios found, the parameters defining the erasure channel model are basically the duration of the erasure and the probability of the erasure. Depending on this values and the t_{delay} wanted configurations and performance of the RS codes will vary. Besides in some of the scenarios not all the needed information is available and configurations and performance rely on assumptions that must be made. Also final performance will rely on final decisions of link layer frame and physical layer packet sizes.

B.1 Undefined parameters and general procedure for RS implementation

in Table B.1 is presented a relation of the undefined parameters of the ANTARES project and the values assumed that are needed for obtaining the RS performance in each scenario.

Parameter	Values assumed
Bitrate R_b	16kbps, 32kbps
LL frame size	256 bytes, 512 bytes
PHY packet size	1024 bits, 2048 bits
Overhead L1/L2	10%

Table B.1: Undefined parameters and values assumed

For Reed Solomon ADT and RSDT tables configurations the next process is followed:

- Fix the delay-aware, t_{delay}, of LL-FEC constrained to $t_{delay} > t_{erasure}$, otherwise all packets could be erased. Besides t_{delay} should be set into a lower value than the most stringent of the traffic CoS TD_{95} if possible. If performance under this value is too bad or $t_{erasure} > TD_{95}$, t_{delay} should be set into a lower value than ET.
- Choose an RS(N,K) code, a physical layer bitrate, a link layer frame size and an encapsulation overhead.
- Compute the number of rows, Nrows, needed for the ADT and RSDT table being known that[1]:

$$t_{delay} = \frac{m \cdot N \cdot N_{rows} + OH(bits)}{R_b}$$

- Build and fill the $ADT_{N_{rows} \times K}$ and $RSDT_{N_{rows} \times T}$ tables.
- Extract information in the tables column wise and add link layer and physical layer headers.
- Select a scenario and generate the erasure channel model.
- Send the information through the channel and de-encapsulate.
- Evaluate CFR performance without using LL-FEC.
- Fill the ADT and RSDT reception tables, read information row wise and correct the errors in the row if less than *T=(N-K)/2* erasures are produced.
- Evaluate CFR performance using LL-FEC and compare with CFR without using LL-FEC.

In Figure B.1 is shown a flux diagram of the process followed.

[1] Detailed explanation on the parameters involving t_{delay} can be found in section 3.5.3

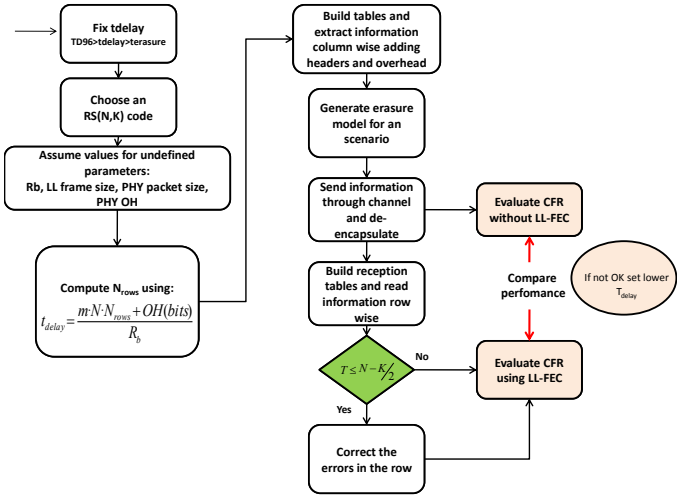

Figure B.1: Flux diagram

B.2 Characteristics of the "Erasures produced by airplanes in the same line of sight with the satellite" scenario

Parameter	Expression	Values obtained/assumed
$t_{erasure}$	$\frac{x}{cos(\theta)\cdot v_{relative}}$	0.04s, 0.3s, 1.15s
$p_{erasure}$	-	$1e^{-4}$-$1e^{-2}$
delay-aware	-	0.68s, 1.5s

Table B.2: Channel parameters

Where x is the length of the aircraft, θ the horizontal angle between the aircrafts and $v_{relative}$ the relative speeds between the two airplanes. Detailed explanation of the $t_{erasure}$ obtention is given in section 3.2.2.2.

B.3 Characteristics of the "Erasures produced by the airplane itself" scenario

Parameter	Expression	Values obtained/assumed
$t_{erasure}$	-	0.5s
$p_{erasure}$	-	$3.4e^{-12}$-$3.4e^{-10}$
delay-aware	-	0.68s

Table B.3: Channel parameters

A detailed explanation of the parameters involving $t_{erasure}$ can be found in section 3.2.2.2.

B.4 Characteristics of the "Erasures produced by the blades" scenario

Parameter	Expression	Values obtained/assumed
$t_{erasure}$	$\frac{1}{RPM_{blades}/60} \cdot (blades_{width})$	0.078
Duty cycle of the erasure	$\frac{t_{erasure}}{\frac{2\pi d_{antenna}}{4} - blades_{width} \cdot \frac{1}{RPM_{blades}/60}}$	*30%*
delay-aware	-	0.68s

Table B.4: Channel parameters

Where the term $d_{antenna}$ is the distance from the rotation axis of the blades to the location of the helicopter antenna. A detailed explanation of the parameters involving $t_{erasure}$ can be found in section 3.2.2.2.

B.5 Characteristics of the "Erasures produced by blades and buildings scenario"

Parameter	Expression	Values obtained/assumed
$t_{erasure}$	$\frac{l}{v_{helicopter}}$	0.9
$p_{building\ erasure}$	can be obtained from real city maps	$1e^{-4}$-$1e^{-2}$
delay-aware	-	1.5

Table B.5: Channel parameters

Where l is the length of the building and $v_{helicopter}$ the speed in m/s of the helicopter. A detailed explanation of $t_{erasure}$ obtention can be found in section 3.2.2.2.

Bibliography

[1] "Multi-Star, Payload Systems", Beam Hopping Techniques for multibeam satellite systems.

[2] "Draft version of System Simulator Architecture: Non Beam Hopping System", Beam Hopping Techniques for multibeam satellite systems.

[3] G.P. Calzolari, M. Chiani, F. Chiaraluce, R. Garello and E. Paolini, "Channel coding for future space missions: New requirements and trends". *Procedings of the IEEE, 95(11):2157-2170, Nov. 2007.*

[4] Jon Hamkins, "Optimal Codes for the Burst Erasure Channel". *IPN Progress Report 42-174, August 2008.*

[5] Amin Shokrollahi, *Senior Member, IEEE*, "Raptor Codes". *IEEE Transactions on information theory, vol. 52, no. 6, pp. 2551-2567, June 2006.*

[6] Jiang Lei, *Student Member, IEEE*, María Ángeles Vázquez-Castro, *Senior Member, IEEE*, and Thomas Sotckhammer, *Senior Member IEEE*, "Link-Layer FEC and Cross-Layer Architecture for DVB-S2 Transmission With QoS in Railway Scenarios". *IEEE Transactions on vehicular technology, vol. 58, no. 8, pp. 4265-4276, October 2009.*

[7] M. Yang and W. E. Ryan, "Performance of efficiently encodable low-density-parity-check codes in noise bursts on the EPR4 channel". *Magnetics IEEE Transactions, vol. 40, no. 2, pp. 507-512, March 2004.*

[8] E. paolini and M.Chiani, "Improved low-density-parity-check codes for burst erasure channels". *Communications,2006. ICC'06. IEEE International Conference on 3:1183-1188, June 2006.*

[9] Gokul Sridharan, Abishek Kumarasubramanian, Andrew Thangaraj and Srikrishna Bhsayam, "Optimizing burst erasure correction of LDPC codes by interleaving". *Information Theory, 2008. ISIT 2008. IEEE International Symposium on, pp- 1143-1147, July 2008.*

[10] Luigi Rizzo, "Effective erasure codes for reliable computer communication protocols", *ACM SIGCOMM Computer communication review, vol. 27, pp. 24-36, 2007.*

[11] "Aeronautical Propagation Channel Model", Antares.

[12] Eriza Hafid Fazli, Markus Werner, "View Angle Statistics of Aircraft Airbone Antenna to GEO satellites", *Satellite and Space Communications, 2009. IWSSC 2009. International Workshop on, pp. 341-345, 2009.*

[13] Y.Y. Tai, L. Lan, L. Zeng, S. Lin, and K.A.S. Abdel-Ghaffar, "Algebraic construction of quasi-cyclic LDPC codes for the AWGN and erasure channels", *Communications IEEE Transactions on, 54(10):1765-1774, October 2006.*

[14] Laura Conde-Canencia, Ali Al Ghouwayel, Emmanuel Boutillon, "Complexity Comparison of Non-Binary LDPC Decoders", ICT-MobileSummit 2009 Conference Proceedings.

[15] Sarah J. Johnson, "Introducing Low-Density Parity-Check Codes".

[16] Antoni Morell, Gonzalo Seco-Granados and María Ángeles Vázquez Castro, "Joint Time Slot Optimization and Fair Bandwidth Allocation for DVB-RCS Systems", *Global Telecommunications Conference, pp. 1-5, November 2006.*

[17] Antoni Morell, Gonzalo Seco-Granados and María Ángeles Vázquez Castro, "Enhanced Dynamic Resource Allocation for DVB-RCS: a Cross-Layer Operational Framework", *Military Communications Conference, pp. 1-7, October 2007.*

[18] Antoni Morell, G. Seco-Granados and M.A. Vázquez-Castro, "Efficient Cross-Layer Algorithm for Fair Dynamic Bandwidth Allocation", *Computer Communications and Networks, Proceedings of 16th International Conference on, pp. 13-18, September 2007.*

[19] Gérard Maral, Michel Bousquet, "Satellite Communications Systems: Systems, Techniques and Techonolyg", *John Wiley & Sons Ltd.*

[20] Thomas M. Cover, Joy A. Thomas, "Elements of Information Theory", *John Wiley & Sons Ltd.*

[21] A. Zanus, L. Gilbert, C. Paquet, "Beam Hopping techniques for multibeam satellite systems", Multi-Star, Payload Systems.

[22] Indra team, "Baseline Scenario Definition for the Multiple Access trade-off, ANTARES.

[23] A. Miglietta, R. Vinci, "Technical Note on Link Budget Analyses", ANTARES.

[24] X. Alberti, J.M. Cebrian, A. Del Bianco, Z. Katona, J. Lei, M.A Vazquez-Castro, A. Zanus, L. Gilbert, N. Alagha, "System Capacity Optimization in Time and Frequency for Multibeam Multi-media Satellite Systems", To be presented.

Resum:

En aquest projecte s'ha analitzat y optimitzat l'enllaç satèl·lit a avió per a un sistema aeronàutic global. Aquest nou sistema anomenat ANTARES està dissenyat per a comunicar avions amb estacions base mitjançant un satèl·lit. Aquesta es una iniciativa on hi participen institucions oficials en l'aviació com ara l'ECAC i que és desenvolupat en una col·laboració europea d'universitats i empreses.

El treball dut a terme en el projecte compren bàsicament tres aspectes. El disseny i anàlisis de la gestió de recursos. La idoneïtat d'utilitzar correcció d'errors en la capa d'enllaç y en cas que sigui necessària dissenyar una opció de codificació preliminar. Finalment, estudiar y analitzar l'efecte de la interferència co-canal en sistemes multifeix. ***Tots aquests temes són considerats només per al "forward link".***

L'estructura que segueix el projecte és primer presentar les característiques globals del sistema, després centrar-se y analitzar els temes mencionats per a poder donar resultats y extreure conclusions.

Resumen:

En este proyecto se ha analizado y optimizado el enlace satélite a avión para un sistema aeronáutico global. Este nuevo sistema, ANTARES, está diseñado para comunicar aviones y estaciones base mediante un satélite. Esta es una iniciativa europea en la que participan varias instituciones oficiales en aviación como el ECAC y es desarrollada en una colaboración europea de universidades y empresas.

El trabajo llevado a cabo en este proyecto comprende básicamente tres aspectos. El diseño y análisis de la gestión de recursos. La idoneidad de usar corrección de errores en la capa de enlace y en caso que sea necesario diseñar una opción de codificación preliminar. Finalmente, estudiar y analizar el efecto de la interferencia co-canal en sistemas multihaz. ***Todos estos temas se consideran solo en el "forward link".***

La estructura que sigue el trabajo es, primero presentar las características globales del sistema, luego centrarse y analizar los temas mencionados para finalmente dar resultados y extraer conclusiones.

Summary:

In this project it is analyzed and optimized the satellite-to-plane link of an aeronautical global system. This new upcoming system called ANTARES is intended for communicating airplanes and ground stations through a satellite system. This is a European initiative involving official institutions in terms of aviation such as the ECAC and developed in a European collaboration of universities and companies.

The work carried out in the project comprehends basically three issues. The Radio Resource Management analysis and design. Analyze the suitability of using Link Layer-Forward Error Correction in the system and in case it is necessary design a preliminary coding option. Finally, study and analyze the effect of the co-channel interference in multibeam systems. ***All these issues are considered only for the forward link of the system.***

The structure of the project is as follows, first present the global characteristics of the system, then focus and analyze the mentioned subjects and finally give results and take conclusions on the work.